May 2023

Allocation and Compilation Methodology for Modular Power Electronic Equipment Metamodels

William J. Koebel
University of Wisconsin-Milwaukee

ALLOCATION AND COMPILATION METHODOLOGY FOR MODULAR POWER ELECTRONIC EQUIPMENT METAMODELS

by

Will Koebel

A Thesis Submitted in
Partial Fulfillment of the
Requirements for the Degree of

Master of Science
in Engineering

at

The University of Wisconsin-Milwaukee

May 2023

ABSTRACT

ALLOCATION AND COMPILATION METHODOLOGY FOR MODULAR POWER ELECTRONIC EQUIPMENT METAMODELS

by

Will Koebel

The University of Wisconsin-Milwaukee, 2023
Under the Supervision of Professor Robert Cuzner

With the ongoing electrification of Navy vessels motivated by increased power demands, evolving operating environments, and more stringent pollution policies, modular distribution networks have been proposed to introduce survivability, affordability, and resiliency into future ship designs. A virtual prototyping process (VPP) has been introduced to produce scalable metamodels for the Leading Edge Architecture for Prototyping Systems (LEAPS) database that enables development of modular distribution networks on the U.S. Navy's Smart Ship System Design (S3D) design platform. This work proposes an allocation and compilation methodology for use in the VPP that modularizes enabling technologies for integration into a modular distribution network through the use of spatial insulation, thermal, conductor, accessibility, and frame allocations. A use case, as distribution bus voltage varies from 5kV to 30kV, is performed on a DC no-load disconnect switch to demonstrate the methodology's applicability. Performance metrics, termed MOP's, are output from the proposed allocation and compilation methodology and provide transparency into performance metric trade-offs introduced once technology is modularized. Calculated MOPS, power density and specific power, suggest diminishing returns on performance gains once a distribution bus voltage of 16kV is reached as insulation coordination requirements begin to dominate space claim.

DEDICATION

I would like to thank my professor Robert Cuzner for his invaluable guidance during my time at UW-Milwaukee. The political science, economics, and journalism departments at UW-Milwaukee for their gracious welcome and patience of my innumerable questions. My parents and sister for their love and support that has been the soil for my growth. And most importantly, my grandmother who's modeled a life worth striving for and imparted the crucial difference between knowledge and wisdom.

TABLE OF CONTENTS

Abstract ii

List of Figures viii

List of Tables xii

Chapter 1: The Problem 1

Chapter 2: Background 5

2.1 Virtual Prototyping Process 5

2.2 Shipboard Ontology 7

2.3 VPP Spatial Allocations 9

2.3.1 Insulation 11

2.3.2 Thermal Management 13

2.3.3 Accessibility 14

2.3.4 Structural 15

2.3.5 Conductors 16

2.3.6 Active Component Models 16

Chapter 3: No-Load Switch Use Case 18

3.1 Place Active Components 19

3.2 Determine and Place Solid Allocations 21
3.3 Determine and Place Supplementary Allocations 21
3.4 Dimensioning Process 25
3.4.1 Nomenclature 26
3.4.2 First-Pass Dimensioning 27
3.4.3 Second-Pass Dimensioning 31
3.5 Compilation Process 35
3.6 MATLAB Metamodel Code 38
3.7 No-Load Switch Metamodel Results 42

Chapter 4: PDM Bay Allocation and Compilation Use-Case 45

4.1 PDM Allocation and Compilation Process 46
4.1.1 No-Load Switch Drawer 46
4.1.2 PDM No-Load Switch Drawer Results 50
4.1.3 PDM Heat Exchanger Drawer 53
4.1.4 PDM Drawer Compartment 58
4.1.5 PDM Connection Compartment 62
4.1.6 PDM Bay 68
4.2 PDM Metamodel MATLAB Code 73
4.3 PDM Bay Metamodel Results 85

Chapter 5: Conclusion and Future Work 90

References 95

Appendix A: Clearance and Creepage Distance Determination for Frequencies Greater than 30k kHz 97

LIST OF FIGURES

2.1 Virtual Prototyping Process 6

2.2 Virtual Prototyping Process as Applied to Use-Case 7

2.3 IPS Based Architecture 8

2.4 IPS/NiPEC Modular Ontology 9

2.5 Allocation Types 11

2.6 Creepage and Clearance Distance for PEBB 1000 SM Drawer 12

2.7 Creepage and Clearance Distance for PEBB 6000 SM Drawer 12

3.1 Allocation and Compilation Process 19

3.2 3-D Rendering of Use-Case No-Load Switch 20

3.3 Active Component Allocations of No-Load Switch 20

3.4 Solid Allocations 21

3.5 No-Load Switch Solid Allocation Placement 22

3.6 Generic Supplementary Allocation Determination 23

3.7 Supplementary Allocation Determination for Three Thermal Solutions . . . 24

3.8 Supplementary Allocation Determination Flowchart for Active Components & Conductor Allocations 25

3.9 Fully Allocated No-Load Switch 25

3.10 Dimension Nomenclature 26

3.11 Allocation Type Nomenclature Convention 26
3.12 First-Pass x Dimensions 28
3.13 First-Pass z Dimensions 29
3.14 First-Pass y Dimensions 29
3.15 First-Pass Section View 1 30
3.16 First-Pass Section View 2 30
3.17 Simplified x Dimensions 32
3.18 Simplified z Dimensions 33
3.19 Simplified y Dimensions 33
3.20 Simplified Section View 1 34
3.21 Simplified Section View 2 34
3.22 Sequence Diagram of No-Load Switch Matlab Code 39
3.23 Width, Height, and Length Results 43
3.24 No-Load Switch Mass Results 44

4.1 Drawer Primary Allocations 46
4.2 Drawer Supplementary Allocation Flowchart 47
4.3 No-Load Switch Drawer Supplementary Allocations 48
4.4 NLSw Drawer Front Dimensioned 49
4.5 NLSw Drawer Side Dimensioned 49
4.6 No-Load Switch Drawer Dimensions 51
4.7 No-Load Switch Drawer Mass 51
4.8 No-Load Switch Drawer Power Density Comparison 52

4.9 No-Load Switch Drawer Specific Power Comparison 53

4.10 Heat Exchanger Primary Allocation 54

4.11 Heat Exchanger Supplementary Allocation Flowchart 55

4.12 Heat Exchanger Supplementary Allocation X-Direction 55

4.13 Heat Exchanger Supplementary Allocation Z/Y-Direction 56

4.14 Heat Exchanger Dimensions X-Direction 56

4.15 Heat Exchanger Dimensions Z/Y-Direction 57

4.16 PDM Compartment Primary Allocations 58

4.17 Heat Exchanger Compartment Primary Allocations 58

4.18 No-Load Switch and Heat Exchanger Compartment Supplementary Allocation Determination Flowchart 59

4.19 No-Load Switch PDM Compartment Supplementary Allocations 59

4.20 Heat Exchanger Compartment Supplementary Allocations 60

4.21 PDM Compartment Drawer Dimensions 60

4.22 PDM Compartment Drawer Dimensions 61

4.23 Heat Exchanger Dimensions Z/Y-Direction 61

4.24 Dimensioned NLSw and HXG Compartment 62

4.25 Active Component Placement of Connection Compartment 63

4.26 Solid Allocation Placement of Connection Compartment 64

4.27 Active Component & Cabling Supplementary Allocation Determination . . 65

4.28 Bus Bar Conductor Supplementary Allocation Determination 65

4.29 Supplementary Allocation Placement of Connection Compartment 66

4.30 First & Second-Pass Dimensioning of Connection Compartment 67

4.31 PDM Bay Active Component Placement 68
4.32 PDM Bay Active Component Placement 69
4.33 Supplementary Allocation Determination for PDM Bay 69
4.34 PDM Bay Supplementary Allocation Placement 70
4.35 PDM Bay Supplementary Allocation Placement 70
4.36 Dimensioned PDM Bay X-Direction 71
4.37 Dimensioned PDM Bay 72
4.38 Dimensioned PDM Bay Connection Compartment X-Direction 72
4.39 Bay Code Sequence Diagram 73
4.40 PDM Bay Dimensions 86
4.41 PDM Bay Mass 87
4.42 PDM Power Density Comparison 88
4.43 PDM Specific Power Comparison 89
4.44 PDM MOP Comparison 89

A.1 High Frequency Creepage Distances 98
A.2 High Frequency Clearance Distances 99

LIST OF TABLES

3.1 Stand_in Array Variables 40

3.2 Iso_in Array Variables 41

3.3 Materials and Densities Informing Mass Calculations 42

CHAPTER 1
THE PROBLEM

New technologies, evolving operating environments, and more stringent pollution policies are motivating the U.S. Navy's development of a fully electric ship [1, 2]. New technologies such as future payloads, sensors, and weapon systems, introduce increased power demands that cannot be met by installed generation capacity [3, 4]. A reconfigurable distribution network is required to enable redirection of the limited installed generation capacity as operating environments and requirements evolve. Addressing this need, several modular distribution architectures have been proposed and are under development. The Integrated Power System (IPS) was the first modular proposal that assembled a distribution network centered around conventionally procured modular electrical distribution equipment and touted gains in survivability, affordability, and resiliency [5]. As research matured an alternative approach to realizing the IPS emerged that was no longer centered around conventionally procured electrical equipment but instead, distribution corridors running longitudinally from aft to port housing modular distribution equipment. This modular approach was termed the Navy Integrated Power and Energy Corridor (NiPEC), and is under development by the Power Electronics Power Distribution System Program (PEPEDS) [6]. A NiPEC provides cost, survivability, and arrangement advantages over the IPES as the concept's increased modularity realizes supply chain economies of scale, redundancy through system reconfiguration, and reduction in electrical-thermal-structural overhead [7]. To ensure that potential technology innovations are incorporated into the NiPEC, early concept design exploration has been prioritized and pursued by the Navy.

The importance of early concept exploration is best captured by a quote by Chalfant in her 2015 conference paper, "One of the truisms of ship design is that the decisions of

greatest impact are made in the early stages of design when the least information and the greatest uncertainty are present"[8]. Because the technology enabling propulsion, mission controls, weapons systems, and support systems may improve during the lengthy design process, often 10 years, design choices, namely technology choices, made early in the design process can leave designers with outdated, sub-optimal technology. To avoid this pitfall ship designers are attempting to gather more information earlier in the process, pushing design decisions until design trade-offs are better understood. This work is being realized through the development of ship design software.

One such tool is the Smart Ship System Design (S3D). S3D is a suite of tools developed by the Electric Ship Research and Development Consortium (ESRDC) to enable concurrent collaboration between engineering disciplines such as electrical, mechanical, thermal, and HVAC [9, 10]. S3D creates, visualizes, and analyzes two-dimensional electrical, mechanical, thermal, and HVAC one-line representations of power systems throughout the ship. The tool produces drawings that can be represented in three-dimensional space to visualize the placement and interaction between equipment and structures.

To enable S3D, the environment draws upon a database of ship design data called the Leading Edge Architecture for Prototyping Systems (LEAPS) [8]. As a catalog of scalable equipment and component object models, equipment's attributes and interfaces are captured to ensure compatibility when used to model modular distribution networks. Attributes include spacial dimensions, weight, and performance metrics. Interfaces include electrical, mechanical, and thermal connections. Cataloged models scale the equipment's size, weight, losses, cost, and reliability as a function of design space variables corresponding to design decisions. In order to accurately scale power generation and distribution equipment, scaling laws must be employed.

Scaling laws and metamodels have been successfully developed for electric machines [11], electromagnetic components [12, 13], and thermal management systems [14] but a robust methodology able to optimize and produce scalable metamodels for the LEAPS

database was not introduced until [15]. The methodology incorporates optimizing objectives, constraints & requirements, exploration variables, technology insertion, and internal infrastructure required to modularize equipment as meta-heuristic scalable models are produced. The metamodels become modular building blocks for use in the NiPEC or IPES modular distribution systems as developed in S3D. Chapter 2 will describe the VPP methodology in detail.

To enable comparison, and ultimately inform design decisions, a means for evaluating equipment performance must be incorporated into the VPP's produced metamodels. Performance metrics are classically organized as Measures of Effectiveness (MOEs), Measures of Performance (MOPs), Technical Performance Metrics (TPMs), and Key Performance Parameters (KPPs) which are a subset of key MOPs and TPMs [16]. These form the basis of performance requirements and the measures by which systems are validated. Due to the complexity and reconfigurability of the modular IPS and NiPEC distribution systems, top-level TPMs most concerning to ship designers, like physical space claim and hull displacement, are difficult to access at the system level. MOPs however, outputs of the metamodels produced by the VPP, do provide this meaningful insight as performance trade-offs such as power density (p), specific power (y), specific cost (a), and efficiency (e) are evaluated and accessed. By evaluating MOPs for each design optimized by the VPP, meaningful design decisions can be made that allow stakeholder needs to be selected for.

This work calculates MOPs, power density and specific power specifically, for a point design already assumed optimized by the VPP. By assuming optimization this work is able to build upon the allocation process first proposed by Cuzner [17] and proposes an updated allocation and compilation methodology that allows existing power electronic technology, or potentially innovative concept designs, to be modularized by adding spatial connection, serviceability, structural support, thermal, and insulation allocations required for integration into the proposed modular distribution networks. MOPs will be calculated for the point design assessed in the use case and provide insight into perfor-

mance trade-offs associated with design decisions, namely DC distribution bus voltage. The following chapters will provide a background to the VPP and the scaling allocations that inform it, introduce the proposed allocation and compilation methodology, apply the methodology to an equipment use-case utilized in the IPS or NiPEC distribution architecture, and ultimately produce a scalable meta-model for use in S3D's LEAPS database. The metamodel will provide designers with system-level MOPs for the modularized assembly.

CHAPTER 2
BACKGROUND

This chapter is dedicated to providing an overview of the VPP, its ontology, and the standards, physics, and engineering experience that inform the VPP's spatial allocations.

2.1 Virtual Prototyping Process

The VPP is a methodology proposed by Cuzner et al. in [17, 18, 19], that accounts for optimizing objects, constraints & requirements, exploration variables, technology insertion, and internal infrastructure required to modularize hardware as it produces meta-heuristic scalable models for use in the Navy's LEAPS database.

The VPP methodology, as presented in fig. 2.1, begins by bringing in present state-of-the-art hardware, or potential innovative designs, system exploration variables (x_v), requirements and constraints (r_v), and optimizing objectives (o_v) into the evolutionary design environment to build active component models for state-of-the-art hardware, or electro-thermal-physical models (ETPMs) for potential innovations. Spatial allocations that scale with system exploration variables (x_v) are brought into the evolutionary design environment and added to active component or ETPM models to account for additional internal infrastructure required when modularizing equipment. Scalable solid spatial allocations account for cooling solutions (a_t), bus & interconnections (a_c), and structural frames (a_f). Supplementary spatial allocations account for dielectric scaling laws (a_d), accessibility (a_a), and thermal management (a_t). As the active component, or ETPM, models are modularized into LRUs, drawers, compartments, and bays spatial scaling allocations are added at each modular level. Once modularized to a bay, design solutions along the Pareto front are output from the evolutionary design environment in the form of optimizing objectives (O_{v1},O_{v2},O_{v3}). These optimizing objectives allow designers the ability

to compare and select viable designs from the Pareto fronts that ultimately inform an optimal single-point design. Optimizing objectives are often identical to the Measures of Performance (MOPs) that the Navy uses to evaluate design performance. With MOPs output, trade-offs between performance metrics can be selected for as informed by stakeholder needs.

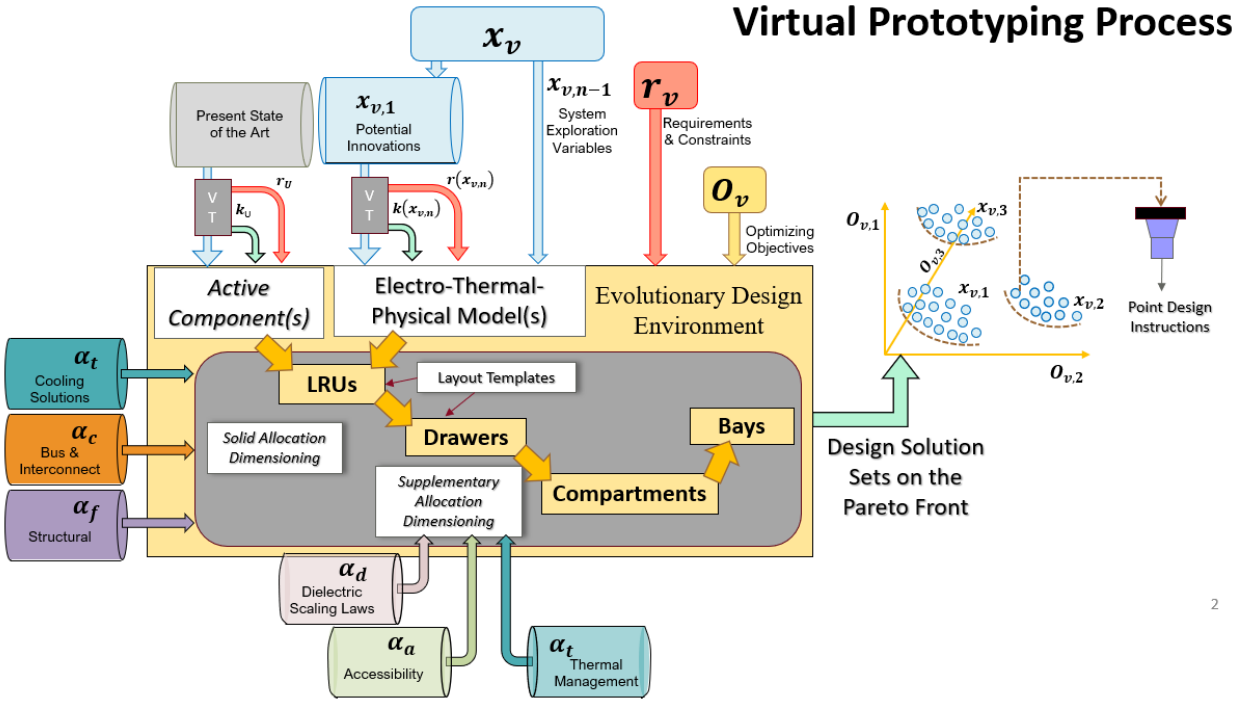

Figure 2.1: Virtual Prototyping Process

Fig. 2.2 shows the virtual prototyping process as adapted to this work. Here, a present state-of-the-art design, a no-load DC disconnect switch [20], is brought into the scaling of point design environment along with rated voltage and rated current as system exploration variables (x_v), and requirements and constraints (r_v), to produce a scalable active component model. Solid and supplementary spatial allocations are brought into the scaling of point design environment to add modularity to the active component model. As the technology is modularized into LRUs, drawers, compartments, and bays scalable metamodels are compiled that evaluate optimizing objective metrics (O_{v1},O_{v2},O_{v3}), or MOPs, for the point design. This output is representative of the VPP's MOP Pareto

front outputs. By comparing MOP outputs designers are able to select optimal designs depending on stakeholder's needs, namely the trade-off between MOPs.

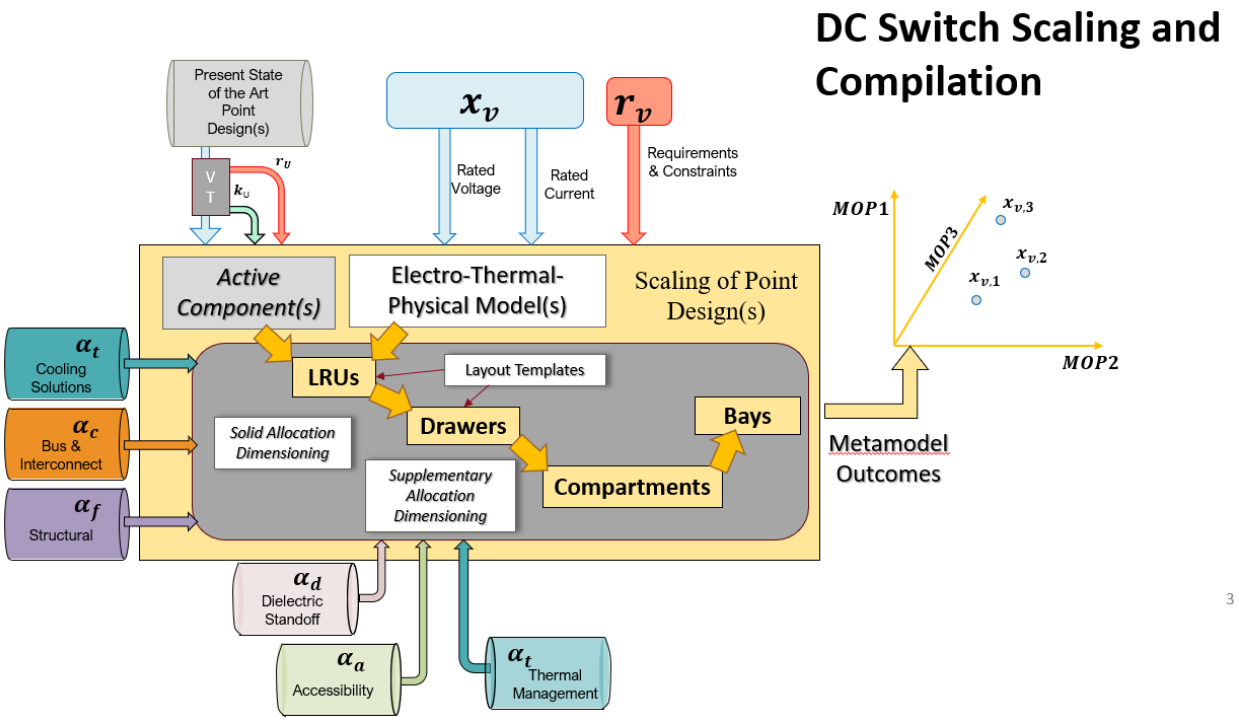

Figure 2.2: Virtual Prototyping Process as Applied to Use-Case

2.2 Shipboard Ontology

The all-electric power train, as pursued by the Navy, has undergone multiple iterations as the trade-offs between cost, survivability, and arrangement have manifested themselves into two prominent power train proposals, the IPS/IPES and NiPEC [6, 1]. The IPS has a long history dating back to 1979 and is the architectural predecessor to the NiPEC. In the IPS/IPES architecture, power flows from generation sources and energy storage devices through distinct, self-contained, power electronic-based modules to vessel loads as shown in fig. 2.3. Each power electronic-based module is defined according to its function within the distribution network with the Power Generation Module (PGM) converting chemical energy to Medium Voltage Direct Current (MVDC) electrical energy, the Power Conversion Module (PCM) converting MVDC energy to Low Volt-

age Direct Current (LVDC) energy, the Power Distribution Module (PDM) distributing MVDC power inter-zonally, a Propulsion Motor Module (PMM) converting MVDC into mechanical propulsion, and the Pulsed Power Module (PMM) converting MVDC energy into directed energy for energy-based weaponry such as the proposed rail gun installation [21, 22].

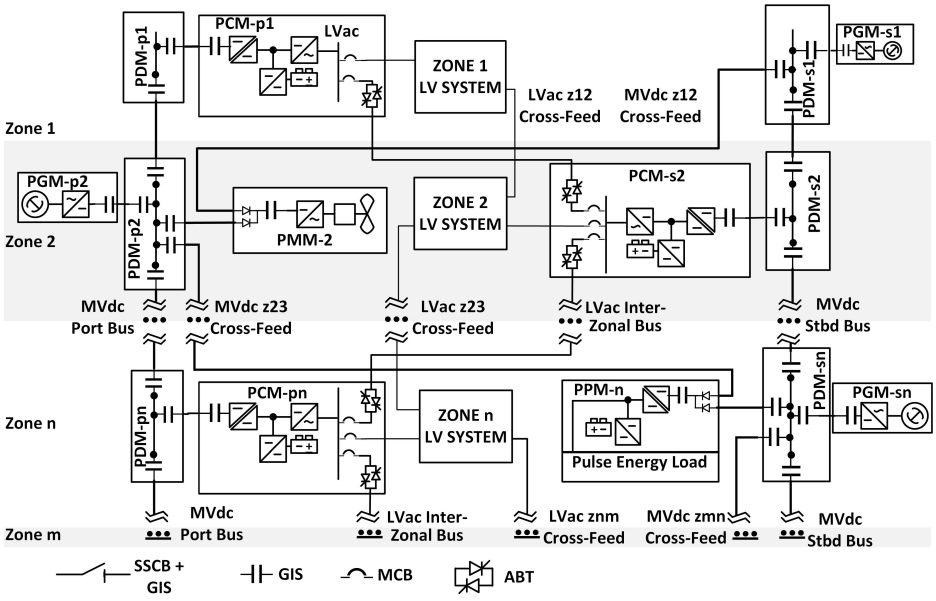

Figure 2.3: IPS Based Architecture

The NiPEC is an iteration of the IPS that does not define the modular distribution equipment by functional modules but instead as a series of modular compartments that run parallel to the ship's center line and are longitudinally connected to one another. In recent years the NiPEC has become the prioritized architecture, but with priorities ever-changing, a robust VPP methodology will allow either IPS or NiPEC, or future power train architectures, to be modeled. The allocation-based methodology proposed in this work provides this robustness by leveraging the foundational modular ontology both architectures share. The ontology underpinning both the IPS and NiPEC is shown in fig. 2.4. The major ontological difference between proposed architectures is that the IPS ontology extends from the LRU to bay while the NiPEC extends from the LRU to Drawers which are then housed in compartments adjacently located along the center line of the

ship to enable a power electronic corridor. The use case used to demonstrate the proposed allocation and compilation methodology is a functional PDM utilized in the IPS architecture but future work will extend this methodology to the NiPEC.

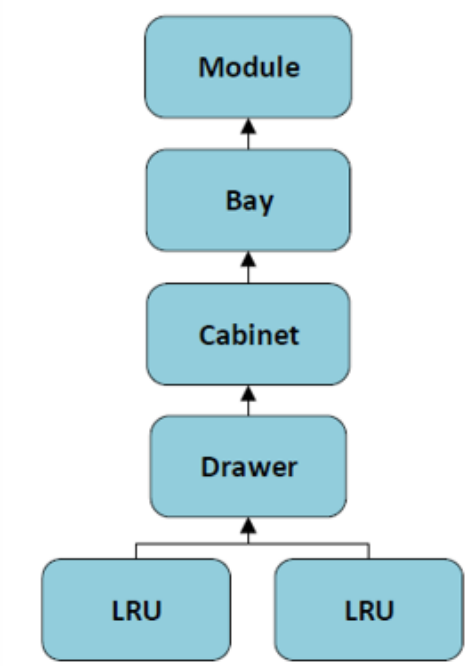

Figure 2.4: IPS/NiPEC Modular Ontology

2.3 VPP Spatial Allocations

The spatial allocations built upon in this work were first introduced by Cuzner et al. [17] as an approach to metamodel development that provided space and mass allocations for cabinet-based modular equipment. Spatial allocations captured the additional internal infrastructure required to modularize technology and included allocations for dielectric stand-offs, thermal management, accessibility, and frame supports. Originally, conservative factors akin to safety factors in mechanical design informed these spatial and mass allocations but as development of the methodology continued physics, standards, and experience-based scaling laws were incorporated. Ideally, all allocations will be informed by physics-based scaling laws as they best capture scaling relationships. The methodol-

ogy utilized in the VPP provides a compromise between the traditional and ideal while experimental research is being pursued to one-day capture the physics-based scaling of spatial allocations and active components. The compromise, as utilized in this work, is an amalgamation of physics, standards, and experience-based scaling relations.

Scaling laws inform the VPP's six generic allocations that when combined are able to model the modularization of any power electronic based technology. The six generic allocations are defined as active components, thermal management, conductors, insulation, accessibility, and structural, as shown in fig. 2.5. Active components are typically procured equipment such as switching modules or in this use-case a DC no-load disconnect switch, but can also include smaller components such as controls and monitoring sensors. Thermal allocations capture any part of the ship's thermal management system which typically includes cold plates, fans, and room for airflow. Thermal management specific to shipboard applications will be discussed in-depth in this chapter. Allocations capturing the conductors that enables electrical distribution throughout the ship are captured by the conductor allocation. Conductor allocations typically represent distribution bus bar and cabling. Insulation allocations represent the physical, or air-gap stand-off, insulation that protects energized equipment from failure modes such as arcing and insulation failure caused by partial discharge. Accessibility allocations account for the space needed to manufacture and service equipment, and is typically highly dependent on the manufacturer and application environment. Structural allocations capture the physical support frames and enclosure paneling needed to house power electronic equipment. Structural allocations can include weight-bearing support structures, sheet metal that encloses the equipment, and other internal support structures.

The following subsections will summarize the physics, standards, and experience-based scaling laws that inform each allocation type as found in the literature and state-of-the-art research.

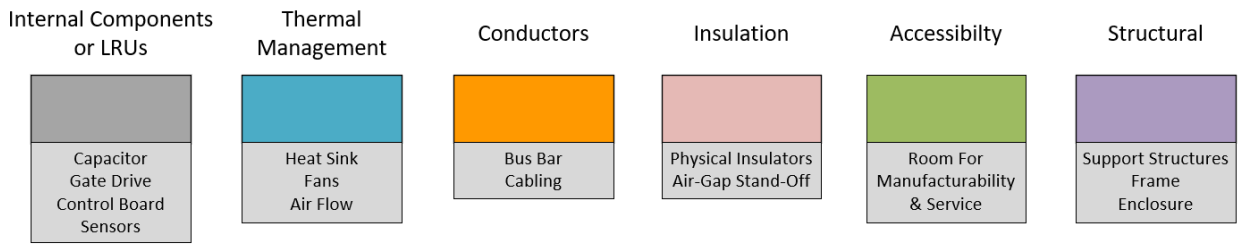

Figure 2.5: Allocation Types

2.3.1 Insulation

Insulation allocations were originally introduced as dielectric standoff allocations in [17]. To present a more inclusive allocation that accounts for both dielectric air-gap standoffs and physical insulation the term insulation allocations is adopted. Guidance on how insulation allocations scale with respect to system, or component voltage is not provided in [17]. Allocations were determined based on engineering experience and found to be appropriate when the cabinet fill-factor percentage was less than 40%. An explicit scaling of insulation allocations was subsequently introduced in [23]. This work explored applicable industry standards to ultimately derive, scalable with voltage, creepage and clearance dielectric air-gap standoff distances from the industry standard IEC 61800-5 [24]. Creepage and clearance air-gap stand-off distances were extrapolated from the industry standard using assumed shipboard environment considerations such as overvolatge category, insulation material, and fault conditions. The prescribed testing voltages and stand-off distances are presented in figs. figs. 2.6 and 2.7.

Prescribed creepage and clearance distances assumed an overvoltage category of three and a material CTI rating of IIIa. This work will inform the scaling of insulation allocations for this work's use-cases.

The approach assumes that shipboard electrical systems are designed to survive a single line to ground fault as is standard in shipboard design [17, 18, 23]. Clearance requirements are determined by taking the maximum standoff distance prescribed by impulse, temporary over-voltage, and working test voltages. Each captures a different over, or

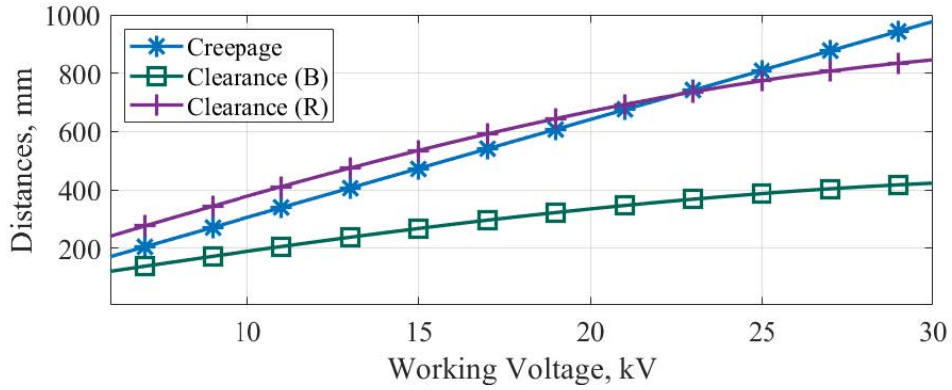

Figure 2.6: Creepage and Clearance Distance for PEBB 1000 SM Drawer

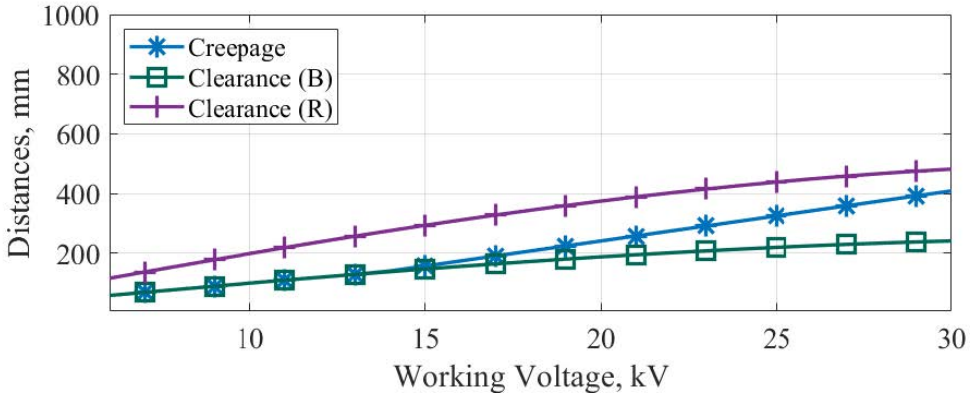

Figure 2.7: Creepage and Clearance Distance for PEBB 6000 SM Drawer

under-voltage, scenario that equipment is expect to be subjected to during operating conditions. Creepage requirements rely only upon working voltage to prescribe creepage distances.

While the IEC-61800 standard-based scaling of insulation allocations provide a reasonable estimate for insulation scaling, ideal scaling laws will capture the physics-based phenomenon that lead to insulation failure, such as partial discharge and treeing. Promising work from [25, 26, 27, 28, 29] is attempting to capture these physics-based relationships but scaling laws have not yet been formalized. As research progresses, physics-based scaling laws can be easily incorporated into the proposed allocation and compilation methodology, and ultimately the VPP.

2.3.2 Thermal Management

As stated in [30] thermal allocations can be spatial allocations representing room for air-flow and fans, considered indirect cooling, or water connections and manifolds, considered direct liquid cooling. The trade-off between choosing indirect or direct liquid cooling comes from the requirement to completely isolate direct liquid cooling manifolds and connections from ground. In order to isolate manifolds and connections from ground additional bracing components are required that when added, often negate power density improvements gained by eliminating the air-flow ”dead space” required for indirect cooling. To capture and analyze this trade-off both indirect and direct liquid cooling must be accounted for by thermal allocations. This approach introduces two distinct thermal allocations, one for physical thermal management components like cold plates that can not serve as insulation or accessibility allocations, and the other, an allocation for air-flow that can occupy the same space as insulation and accessibility allocations. The distinction is presented in fig. 2.5 with the dark blue allocation representing physical thermal management components and the light blue, air-flow allocations.

In [17], Cuzner introduces a further challenge when implementing a thermal management system in a shipboard environment. He states that in shipboard environments electrical equipment shall not produce heat, thus forcing the designer to implement a thermal management system that withdraws heat through a liquid-cooled cold plate or an air-to-water heat exchanger that provides forced-air convection.

An applicable guiding standard, MIL-E-917E, states that cooling of electrical equipment shall be equipment specific but can be accomplished in one of the following manners, in order of preference: Natural convection, conductor, and radiation, forced air (self-contained), forced air (not self-contained), fresh water air cooler, salt water air cooler, and other methods such as cooling oil or water in indirect contact with active electrical equipment [31]. The standard provides guidance that heat exchangers should be located so that water from leaks and condensation does not fall on electrical circuitry and that heat ex-

changers be easily removable without removal of, or damage to, adjacent parts. Guidance for direct liquid cooling states that electronic cooling water (ECW) systems are preferred in surface ships but that deionization systems, which are self-contained with purification equipment, purity sensors, and alarm systems, are also acceptable.

While not used this work's use case, physics-based scaling laws have been incorporated into the VPP by creating equivalent thermal circuits for active components and solid allocations that prescribe air-flow distances for natural, or forced-air convection by calculating pressure drop between components [32].

2.3.3 Accessibility

Accessibility allocations as introduced in [17] and elaborated on in [33, 34] are difficult to model as they are highly subjective to the manufacturer and application environment. Accessibility allocations are primarily used to account for the physical space required to manufacture, perform maintenance, and functionally operate the equipment. Cuzner provides no guidance on accessibility allocation selection in his initial methodology [17]. In this study, accessibility allocations range from .0127 (.5″) to .0413 meters (1.62″) depending on the application and modularization level.

The only standard-based accessibility guidance is around conductors, naming cabling and bus-bar. MIL-DTL-32483 *Switchgear, Power, Hard-Mounted, Medium Voltage, Naval Shipboard* states that a minimum clearance of 1/4 inch is required between cabling and bus bar to prevent abrasion under conditions of vibration [35]. MIL-E-917E prescribes not less than a 3/4 inch distance between exposed, nonarcing, current-carrying parts, specifically bus-bar and the enclosure [31]. Both accessibility prescriptions are incorporated into this work's metamodels.

2.3.4 Structural

As introduced in [17] frame supports, defined as structural allocations in this work, must meet shock and vibration requirements for the shipboard environment. Cuzner writes, "As a rule of thumb, for shock-hardened systems, the total frame support weight should be less than 25% of the sum of the individual component weights it supports". This 25% rule of thumb informed frame allocations in the initial VPP methodology, and will be employed in the work's use-cases. Ideally, structural supports will scale according to column and beam buckling analysis, physics-based scaling laws, but this has yet to be incorporated and is left to future investigations.

Military standard, MIL-E-917 *Electric Power Equipment Basic Requirements* is the guiding standard for shipboard power electronics and refers to military standards MIL-S-901-D, *Shock Test. H.I. (High-Impact) Shipboard Machinery, Equipment, and Systems* and MIL-STD-167-1, *Mechanical Vibrations of Shipboard Equipment* for shock and vibration requirements [31, 36, 37]. Shock considerations depend upon a number of factors which include applicable shock grade, equipment class, shock test type, and mounting considerations. Aboard naval vessels, a shock grade of A can be assumed for electrical distribution equipment as it is "essential to the safety and continued combat capability of the ship". Equipment class III can be assumed as resident mountings may or may not be used to pass shock testing requirements, and a test type A is assumed at the bay level as the bay module is a medium-weight shock test or heavyweight shock test is used to qualify the specified requirements. A medium-weight shock test prescribes dropping a weighted hammer 6 times at varying heights as informed by the equipment's weight. The equipment passes when no damage is evident. Heavyweight testing prescribes detonating 4 explosive charges below surface level at varying distances from the hull. Because this guidance provides no scaling for shock-hardened frame structures, physical testing of assembled equipment is the only approach to verify frame allocations' suitability for the shipboard environment.

Vibration requirements guided by MIL-STD-167-1 are intended to locate equipment resonances [36]. To meet vibration requirements equipment must pass a two-hour endurance test at the most damaging amplitude and frequency expected in the shipboard environment. Amplitude is defined as the maximum displacement of simple harmonic motion, oscillation defined as displacement from the equipment's point of rest, and both must be within the bounds specified by the standard for each testing frequency selected by the testing engineer. Testing frequencies range from 4hz to 50hz and must be tested for five minutes, for a total of 2-hours of testing, at each selected test frequency. With only pass/fail testing guidance provided by military standards for vibration-hardened equipment, no frame scaling laws can be derived from applicable standards. The 25% of mass engineering-based scaling remains the most applicable scaling law for support structures.

2.3.5 Conductors

Guidance for conductor sizing as current scales in shipboard environments is limited to bus-bar prescriptions from MIL-DTL-32483 *Switchgear, Power, Hard-Mounted, Medium Voltage, Naval Shipboard*. The standard is found to be the most applicable military standard for MV electrical distribution equipment as modular power electronic equipment is the replacement technology for traditional switchgear distribution equipment. The sizing prescribed by [35] is used to scale bus-bar allocations, conductor allocations, as system current scales in this work's use-cases.

Cable sizing, the other option for distribution conductors, is provided no guidance by applicable military standards. Here, engineering experience is used to size cabling connections in this work's use-cases

2.3.6 Active Component Models

Active component allocations, a new allocation type proposed by this methodology, allows the previously introduced allocation types to be applied at every level of the VPP

ontology. Previous work [17, 30, 18] implies its use but this work makes it an explicit allocation type. At each level of the ontology, the previous level is considered an active component. This concept is leveraged in chapter 4 as no-load switch drawers, comprised of two modularized no-load switches, are considered active components of the compartment. The modularized no-load switches of chapter 3 were modularized from the no-load switch's pressurized contactor cylinder, actuator cylinder, and power electronic controller active components. Active components will make up every level of the VPP ontology. No-load switches are active components of the drawers, drawers the active components of the compartment, and compartments the active components of the bay.

CHAPTER 3
NO-LOAD SWITCH USE CASE

This chapter introduces the allocation and compilation methodology proposed in this work. Through the use of generic allocations the methodology modularizes power electronic technologies as it produces scalable meta-huertistic models that reflect design decisions. A use case, that will become the building block of the functional PDM modeled in chapter 4, is employed to demonstrate the multi-step process. Fig. 3.1 represents the allocation and compilation process as a series of steps resulting in the calculation of volume and weight as a function of design exploration variables. sections 3.1 to 3.5 outline the process in detail.

The no-load switch, as represented in fig. 3.2, is chosen as a use case for two reasons. The first is that all six generic allocations are present in the allocation of the chosen no-load switch which lends itself to a comprehensive demonstration of the generic allocation and compilation process. The second is that the no-load switch becomes the modular building block of the modularized functional PDM module in chapter 4. This allows demonstration of the generic allocation and compilation methodology at every level of a modularized distribution network. The no-load switch is a current limiting disconnect switch designed to replace traditional circuit breakers when incorporated into a power electronic distribution network. The no-load switch provides galvanic isolation as copper contactors open once current has been driven to zero by power electronic converters adjacent in the distribution network. This work's representation of the switch is modeled after a no-load switch rated to 6kV for DC connections as introduced in [20]. This, in relation to the VPP, is considered state-of-the-art technology which can be brought into the evolutionary design environment along with system exploration variables (x_v), requirements and constraints (r_v), and optimizing objectives (o_v) to produce active component

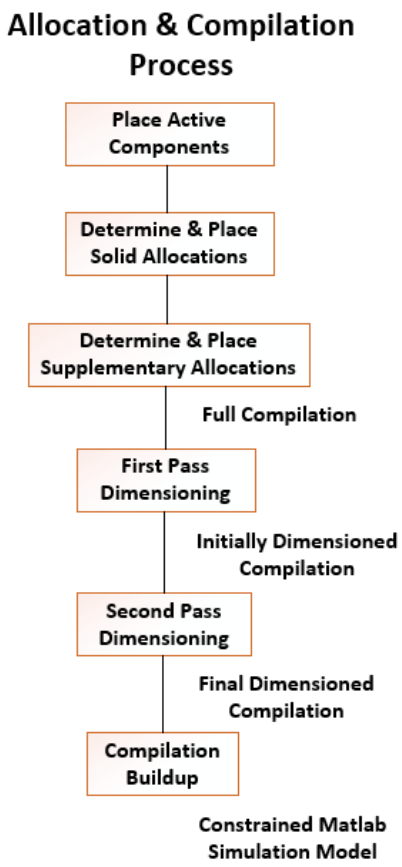

Figure 3.1: Allocation and Compilation Process

models that can be modularized.

3.1 Place Active Components

The allocation process begins by placing active components representing all enabling technologies. The key enabling technologies of the no-load switch are a pressurized contact cylinder that provides galvanic isolation once opened and an actuator cylinder that will force the contactor's opening and closing. These are represented by grey allocations and placed as active components in fig. 3.3.

The reader will notice two things in figs. 3.2 and 3.3. The first, as seen in fig. 3.2, is that the actuator cylinder is comprised of multiple sub-components, yellow cylinders, and a grey end cap with protruding features. Because the final compilation model is only con-

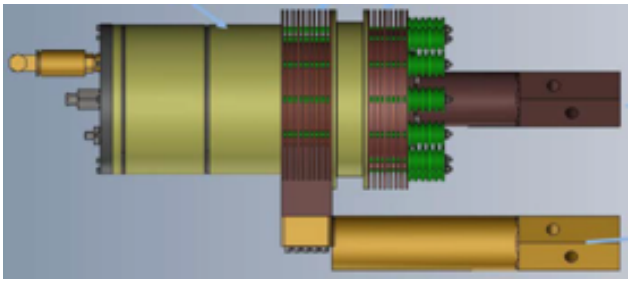

Figure 3.2: 3-D Rendering of Use-Case No-Load Switch

Figure 3.3: Active Component Allocations of No-Load Switch

cerned with overall equipment volume, the sub-components that make up the actuator cylinder are not represented as sub-components but instead as one active component allocation. As long as the total width, height, and length of the assembled sub-components are accounted for in the aggregate active component model precise differences between sub-components can be ignored. The second, is that an additional power controller represented by a grey active component allocation is placed to the left of the no-load switch. The allocation is added because in practical application the no-load switch will require a power controller to functionally operate the actuator cylinder. This addition of active components to a state-of-the-art technology highlights the inherent benefits of modeling equipment with allocations. Any amount of auxiliary technology can be added to the active component models as applications demand it. Chapter 4 will expand on this benefit and demonstrate that any number of design parameters can be captured, making this

method flexible to any technology.

3.2 Determine and Place Solid Allocations

To begin modularizing the technology, solid allocations, as presented in fig. 3.4, are added to the placed active components. As seen in fig. 3.2 outgoing conductors, cooling fins, and bushings surround the pressurized contact cylinder and actuator cylinder. As physical structures, they are represented by solid allocations. The incoming and outgoing conductor connections are represented by conductor allocations, the cooling fins used to minimize contact losses are represented by thermal management allocations, and the insulation bushings are represented by insulation allocations. The three solid allocations, in addition to allocations for frame supports, are added to the active component allocations are presented in fig.**??**

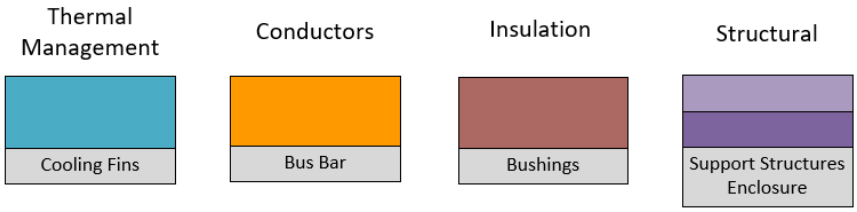

Figure 3.4: Solid Allocations

Fig. **??** captures the end of the determine and place solid allocations step of the compilation and allocation process with all solid allocations having been added to the active component allocations. Notice that solid frame and enclosure allocations have been added around the placed active components and solid allocations.

3.3 Determine and Place Supplementary Allocations

With active components and solid allocations determined and placed, the process moves to the third step shown in Fig. 3.1, determining and placing supplementary allocations. This step allocates space for thermal management, insulation, and room for manufac-

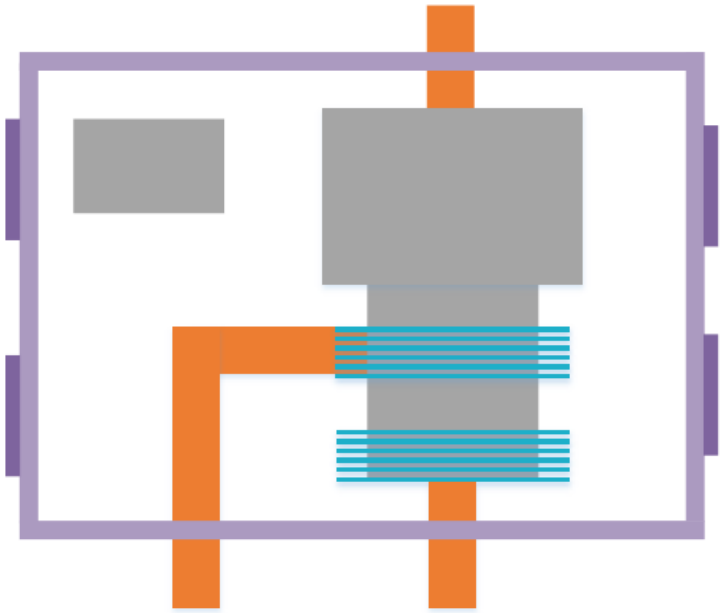

Figure 3.5: No-Load Switch Solid Allocation Placement

turability that is required when individual components are modularized into a modular assembly. Insulation and thermal management supplementary allocations are dictated by system exploration variables (x_v), design choices, such as typology, thermal management system, and grounding scheme with variable selection bounded only by applicable design choices. Once dictated by design decisions, insulation and thermal management supplementary allocations are added to each active component and solid allocation. Supplementary accessibility allocations are not dictated by design decisions but instead are uniformly added to every active component and solid allocation. This ensures space is available to physically place the physical components at the LRU level and ensure serviceability once modularized into drawers, compartments, and bays.

Fig. 3.6 represents determining each active component's and solid allocation's supplementary allocations as a formalized flowchart where each decision node is a system exploration variable (x_v), or design decision. When made, design decisions result in insulation, thermal management, and accessibility allocations being added to each active component and solid allocation. Examples of design decisions impacting insulation coordination are

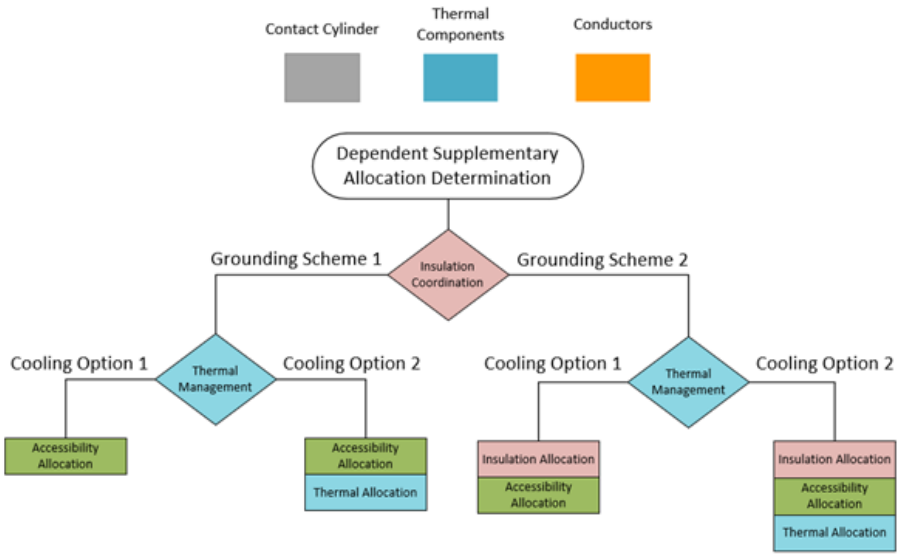

Figure 3.6: Generic Supplementary Allocation Determination

distribution level voltage, as creepage and clearance requirements are a function of energized voltage, and grounding scheme, as components are either hull-grounded or left ungrounded at system potential, termed floating in shipboard applications. Examples that impact thermal management allocations include determination of a thermal management solution, which as prioritized by the Navy can be selected as natural convection, forced-air convection, and liquid cooling through the use of cold plates.

Fig. 3.7 demonstrates a more complicated supplementary allocation determination where three system-level design choices, (x_v), are considered. Here, three thermal management solutions are considered with each dictating its own dependent supplementary allocations. The adaptability of the proposed allocation and compilation methodology is demonstrated here in fig. 3.7 as any number of design solutions can be considered, with each prescribing its own supplementary allocation determination.

To determine the dependent supplementary allocations required for each active component and solid allocation in the modeled no-load switch, a supplemental allocation flowchart is developed. For the no-load switch, the system exploration variables (x_v) considered are floating or hull-grounding active components, and cooling the pressurized

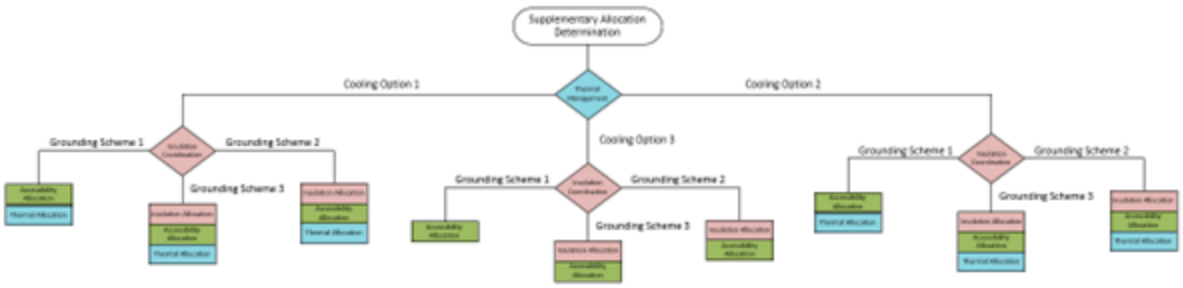

Figure 3.7: Supplementary Allocation Determination for Three Thermal Solutions

contactor cylinder by natural convection or liquid cooling. In the modeled application, and practically, internal components are not hull-grounded but left floating. As noted, floating denotes that the hardware is not directly grounded to the hull of the ship, therefore leaving a voltage potential between the charged equipment and hull that must be accounted for by insulation coordination. The choice to provide thermal management through natural convection or liquid cooling has already been made for the designer as the modeled no-load switch is designed to cool the pressurized contactor cylinder through an angular finned heat-sink. Conductor and active component allocations will not receive supplementary air-flow thermal allocations because the thermal management allocations representing the angular finned heat-sink is assumed to provide a thermal management solution for the assembled no-load switch with no additional space required for air-flow.

Fig. fig. 3.8 presents the supplementary allocation determination flowchart for the no-load switch's active components, conductor allocations, and thermal management allocations. From fig. 3.8 active components and solid allocations are prescribed insulation and accessibility allocations.

With supplementary insulation and accessibility allocations placed around active components, conductor allocations, and thermal allocations, a full compilation is the output of step three in the allocation and compilation process. The fully allocated no-load switch is shown in fig. 3.9.

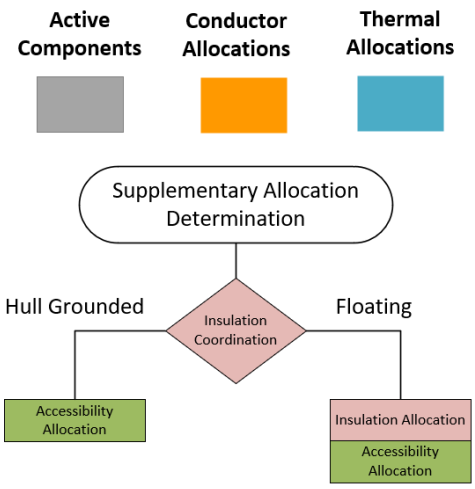

Figure 3.8: Supplementary Allocation Determination Flowchart for Active Components & Conductor Allocations

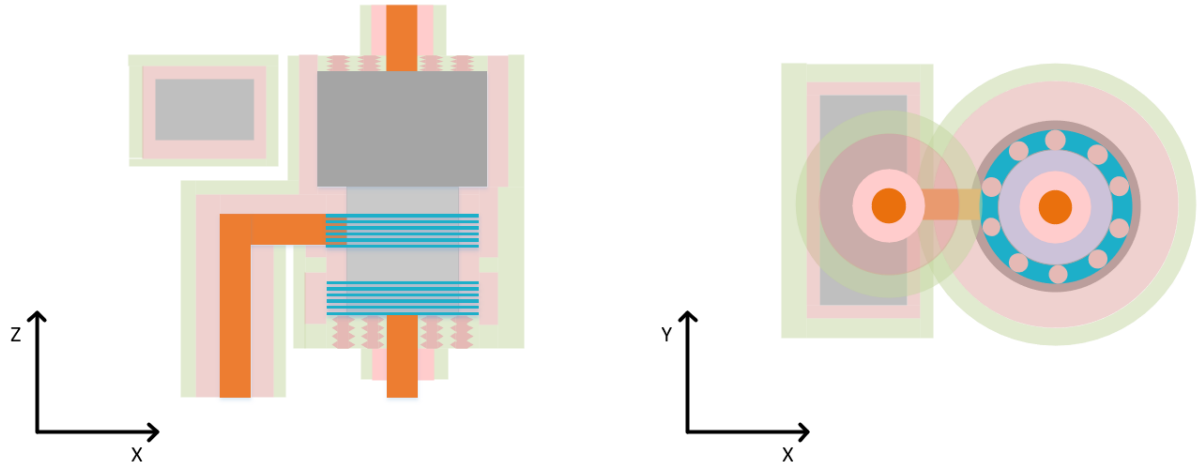

Figure 3.9: Fully Allocated No-Load Switch

3.4 Dimensioning Process

To begin building up the component's width, height, and length, dimensioning of the active components, solid allocations, and supplementary allocations must be addressed. Before proposing a dimensioning method it is important to reiterate the purpose of this process; namely, to account for physical space requirements between adjacent parts that will scale with system exploration variable (x_v). With this in mind, multiple dimensioning

and build-up approaches producing identical and equally informative build-ups can be imagined. This methodology proposes the following for the dimensioning and build-up process as a baseline methodology to ensure that appropriate insulation, thermal, and accessibility considerations are included in the final build-up. As designers become well-versed in the purpose and process of dimensioning, it is expected that the initial first-pass dimensioning process can be simplified and eventually subsumed into the simplifying dimensions process. Nevertheless, the method proposed should be used when initially implementing the process.

3.4.1 Nomenclature

To begin, a nomenclature regarding how each dimension is denoted must be established. Figure 3.10 introduces the 5-6 alpha-numeric nomenclature proposed to denote each dimension. The first identifier signifies which allocation type is being captured. Fig. 3.11 shows the one-letter identifiers associated with each allocation type.

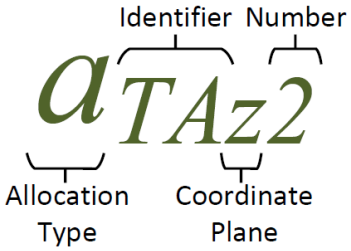

Figure 3.10: Dimension Nomenclature

Allocation Naming Convention	
Active Componet	i
Conductor	c
Thermal Management	t
Accessibility	a
Insulation	d
Frame	f

Figure 3.11: Allocation Type Nomenclature Convention

The second identifier is the equipment identifier signaling which piece of equipment is being represented. For the no-load switch test case, the equipment identifier SW is chosen which indicates that all dimensions with the equipment identifier SW belong to the no-load switch allocation and compilation process. Any 2 letter identifier can be chosen, but it is best practice to chose intuitive identifiers. For example, when in chapter 4 two no-load switches are modularized into a modular drawer assembly, the two-letter equipment identifier DS, drawer switch, is chosen. When the modularized drawers are later modularized into a bay assembly, BS, for bay switch, is chosen.

The third identifier captures the plane the dimension is being made in. The three choices are naturally x, y, and z as this process is done in the cartesian coordinate system. Further research, especially when the equipment is largely cylindrical such as in motors and pumps, may find it beneficial to perform dimensioning in the cylindrical coordinate frame.

The fourth and final identifier is a numeric identifier that allows each dimension of like allocation to be uniquely identified. If this identifier was not added all accessibility dimensions in the x direction would be denoted as a_{SWx} without the ability to reference a single dimension.

3.4.2 First-Pass Dimensioning

The first-pass dimensioning process begins in the top left-hand corner of every allocated 2-D drawing and moves subsequently along a selected coordinate plane. The dimensions follow the nomenclature identified in fig. 3.10 and correspond to the allocation types previously introduced. Dimensions are indexed in ascending order, initialized at one, and indexed by one as allocations are given dimensions. Fig. 3.12 demonstrates this with accessibility and dielectric allocations initialized as a_{SWx1} and d_{SWx1} to the left of the internal power controller, and i_{SWx1}. a_{SWx2} and d_{SWx2} to the right of the power controller. Accessibility and dielectric allocations dimensioned from the left and right of the actuator

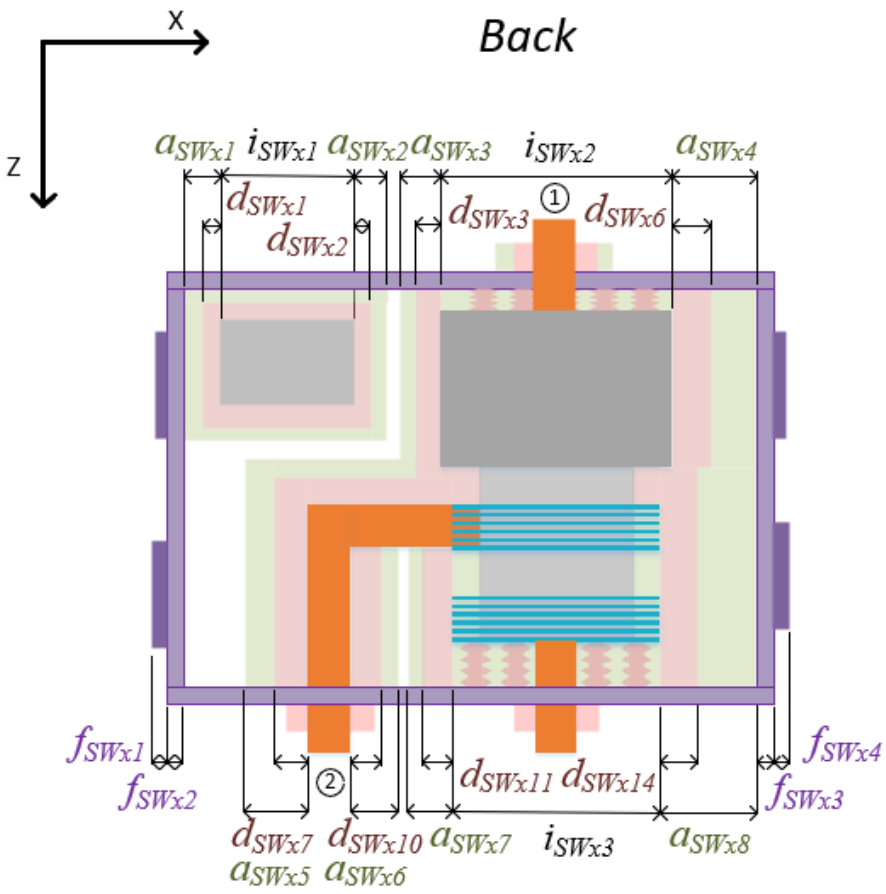

Figure 3.12: First-Pass x Dimensions

cylinder are placed and indexed to a_{SWx3} and d_{SWx3}, and a_{SWx4} and d_{SWx6} respectively. Insulation allocations d_{SWx4} and d_{SWx5} are indexed in fig. 3.15, a section view of fig. 3.12, to provide more dimensioning detail. Indexing continues until all dimensions on a given side of a coordinate plane have been dimensioned.

When first-pass dimensioning is completed along one side of the selected coordinate plane, the process is repeated along the opposite side. Dimensions a_{SWx5}, d_{SWx7}, a_{SWx6}, and d_{SWx10} are initialized around c_{SWx2}, one of three outgoing conductors. Dielectric allocations d_{SWx8} and d_{SWx9} are dimensioned in fig. 3.16 around c_{SWx2}, the outgoing conductor allocation. This repeats with d_{SWx12} and d_{SWx13} added around c_{SWx3}. Frame allocations f_{SWx1},f_{SWx2},f_{SWx3}, and f_{SWx4} are dimensioned along the lower x-coordinate plane but could be dimensioned along the upper plane to the same effect. As components

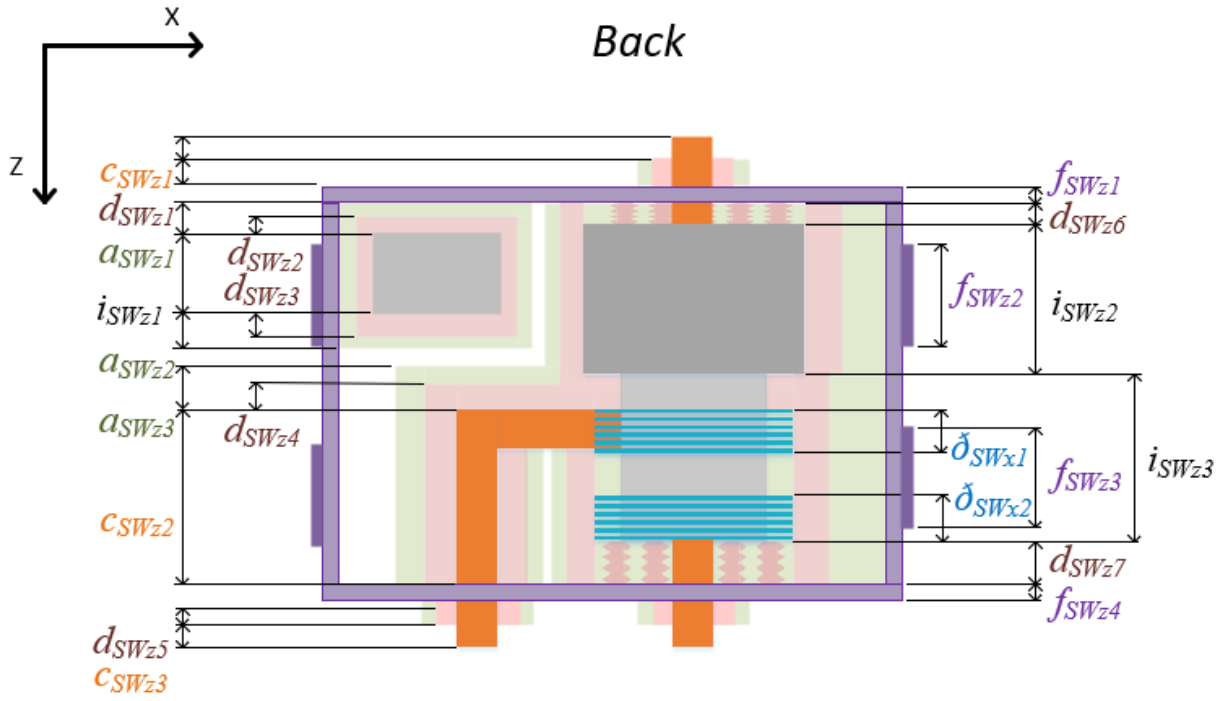

Figure 3.13: First-Pass z Dimensions

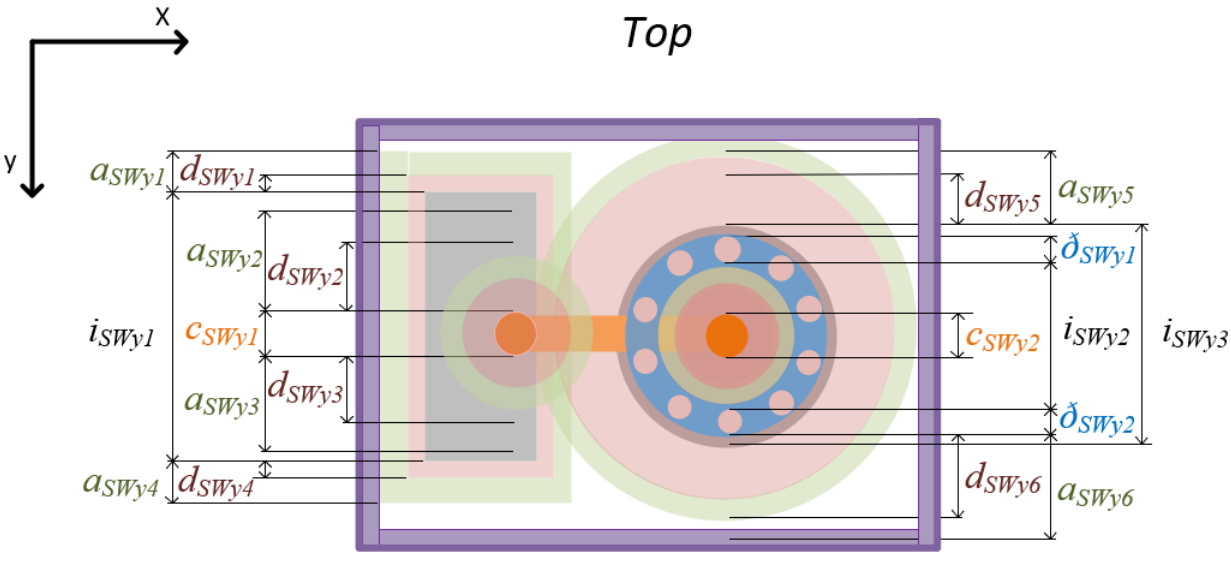

Figure 3.14: First-Pass y Dimensions

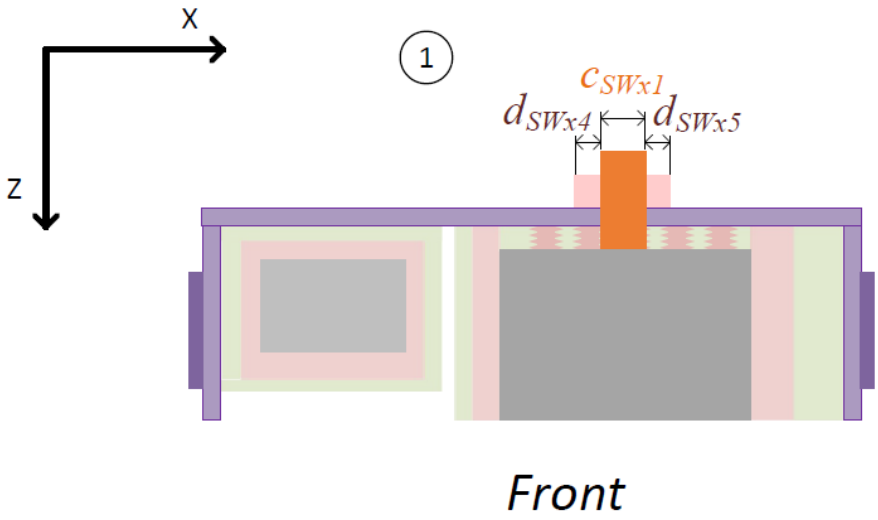

Figure 3.15: First-Pass Section View 1

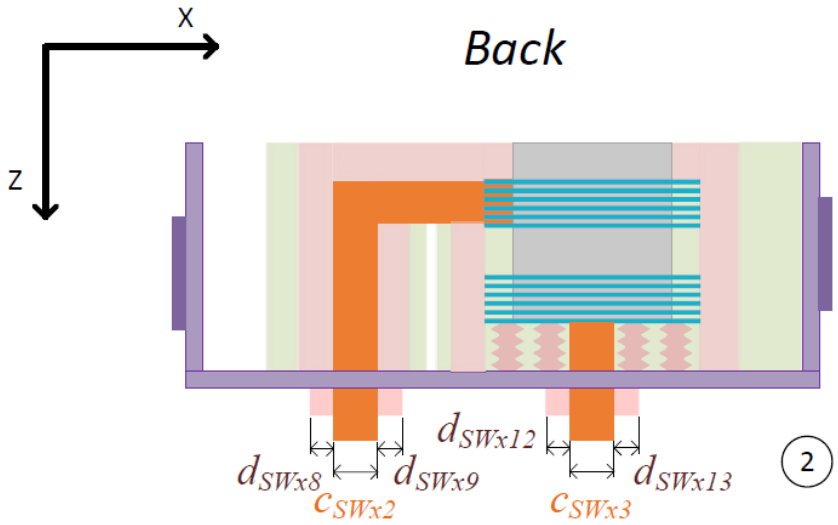

Figure 3.16: First-Pass Section View 2

increase in complexity the dimensioning process can become congested and multiple-dimensioned figures may be required to denote allocations.

An identical process is repeated in the y and z coordinate planes of figs. 3.13 and 3.14. Conductor, dielectric, and accessibility allocations are initialed as c_{SWxz1}, c_{SWxy1}, d_{SWz1}, d_{SWy1}, and a_{SWxz1}, a_{SWxy1} and indexed by one as subsequent allocations are dimensioned. First-pass dimensioning in the y and z coordinate plane completes the first-pass dimensioning process and the process of second-pass dimensioning can be initiated.

3.4.3 Second-Pass Dimensioning

In this section, a reductive second-pass dimensioning process is performed to combine repetitively dimensioned allocations. Fig. 3.17, presents a completed second-pass dimensioning of the x-direction. Along the rear of the no-load switch, d_{SWx2} and d_{SWx3} have been combined into a single reinforced insulation allocation denoted as d_{SWx2} which represents the reinforced insulation required between the controller and the contactor housing. Reinforced insulation is required as the controller is energized by a low voltage power supply with a supply voltage assumed to be between 5VDC – 120VAC, giving it a decisive voltage class (DVC) of A. A DVC of D is prescribed by IEC 61800-5, for the contactor cylinder as it will be energized to the distribution bus voltage which ranges from 5kV to 30kV in this use-case. When energized components of different DVCs are adjacent to one another reinforced insulation is required as prescribed by IEC 61800-5 [24, 23].

In fig. 3.15 the dimensions d_{SWx4} and d_{SWx5} from fig. 3.20, are simplified to d_{SWx3}. Note that because d_{SWx2} and d_{SWx3} have been simplified to d_{SWx2} the next insulation allocation becomes indexed to d_{SWx3}. This re-indexing is done throughout the second-pass dimensioning process and is demonstrated by d_{SWx4} in fig. 3.16 being re-indexed to d_{SWx6} in fig. 3.20. In the x direction, d_{SWx10} and d_{SWx11} are simplified to d_{SWx7} as the two insulation allocations become redundant. Each insulation allocation physically represents the space allocated for the required clearance distance between components

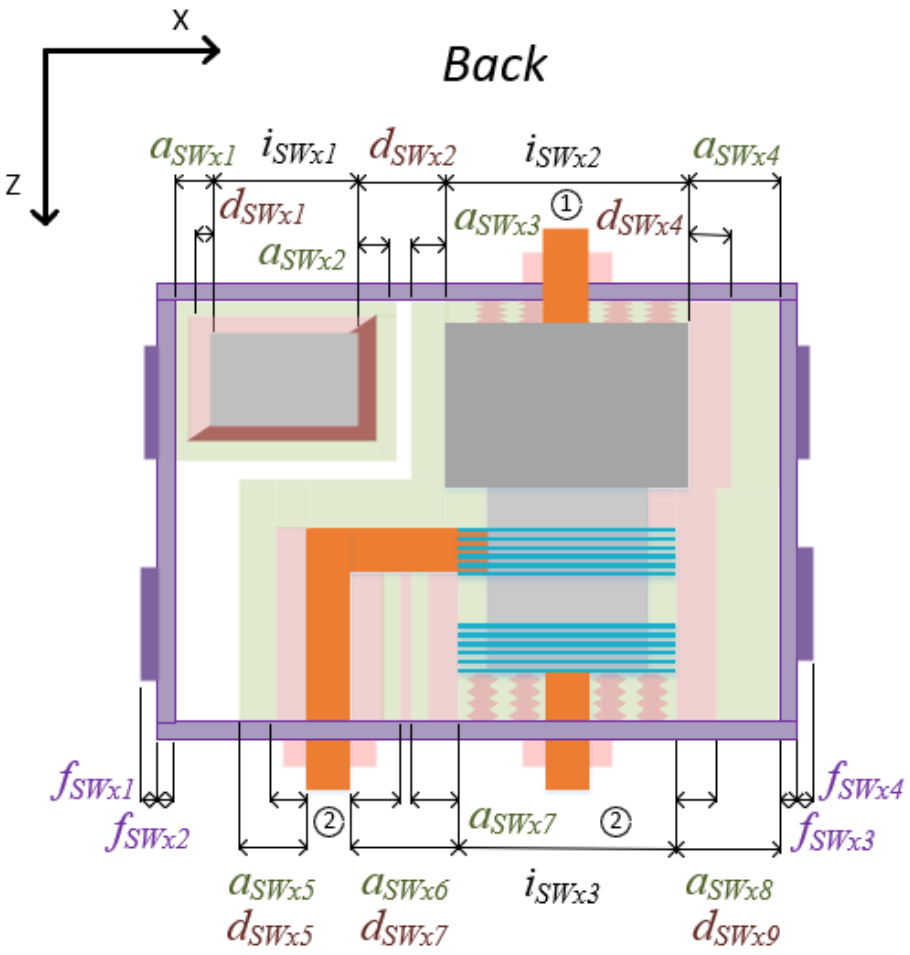

Figure 3.17: Simplified x Dimensions

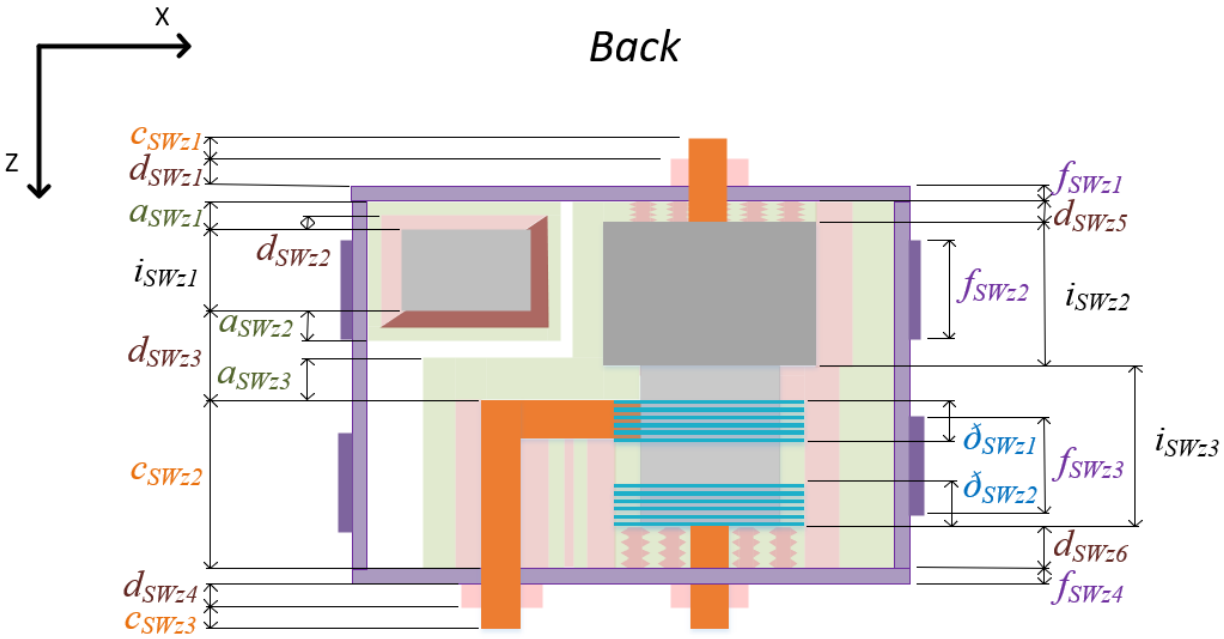

Figure 3.18: Simplified z Dimensions

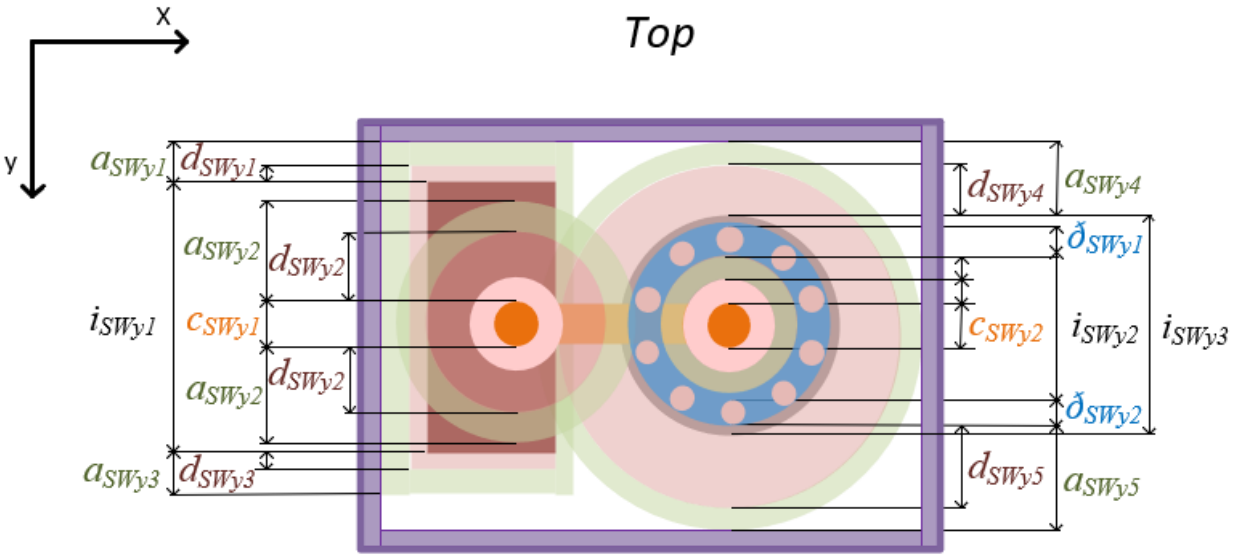

Figure 3.19: Simplified y Dimensions

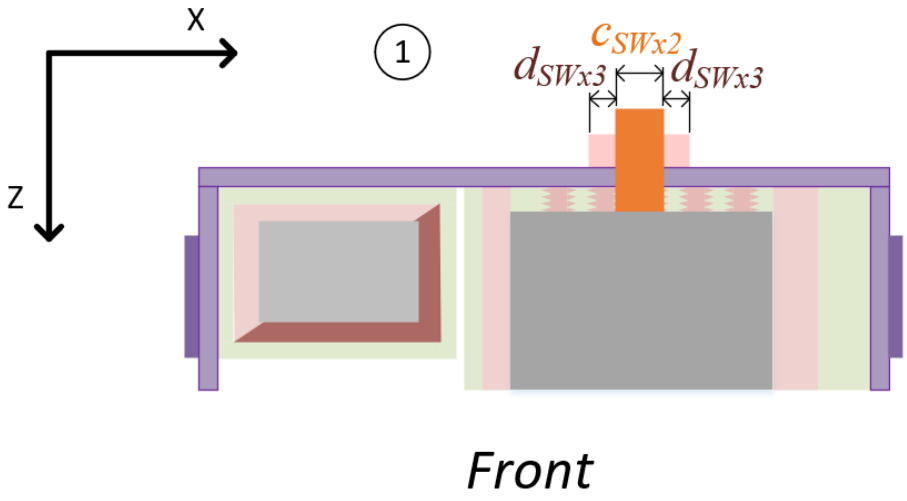

Figure 3.20: Simplified Section View 1

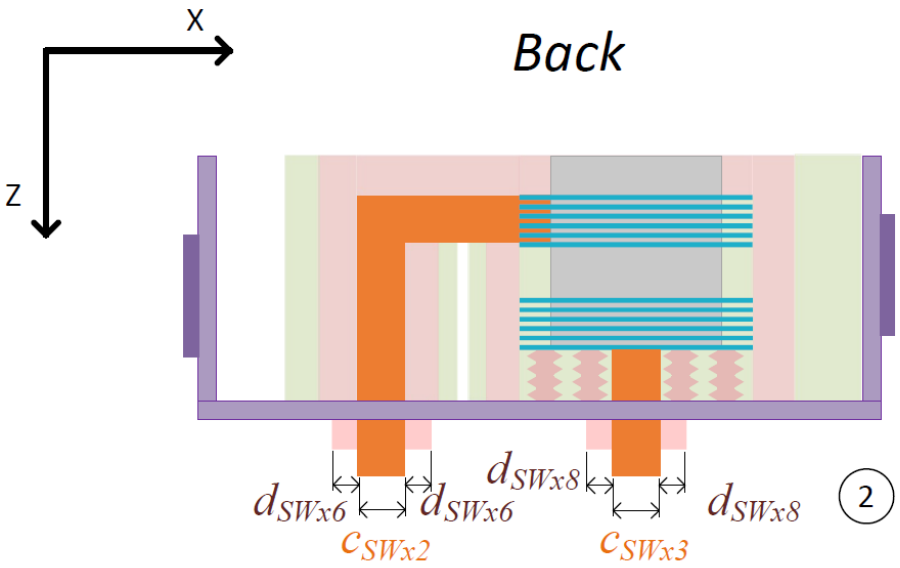

Figure 3.21: Simplified Section View 2

of similar DVC. Both components are of DVC D as the conductor, c_{SW2}, and fins, are assumed energized to the same system voltage. If both insulation allocations were kept, air-gap standoffs would be double counted, ultimately allocating twice the space required for insulation coordination and increasing the no-load switch's width unnecessarily.

In the y-coordinate plane, no simplifications are made. Note though, that d_{SWy2} and d_{SWy3} can, and will, be set equal to each other in the subsequent compilation process of section 3.5. Required insulation air-gap standoffs are symmetrical above and below the conductor, c_{SWy1}, as the insulation requirement is radial from the conductor. The same is true of d_{SWx5} and d_{SWx6}. These are not simplified to the same dimension in 3.19 because this work seeks to capture the generic situation that may include different insulation coordination solutions above and below the conductor. The second-pass dimensioning process is repeated in the z-coordinate plane with no simplifications to produce a final dimensioned compilation.

3.5 Compilation Process

With the second-pass dimensioning complete and a fully dimensioned compilation as its output, the compilation build-up process is undertaken to produce a fully constrained Matlab simulation. The goal of this step is to capture, in each dimension, every combination of adjacent dimensions that will drive the overall width, height, and length of the modeled equipment. Each combination of adjacent dimensions is referred to as a buildup. In the x-direction, two possible buildups exist and are captured by eqs. (3.1) to (3.3).

$$\begin{aligned} w_{NLSw1} = {} & f_{SWx1} + f_{SWx2} + max(d_{SWx1}, a_{SWx1}) + i_{SWx1} + max(d_{SWx2}, a_{SWx2}, a_{SWx3}) \\ & + i_{SWx1} + max(d_{SWx4}, a_{SWx4}) + f_{SWx3} + f_{SWx4} \end{aligned} \tag{3.1}$$

$$w_{NLSw2} = f_{SWx1} + f_{SWx2} + max(d_{SWx5}, a_{SWx5}) + c_{SWx2} + max(d_{SWx7}, a_{SWx6}, a_{SWx7}) + i_{SWx3} + max(d_{SWx9}, a_{SWx8}) + f_{SWx3} + f_{SWx4} \tag{3.2}$$

$$w_{NLSw} = max(w_{NLSw1}, w_{NLSw2}) \tag{3.3}$$

Equation 3.1 captures the adjacent dimensions in the rear of the no-load switch while Eq. 3.2 captures the adjacent dimensions in the front of the switch. Notice that around i_{SWx1}, the power controller, insulation and accessibility allocations are taken as a maximum. Because air-gap standoffs required for clearance between energized parts and space for manufacturability can occupy the same physical space without interfering with each other, the maximum between the two is taken. A maximum is taken where ever insulation, specifically air-gap standoffs, and accessibility allocations overlap. If physical insulation is used instead of air-gap creepage and clearance standoffs then the maximum between the two allocations is not appropriate. Instead, a simple addition of the allocations is required.

In the y-coordinate plane, four buildups are accounted for. Equations (3.4) to (3.7) capture the driving dimensions of the controller, insulation, and accessibility around the PC, i_{SWy1}, outgoing conductor, c_{SWy1}, contactor, i_{SWy2}, and cylinder, i_{SWy3}. Again, the maximum of the four build-ups is taken to drive the no-load switch's height as captured by eq. 3.8.

$$h_{NLSw1} = f_{SWy1} + f_{SWy2} + a_{SWy1} + i_{SWy1} + max(d_{SWy1}, a_{SWy2}) + f_{SWy2} + f_{SWy1} \tag{3.4}$$

$$h_{NLSw2} = f_{SWy1} + f_{SWy2} + max(d_{SWy2}, a_{SWy3}) + c_{SWu1} + max(d_{SWy3}, a_{SWy4}) + f_{SWy2} + f_{SWy1} \tag{3.5}$$

$$h_{NLSw3} = f_{SWy1} + f_{SWy2}) + max(d_{SWy4}, a_{SWy5}) + i_{SWy2} + max(d_{SWy5}, a_{SWy6}) + f_{SWy2} + f_{SWy1} \tag{3.6}$$

$$h_{NLSw4} = f_{SWy1} + f_{SWy2} + a_{SWy7} + i_{SWy2} + a_{SWy8} + f_{SWy2} + f_{SWy1} \tag{3.7}$$

$$h_{NLSw} = max(h_{NLSw1}, h_{NLSw2}, h_{NLSw3}, h_{NLSw4}) \tag{3.8}$$

In the z-coordinate plane, two buildups are accounted for. Equations (3.9) and (3.10) capture the driving dimensions of the controller, insulation, and accessibility around the PC, i_{SWz1}, outgoing conductor, c_{SWz2}, contactor, i_{SWz2}, and cylinder, i_{SWz3}. Again, the maximum of the two build-ups is taken to drive the no-load switch's length as captured by eq. 3.11.

$$l_{NLSw1} = c_{SWz3} + d_{SWy4} + f_{SWz1} + f_{SWz2} + c_{SWz2} + max(d_{SWz3}, a_{SWz2}, a_{SWz3}) + i_{SWz1} + max(d_{SWz2}, a_{SWz1}) + f_{SWy2} + f_{SWy1} + d_{SWz1} + c_{SWz1} \tag{3.9}$$

$$l_{NLSw2} = c_{SWz1} + d_{SWz1} + f_{SWz1} + max(d_{SWz5}, a_{SWz4}) + i_{SWz2} + i_{SWz3} + max(d_{SWz6}, a_{SWz5}) + f_{SWz4} + d_{SWz4} + c_{SWz3} \tag{3.10}$$

$$l_{NLSw} = max(l_{NLSw1}, l_{NLSw2}) \tag{3.11}$$

The no-load switch's volume is found by eq. 3.13 and informs the power density calculation in the section 3.6.

$$v_{NLSw} = w_{NLSw} * h_{NLSw} * l_{NLSw} \tag{3.12}$$

With the width, height, and length equations synthesized from the fully dimensioned no-load switch, the allocation and compilation process is complete. The following section walks the reader through the Matlab metamodel code that calculates MOPs, specifically power density and specific power, for the no-load switch.

$$v_{NLSw} = w_{NLSw} * h_{NLSw} * l_{NLSw} \tag{3.13}$$

3.6 MATLAB Metamodel Code

Fig. 3.22 is a sequence diagram depicting how the no-load switch metamodel code is constructed and passes data between its two sub-functions. The main code scales and compiles the test article while is housed in NLSw.m while scaling with rated voltage creepage

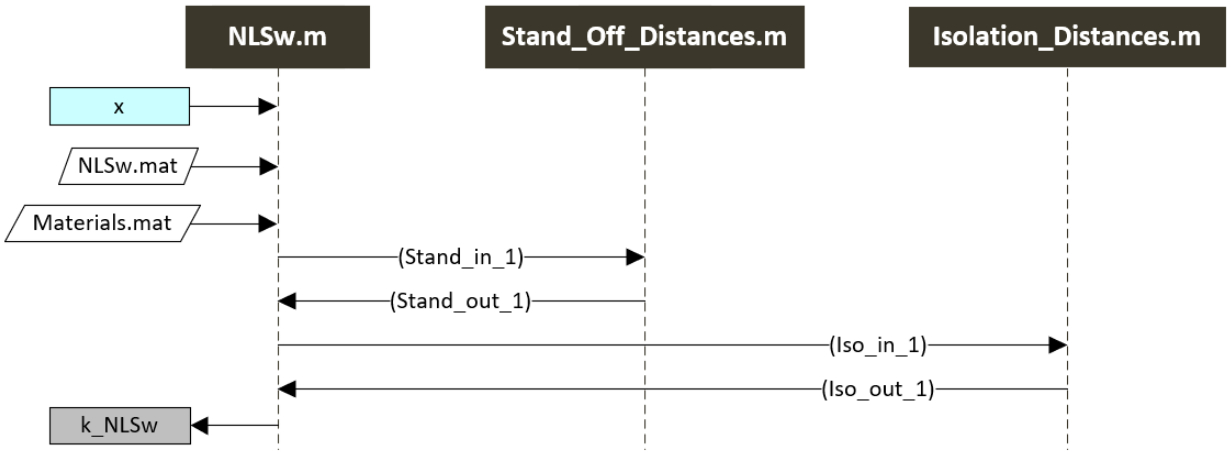

Figure 3.22: Sequence Diagram of No-Load Switch Matlab Code

and clearance distances are calculated in the sub-functions Stand_Off_Distances.m and Isolation_Distances.m. To begin the scaling, NLSw.m brings in the variable *x* housing the required design spaces variables. For the single no-load switch compilation shown here, rated voltage and rated current are design space variables specified by the designer. In chapter 4 when the complete PDM bay is compiled more design space variables are considered. Next, NLSw.m loads the initialized allocations of the test article no-load switch designed to 6kV and 2kA from the input NLSw.mat file. The test article's initialized allocations housed in NLSw.mat are taken from the no-load switch modeled in fig. 3.2 as found in [38]. Materials.mat is brought in to initialize the densities used for later weight calculations, modulus of elasticities for column buckling analysis, and insulation constants. From there, NLSw.m begins the scaling process. The model finds a scaling ratio between the test article no-load switch and the rated current passed in as a design space variable (x). The scaling ratio, defined as *Iratio*, is derived from the test article's initialized internal resistance to find a scaled resistance that is used to calculate the power loss of the scaled NLSw. The scaling ratio and the individual no-load switch's power losses are found by eqs. (3.14) and (3.15).

$$Iratio = I_{scaled}/I_{testarticle} \tag{3.14}$$

$$PowerLoss = RatedCurrent^2 * ScaledResistance \tag{3.15}$$

Once scaled power losses are found, NLSw.m uses the scaling ratio to scale the conductor diameters, width of the cylinder housing the contactors, and the number of heat-sink fins, all of which are assumed to scale with current and subsequently power. Creepage and clearance distances informing insulation allocations are then calculated in the sub-functions Stand_Off_distances.m and Isolation_Distances.m by sending the array of input variables Stand_in_1 and Iso_in_1 to each sub-function. Fig. 3.22 presents each of these arrays as a single variable but in practice, Stand_in_1 and Iso_in_1 are arrays containing the variables found in table 3.1.

Variable	Description
OVCat	Over Voltage Category
UAC	UDC/sqrt(2)*.98/2
UDC	Rated Voltage/2
ku	Voltage Tolerance
kr	Voltage Ripple
kp	Line-to-Gound Pulsing Factor
fr	AC Frequency
U_Nom	Line-to-Line Functional Insulation
U_INSUL_L	Line-to-Ground Functional Insulation
DC	DC System Marker

Table 3.1: Stand_in Array Variables

The variable arrays *Stand_out* and *Iso_out* are returned to NLSw.m with both arrays housing a prescribed air-gap clearance and creepage distance, denoted as *dClr* and *dCrp*, informed by the inputs of *Stand_in* and *Iso_in*. Each insulation allocation captured in figs. 3.17 to 3.21 is assigned its appropriate *dClr* or *dCrp* value. The compilation of the no-load switch's width, height, length, and mass can now begin as all allocations have been initialized through either NLSw.mat, or Stand_Off_distances.m and Isolation_Distances.m.

Width, length, and height equations for the no-load switch are compiled from the sec-

Variable	Description
OVCat	Over Voltage Category
U1	Rated Voltage 1
U2	Rated Voltage 2
ku1	Voltage Tolerance 1
ku2	Voltage Tolerance 2
kr1	Voltage Ripple 1
kr2	Voltage Ripple 2
kp1	Line-to-Gound Pulsing Factor 1
kp2	Line-to-Gound Pulsing Factor 2
fr	AC Frequency
U_Nom_1	Line-to-Line Functional Insulation 1
U_Nom_2	Line-to-Line Functional Insulation 2
DC1	DC System Marker 1
DC2	DC System Marker 2

Table 3.2: Iso_in Array Variables

ond pass dimensions drawings shown in figs. 3.17 to 3.21. Each directional compilation can, and in this use-case will, have multiple driving compilations which were presented in section 3.5 and captured by eqs. (3.1), (3.2), (3.4) to (3.7), (3.9) and (3.10) and **??**.

With the NLSw's scaled width, length, and height found, only the no-load switch's mass remains to be calculated. The mass of each component or allocation type is found by calculating each allocation type's volume and multiplying its volume by the density corresponding to the allocation. The controller, frame supports, and frame enclosure volume are directly scaled from the test article's initialized volume with the scaling factor employed earlier. The volumes of the cylinder housing the contactors, the conductors, and the heat-sink surrounding the contactor cylinder are not directly scaled by the scaling factor but instead through the individual scaling of their allocations as produced by the scaling process. To find mass, the scaled volumes are multiplied by the densities brought in by Materials.mat. The assumed densities are presented in table 3.3.

With component and allocation masses determined, the masses are summed together to compute the total mass of the no-load switch in kilograms. This ends the compilation

Mass Contributor and Material and Density (kg/m^3)		
Controller	Assembly	75
Frame Supports	Aluminum 1100	2720
Frame enclosure	Aluminum 1100	2720
Contactor Cylinder	Aluminum 1100	2720
Conductors	Copper	8940
Heat Sink	Aluminum 1100	2720

Table 3.3: Materials and Densities Informing Mass Calculations

of the individual no-load switch's width, length, height, and mass. Each is stored in the array *k_NLSW* and returned from NLSw.m as outputs.

To summarize, NLSw.m takes in rated voltage and current, initializes the model the output will be scaled from and the materials used, calls two sub-functions to determine scaling insulation requirements, determines the width, length, height, and mass of the scaled no-load switch based upon a scaling factor determined by the inputted rated voltage and current, and ultimately calculates the width, length, height, and mass of the scaled no-load switch. While the model described calculates only one voltage-dependent output of the scaled no-load switch for use in S3D's LEAPS database, an additional wrapper function executing this code over a specified voltage range will produce figures demonstrating how these calculated parameters change with voltage. The next section will present such figures and comment on their findings.

3.7 No-Load Switch Metamodel Results

The outputs of the no-load switch metamodel are presented in figs. 3.23 and 3.24. Fig. 3.23 shows the no-load switch's overall modular width, height, and length as distribution bus voltage increases from 5kV to 30kV. Notice that height and length increase seemingly linearly as voltage increases. This is due to insulation creepage and clearance distances, namely d_{SWy1}, d_{SWy3}, d_{SWy4}, and d_{SWy5} for height, and d_{SWz1} and d_{SWz4} for length, increasing linearly as voltage increases as seen in fig. 2.7. Note that the overall width does

not begin to scale linearly with voltage until 16kV. The overall width's transition to linear scaling at 16kV is caused by thermal and accessibility allocations initialized from the state-of-the-art hardware our model represents being larger in magnitude than prescribed creepage and clearance distances when distribution bus voltage is less than 16kV. Once a system voltage of 16kV is reached the IEC 61800-5 dictated creepage and clearance air-gap standoff distances overtake initialized thermal and accessibility allocations and continue driving total width until 30kV.

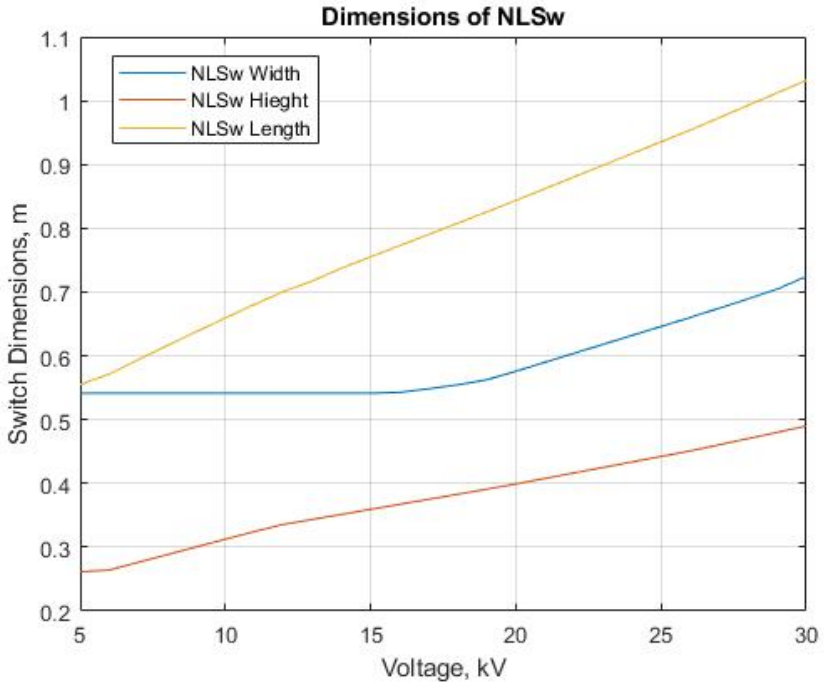

Figure 3.23: Width, Height, and Length Results

The overall mass, in kilograms, of the no-load switch as it scales from 5kV to 30kV is presented in fig. 3.24, and reflects the trends found in fig. 3.23. Mass increases approximately linearly from 5kV to 16kV and then increases in slope until the study's limit of 30kV. The increase in mass as voltage increases is due to the overall width experiencing the same linear increase at 16kV. Air-gap creepage and clearance distances do not contribute to the overall mass of the no-load switch, as air-gap allocations do not constitute mass, but do cause the width of the frame structures to increase, which consequently

increases overall weight as shown in fig. 3.24.

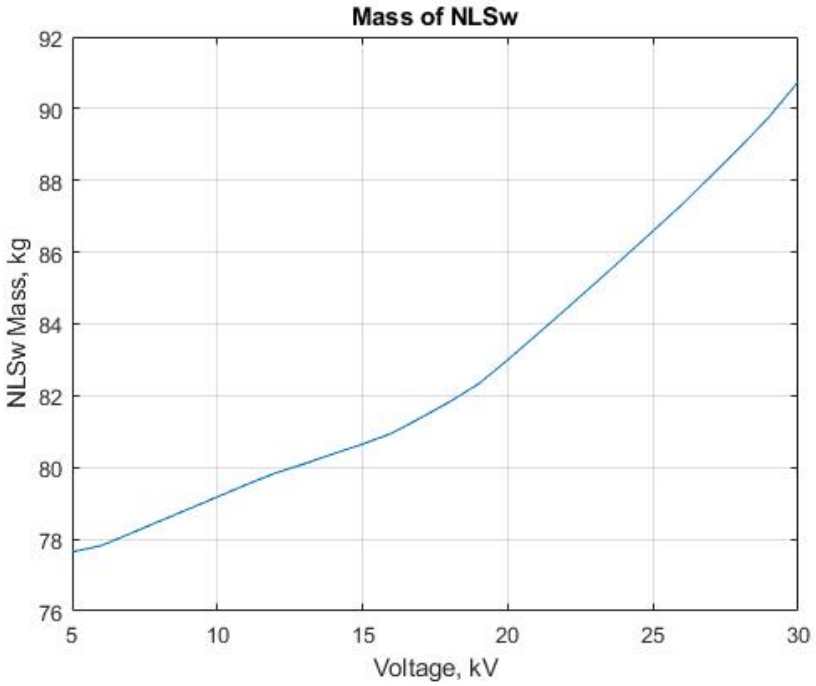

Figure 3.24: No-Load Switch Mass Results

CHAPTER 4

PDM BAY ALLOCATION AND COMPILATION USE-CASE

This section builds upon the use-case employed in Section 3 to model a functional power distribution module (PDM) with the capability to electrically isolate upstream and downstream equipment by providing galvanic isolation through a DC no-load switch. Included in a functional PDM are the galvanic isolating no-load switches, heat exchangers to provide thermal management, bus connections for each no-load switch, and supply and feeder cabling in and out of the PDM. To build a functional PDM, two no-load switches, for the positive and negative leg of the DC distribution network, are packaged into drawers. Drawers are stacked on top of each other into a compartment until the imposed height constraint necessitates adding additional compartments. Each additional compartment is adjacently attached to the prior compartment until the required number of disconnects is achieved. The adjacent compartments, in addition to allocations for compartment-specific heat exchangers, interconnections, and cabling, are considered a PDM bay.

The rest of this chapter will demonstrate the allocation and dimensioning process of the no-load switches modularized into drawers, demonstrate how drawers are modularized into compartments and bays using the allocation and dimensioning process, outline the model specifications used to find metamodel results as voltage changes from 5kV-30kV, describe the operation of the metamodel MATLAB code, and finally present and comment on the metamodel's results.

4.1 PDM Allocation and Compilation Process

4.1.1 No-Load Switch Drawer

As previously mentioned, a positive leg no-load switch and negative leg no-load switch are used as disconnects in the functionally defined PDM. The positive and negative leg switches are modularized side by side into drawers to take advantage of minimizing EMI through the properties of symmetry [17]. What was a complete build-up of the no-load switch with active component, insulation, thermal, accessibility, frame, and conductor allocations in section 3, now becomes an active component of the modular drawer. Following the allocation and compilation process introduced in the previous section, and as shown in fig. 3.1, the process begins by placing active components. Two modular no-load switches, LRUs in the VPP ontology, are placed adjacently as active components of the PDM no-load switch drawer. Fig. 4.1 shows the placed active components.

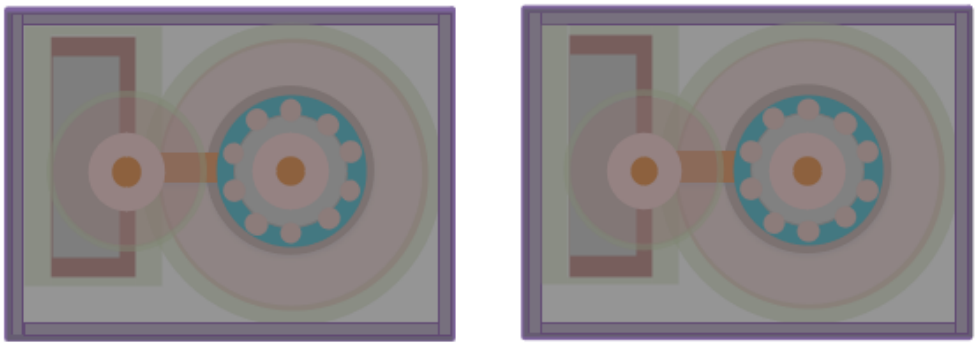

Figure 4.1: Drawer Primary Allocations

Frame allocations are the only solid allocations added to active components in the PDM no-load switch drawer. Thermal allocations are not placed because forced-air convection is chosen as the PDM's cooling solution. If instead, direct cooling was selected as a design choice, a solid thermal management allocation would be added. Conductors will be added in the subsequent connection compartment compilation requiring no solid conductor allocations to be accounted for in the drawer.

Determining and adding supplementary allocations is the next step in the allocation

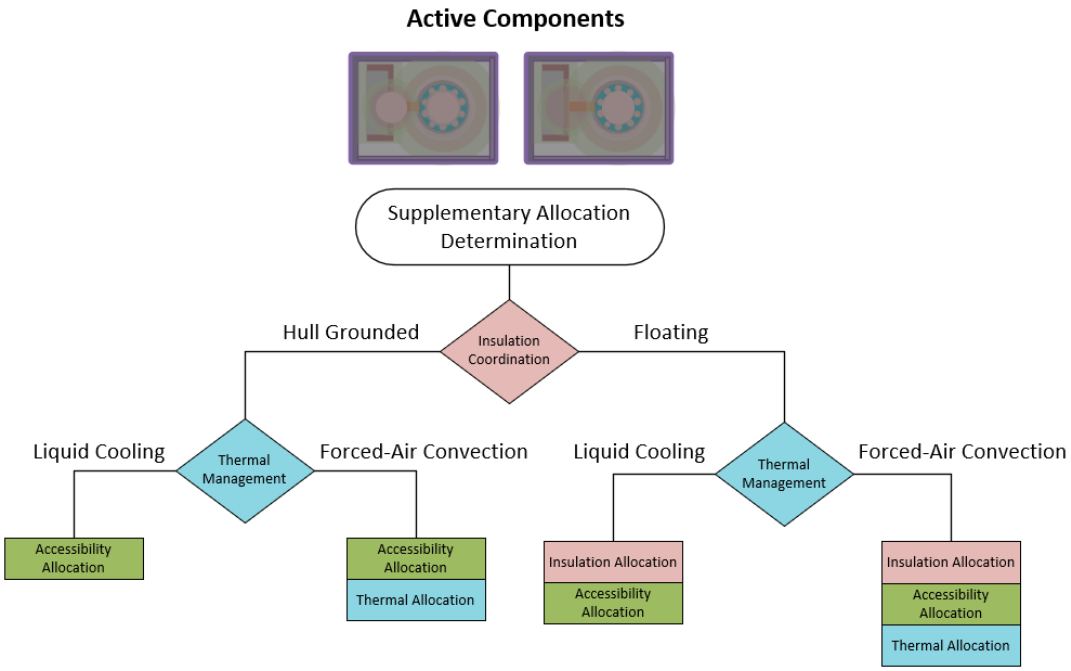

Figure 4.2: Drawer Supplementary Allocation Flowchart

and compilation process. Here, dependent thermal management, insulation, and accessibility supplementary allocations are added to active components and solid allocations. Similar to fig. 3.1 from section 3, an allocation determination flowchart is employed to help visualize the supplementary allocation determination process. As with the no-load switch's supplementary allocation flowchart, Fig. 4.2 visualizes the impact insulation coordination and thermal management design decisions have on supplementary allocation additions. The two design decisions captured in 4.2 are identical to the no-load switch and are between hull-grounding or floating the individual no-load switches, and using forced-air convection or liquid cooling as thermal management solutions.

Either selection of design decisions is viable for shipboard applications, but in this model the no-load switches are left floating at system potential and forced-air convection is chosen as a cooling solution. From these design choices, and in accordance to Fig. 4.2, each no-load switch requires insulation, accessibility, and thermal airflow supplementary allocations. These supplemental allocations are added around each switch and when

fully allocated build to fig. 4.3. All three supplementary allocations occupy the same physical space, as room for air-flow also functions as room for air-gap creepage or clearance requirements, and the physical space required to service or replace the packaged no-load switches. This is a full compilation and the output of step 3 in the allocation and compilation process.

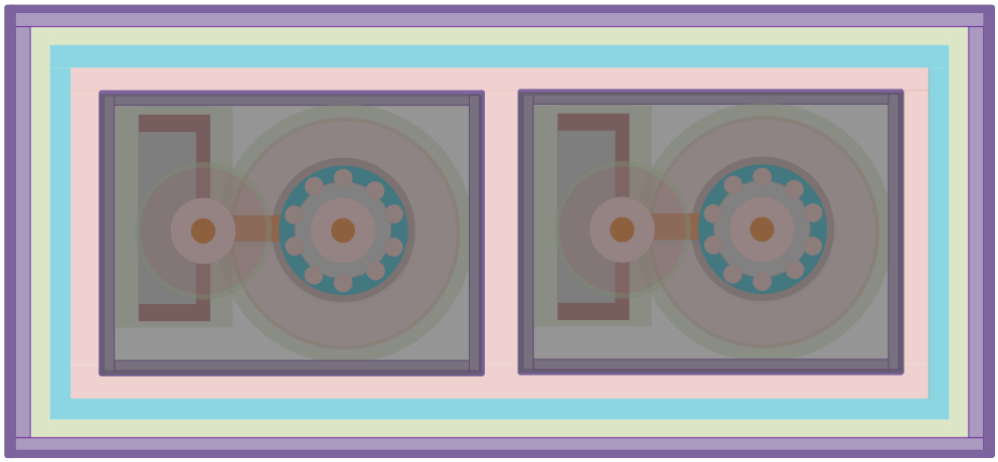

Figure 4.3: No-Load Switch Drawer Supplementary Allocations

Step 4 in the allocation and compilation process, requires first pass dimensioning of the modularized no-load switches as shown in figs. 4.4 and 4.5. This is an initially dimensioned compilation. Because no allocations can be combined or simplified figs. 4.4 and 4.5 also serve as outputs of the second pass dimensioning step. With a final dimensioned compilation the compilation buildup can begin.

From figs. 4.4 and 4.5 the width, height, and length compilation buildup equations are synthesized into eqs. (4.1) to (4.3). These form a fully constrained compilation that can be captured by the MATLAB metamodel. With this, the allocation and compilation process is complete for the modular drawer of a PDM.

$$\begin{aligned} w_{DS} = {} & f_{DSx1} + f_{DSx2} + max(a_{DSx1}, max(th_{DSx1}, d_{DSx1})) + i_{DSx1} + d_{DSx2} + i_{DSx2} \\ & + max(a_{DSx2}, max(th_{DSx2}, d_{DSx3})) + f_{DSx2} + f_{DSx1} \end{aligned} \tag{4.1}$$

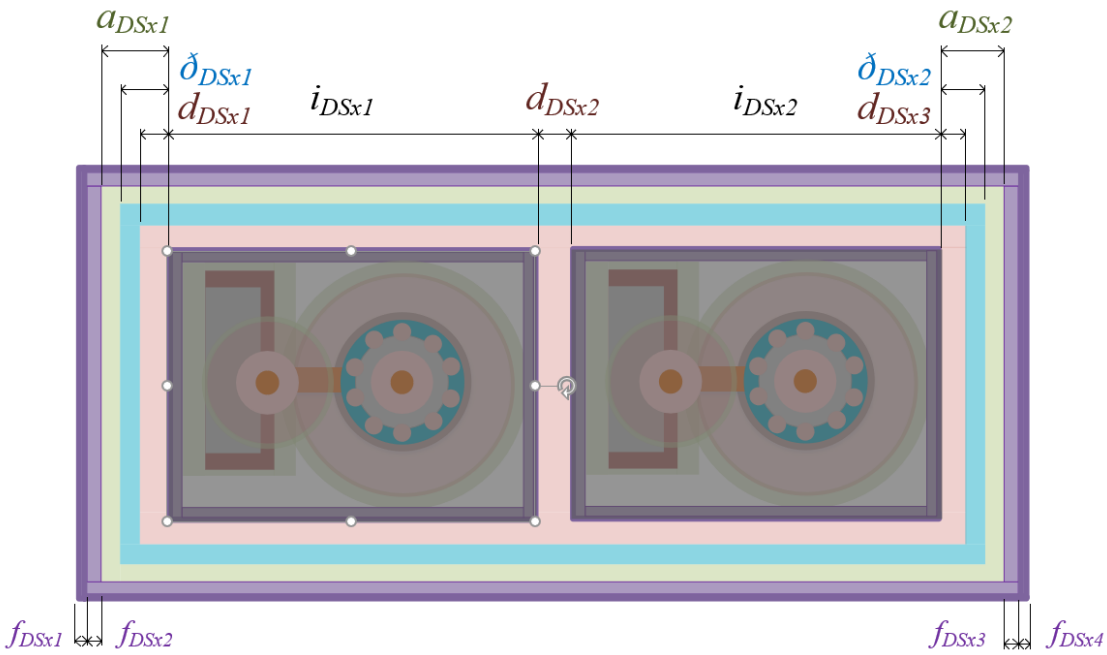

Figure 4.4: NLSw Drawer Front Dimensioned

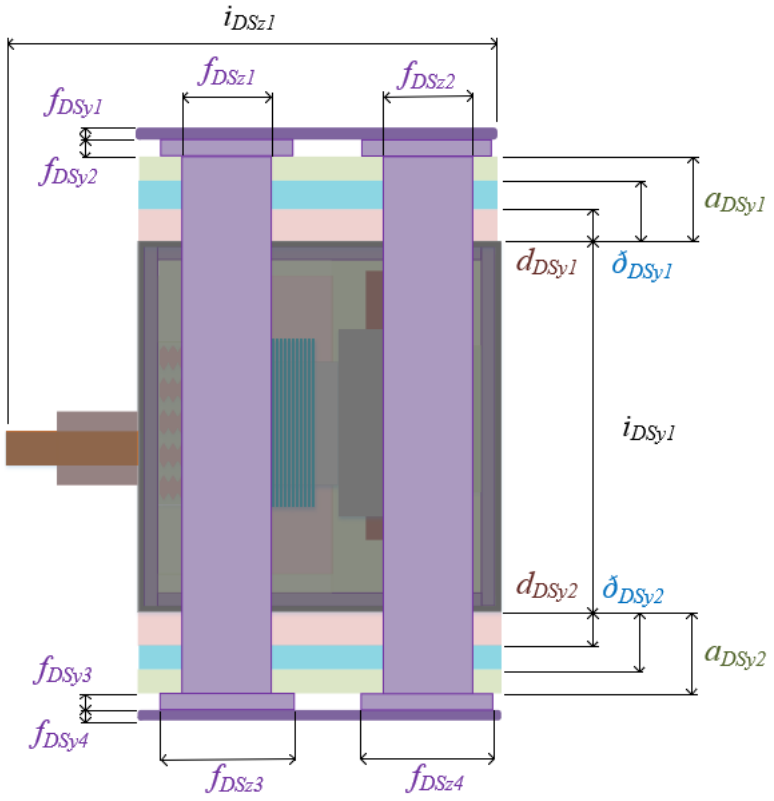

Figure 4.5: NLSw Drawer Side Dimensioned

$$h_{DS} = f_{DSy1} + f_{DSy2} + max(a_{DSy1}, max(th_{DSy1}, d_{DSy1})) + i_{DSy1} + max(a_{DSy2}, max(th_{DSy2}, d_{DSy2})) + f_{DSy2} + f_{DSy1} \tag{4.2}$$

$$l_{DS} = i_{DSz1} \tag{4.3}$$

4.1.2 PDM No-Load Switch Drawer Results

The outputs of the no-load switch drawer metamodel are presented in figs. 4.6 to 4.9. Fig. 4.6 shows how the modular no-load switch drawer dimensions scale with voltage from 5kV to 30kV. As with the no-load switch LRU, the drawer's height and length increase linearly with voltage as driven by increasing insulation creepage and clearance requirements. This correlation between modular ontological units is expected as the drawer is comprised of two LRUs, no-load switches, and the LRU's impact on design metrics will inform every ontological. The drawer width is also informed by the no-load switch's width. Overall drawer width does not begin increasing until 16kV just as in the no-load switch when creepage and clearance distances begin to drive overall width. This correlation again highlights how design decisions or technology selection at the base LRU ontological level will inform every modular level that incorporates the LRU as a building block.

Fig. 4.7 presents the drawer's overall mass which correlates closely with the individual no-load switch's weight as seen in fig. 3.24. As overall width begins to increase linearly at 16kV due to driving insulation allocations, mass also experiences a change in slope and begins increasing more rapidly. As with the no-load switch, the increase in overall weight is due to an increase in frame weight as the frame widens to allow for prescribed creepage and clearance stand-offs.

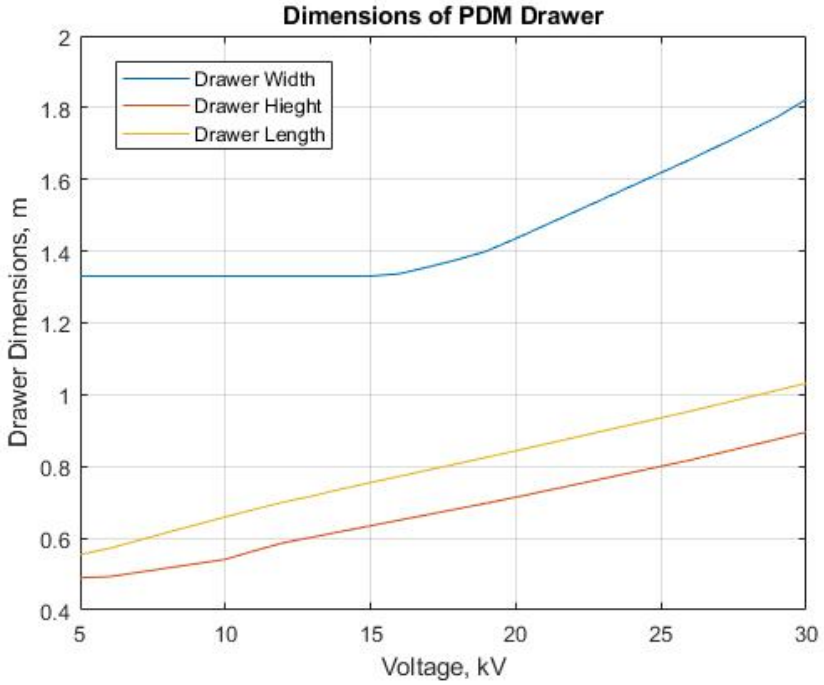

Figure 4.6: No-Load Switch Drawer Dimensions

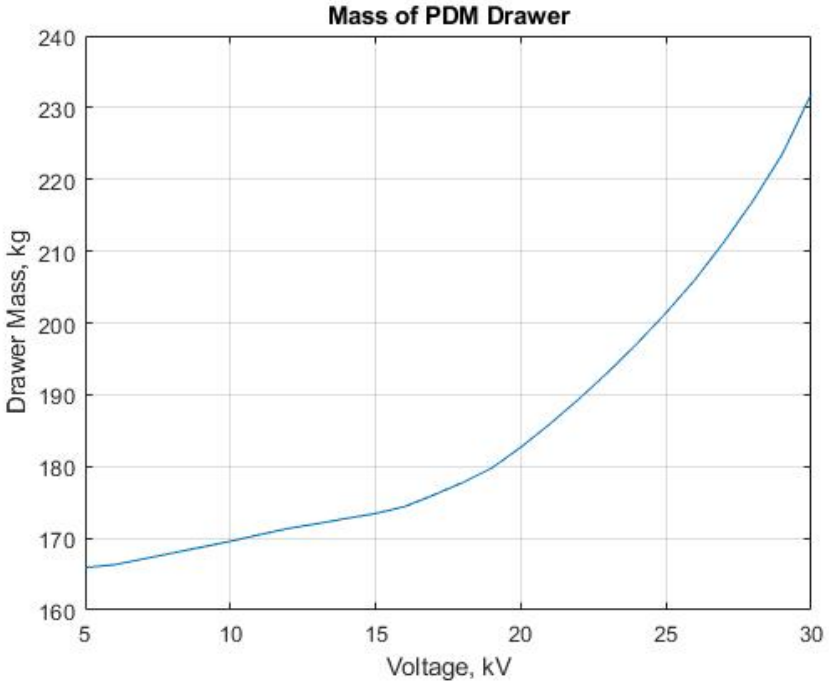

Figure 4.7: No-Load Switch Drawer Mass

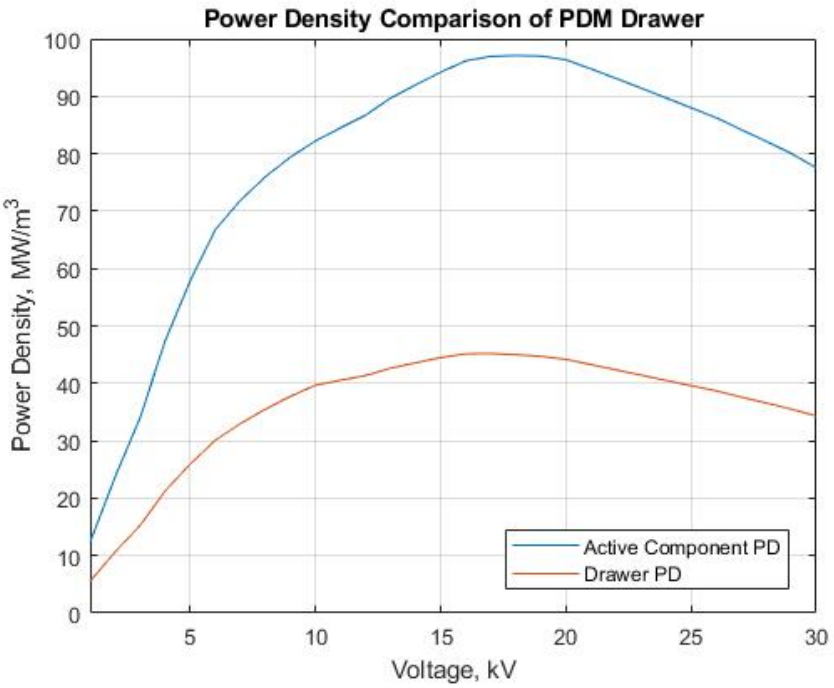

Figure 4.8: No-Load Switch Drawer Power Density Comparison

Fig. 4.8 compares the power density of the modularized no-load switch drawer to the power density of two LRU no-load switches. The comparison demonstrates the loss in power density, design metrics in a general sense, as technologies are modularized and built into a modular distribution network. The drawer's power density is labeled Drawer PD and shown in red while the no-load switch's power density is labeled Active Component PD and shown in blue. As seen in the figure, once insulation, thermal, and accessibility allocations are added to the drawer its power density peaks at 43 MW/m^2 at 16kV compared to the no-load switch's 97 MW/m^2.

Fig. 4.9 compares specific power between the modularized drawer and its LRU, no-load switch, building blocks. The loss in specific power between the modularized drawer and no-load switch, active component, is less pronounced than power density. This is because while increasing creepage and clearance requirements do drive overall volume, which in turn drives frame weight, the added air-gap standoffs do not contribute to overall weight. At 16kV, the drawer's specific power no longer increases linearly and begins

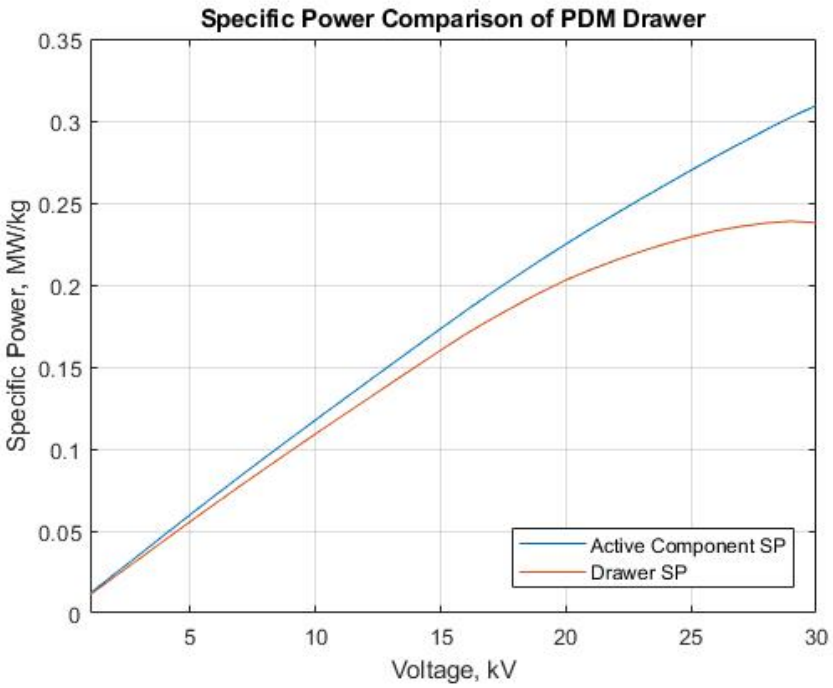

Figure 4.9: No-Load Switch Drawer Specific Power Comparison

to lessen until flattening at 30kV. The frame's weight begins to dominate the weight of active components and causes no further gain in specific power as voltage is increased.

4.1.3 PDM Heat Exchanger Drawer

A fully functional PDM requires active thermal management to efficiently cool the no-load switches housed within the bay. For this use-case, a fan-driven heat exchanger is selected as the PDM's thermal management solution. The heat exchanger will be packaged into a drawer housed in the same compartment as the no-load switch drawers. Each compartment will have one heat exchanger, located at the top of the compartment, to facilitate air-flow cooling.

The heat exchanger's allocation and compilation process will be performed and demonstrated as it becomes a modular building block in the modular distribution network. This highlights the adaptability of this methodology; namely that any technology, in this case not power electronic equipment, can be accounted for in the metamodel produced by the

allocation and compilation process.

As with the no-load switch drawer, the heat exchanger's allocation and compilation process begins by placing active components. Because the heat exchanger is assumed to be a procured technology, the heat exchanger is placed as an active component in step one of the process as reflected in fig. 4.10.

Figure 4.10: Heat Exchanger Primary Allocation

With no solid allocations required, the heat exchanger is assumed a fully functional procured piece of equipment, next is the placement of supplementary allocations. Fig 4.11 shows the allocation flowchart used to determine supplementary allocations. The two decisions captured in fig. 4.11 are between floating or hull-grounding the heat exchanger within the drawer and the use of forced-air convection or liquid cooling thermal management solutions. Unlike the packaged no-load switches, the heat exchanger is assumed to be hull grounded in this use-case and forced-air convection cooling is implicit in the choice of a heat-exchanging fan. Choosing hull-grounded at the insulation coordination decision node, and forced-air convection at the thermal management node, accessibility and thermal supplementary allocations are prescribed for the heat exchanger's active component. These additions are reflected in figs. 4.12 and 4.13.

First and second-pass dimensioning is subsequently performed. Because no dimensions can be subsumed between first and second pass dimensioning, figs. 4.14 and 4.15 presents the fully dimensioned heat exchanger.

The compilation equations that fall out of the fully dimensioned heat exchanger are

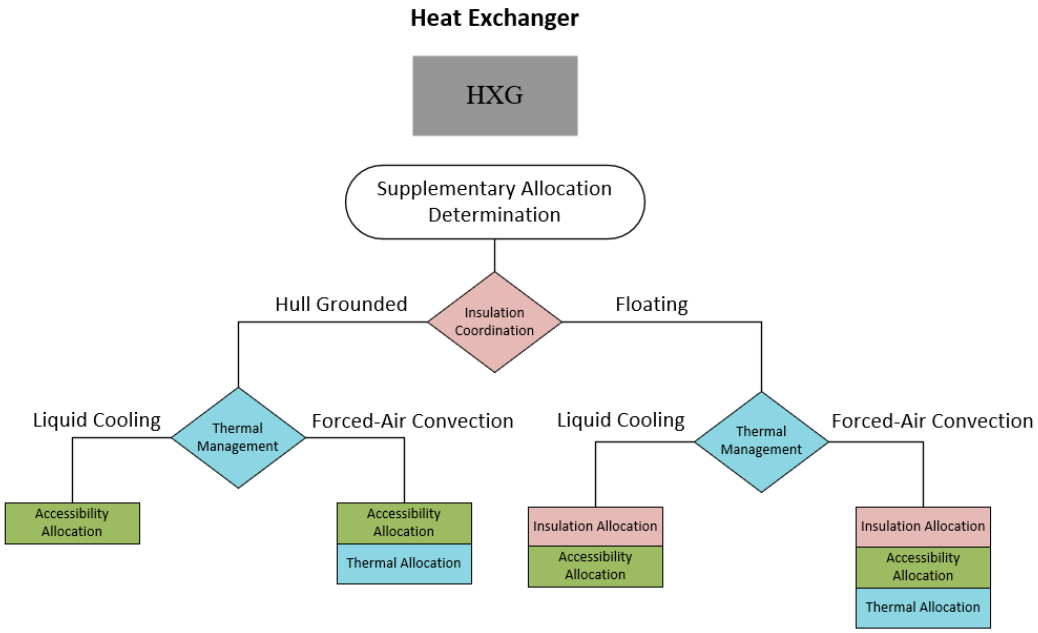

Figure 4.11: Heat Exchanger Supplementary Allocation Flowchart

Figure 4.12: Heat Exchanger Supplementary Allocation X-Direction

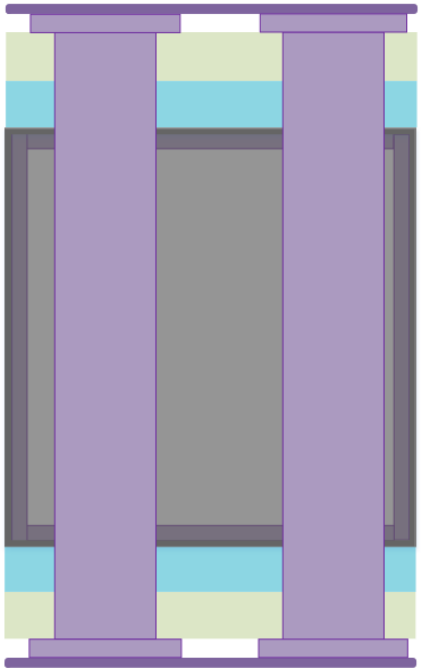

Figure 4.13: Heat Exchanger Supplementary Allocation Z/Y-Direction

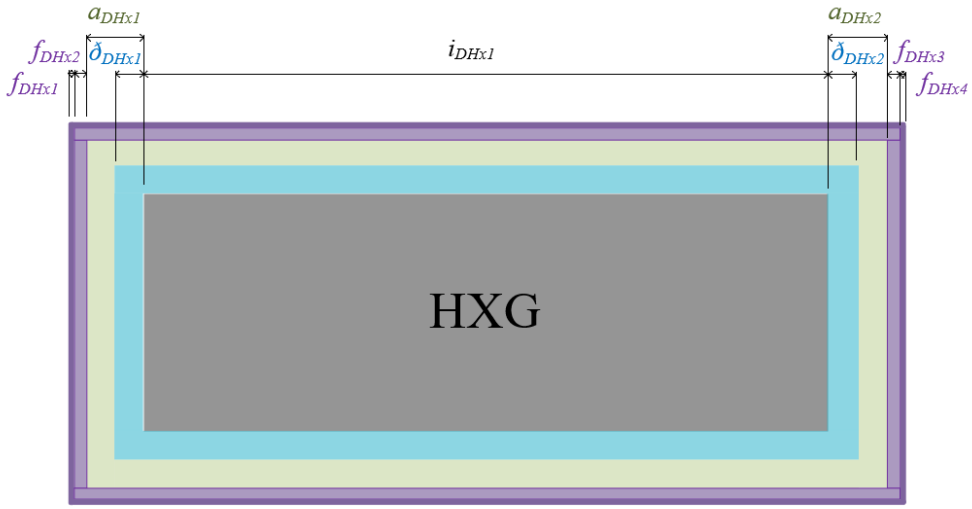

Figure 4.14: Heat Exchanger Dimensions X-Direction

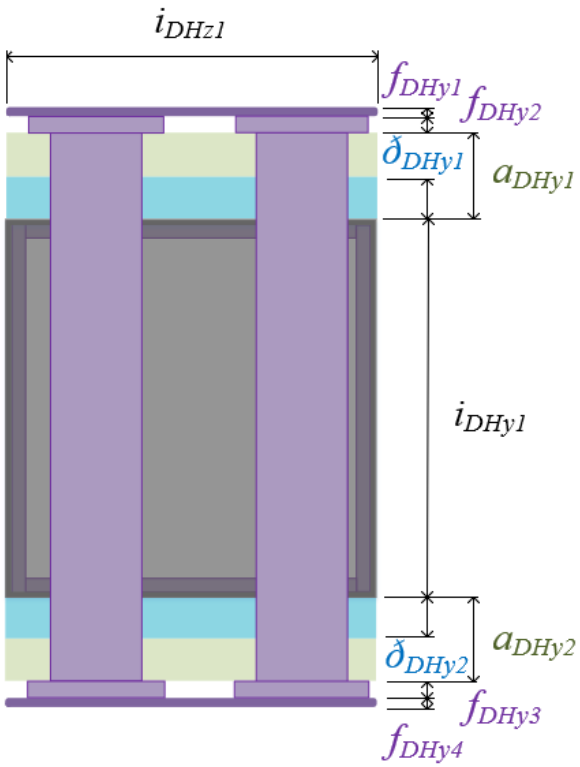

Figure 4.15: Heat Exchanger Dimensions Z/Y-Direction

captured by eqs. (4.4) to (4.6):

$$w_{DH} = f_{DHx1} + f_{DHx2} + max(a_{DHx1}, th_{DHx1}) + i_{DHx1} + max(a_{DHx2}, th_{DHx2}) + f_{DHx3} + f_{DHx4} \tag{4.4}$$

$$h_{DH} = f_{DHy1} + f_{DHy2} + max(a_{DHy1}, th_{DHy1}) + i_{DHy1} + max(a_{DHy2}, th_{DHy2}) + f_{DHy3} + f_{DHy4} \tag{4.5}$$

$$l_{DS} = i_{DHz1} \tag{4.6}$$

4.1.4 PDM Drawer Compartment

At the compartment level, the allocation and compilation process assembles the no-load switch and heat exchanger drawers into compartments. The no-load switch and heat exchanger drawers now become active components of the compartment, with active components placement presented in figs. 4.16 and 4.17. Note that the compartment active component placement is almost identical to the drawer primary placement, highlighting again the generic and adaptability of this methodology to all levels of modularization.

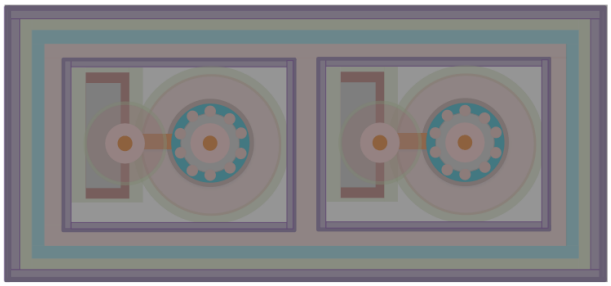

Figure 4.16: PDM Compartment Primary Allocations

Figure 4.17: Heat Exchanger Compartment Primary Allocations

Once placed, supplementary allocations are added to active components as determined by the flowchart presented in fig. 4.18. Insulation coordination becomes the only decision node present as thermal management, or space for air-flow, has previously been added to the drawer. The choice, as before, is between hull-grounding the drawer or floating the drawer at system potential. Because additional insulation allocations have already been added to the no-load switch assembly at the drawer level, and the heat exchanger is

assumed hull-grounded, hull-grounded has been implicitly chosen. Hull-grounding prescribes only accessibility allocations to both the no-load switch and the heat exchanger drawer. Figures 4.19 and 4.20 shows the accessibility allocations added to the active component no-load switch and heat exchanger drawers.

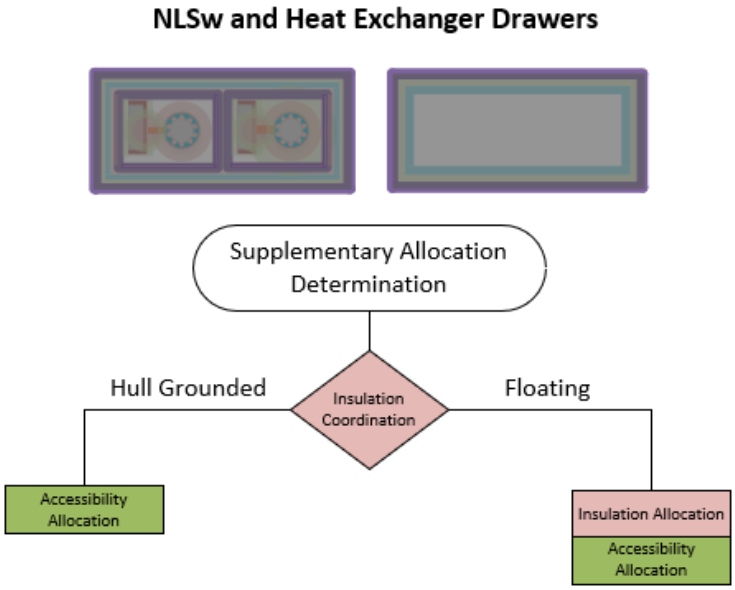

Figure 4.18: No-Load Switch and Heat Exchanger Compartment Supplementary Allocation Determination Flowchart

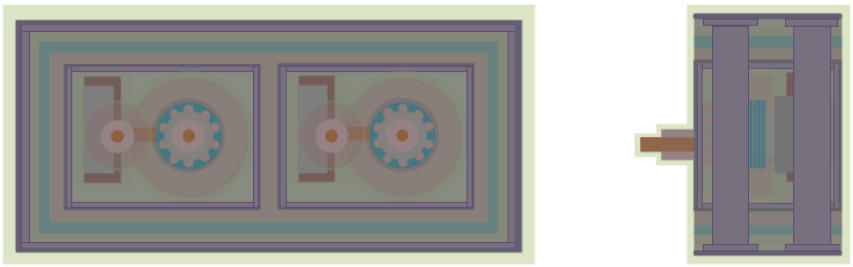

Figure 4.19: No-Load Switch PDM Compartment Supplementary Allocations

First and second-pass dimensioning get subsumed into a single step as no overlapping dimensions exist during first-pass dimensioning. Figs. figs. 4.21 to 4.23 represent fully dimensioned compartment drawers. Note that the heat exchanger's indexed dimensions as presented in 4.20 are indexed from the no-load switch drawer dimensions seen in figs. 4.21 and 4.22 instead of zero. Active component, solid allocation, and sup-

Figure 4.20: Heat Exchanger Compartment Supplementary Allocations

plementary allocation dimensions are indexed in reference to each other when housed in the same modular assembly. This was the case in chapter 3 when a power controller active component was added to the no-load switch's active components, and indexed in reference to the no-load switch's active components. The same occurs in the compartment as both the no-load switch and heat exchanger drawer are part of the same modular compartment assembly.

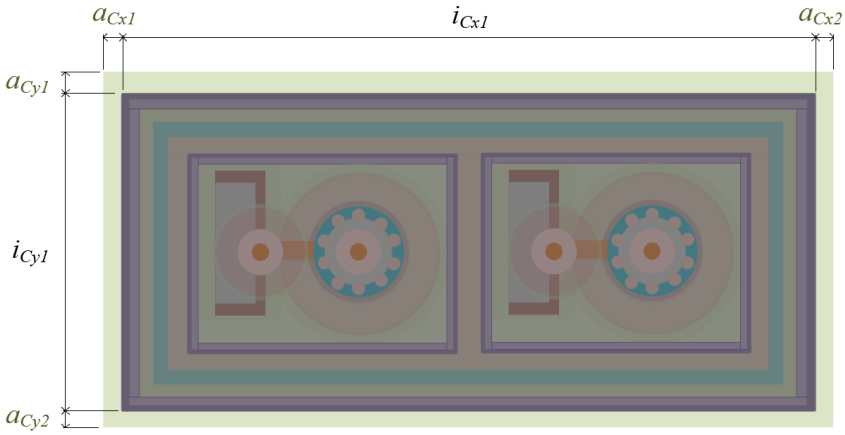

Figure 4.21: PDM Compartment Drawer Dimensions

The drawer compartment build-up equations are captured in section **??** as the build-up equations depend upon the number of no-load switch drawers required in each drawer compartment. They will be compared against the connection compartment build-up equations with the maximum driving overall bay dimensions.

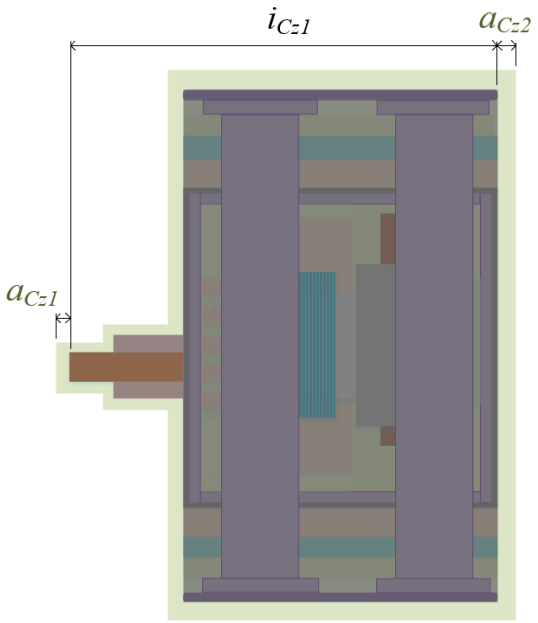

Figure 4.22: PDM Compartment Drawer Dimensions

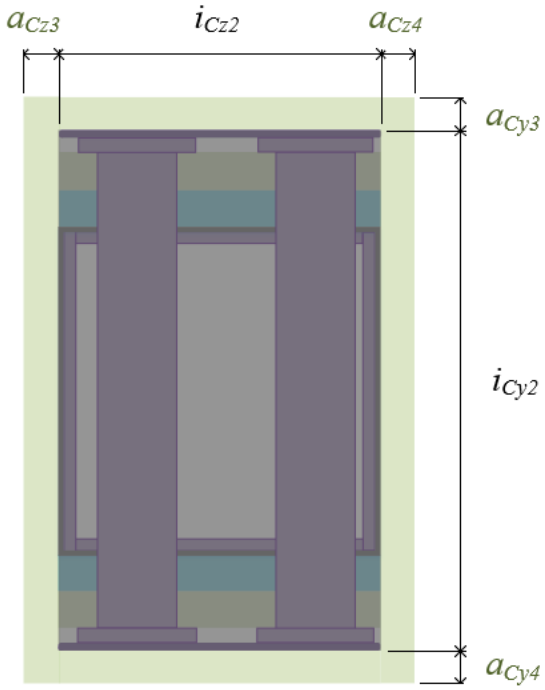

Figure 4.23: Heat Exchanger Dimensions Z/Y-Direction

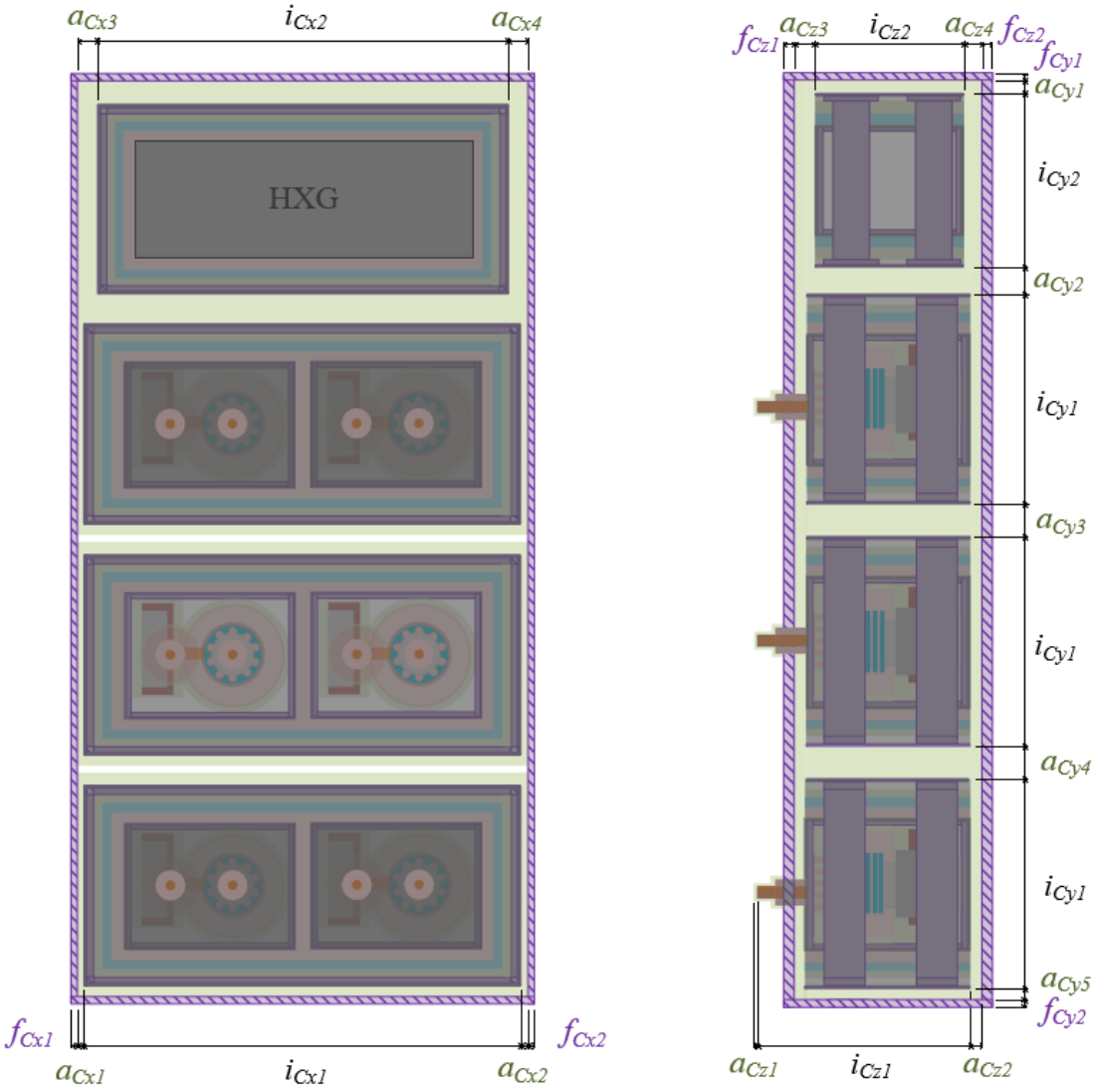

Figure 4.24: Dimensioned NLSw and HXG Compartment

4.1.5 PDM Connection Compartment

The PDM requires a connection compartment be added to account for cabling and bus bar connections required for connection to the assumed modular distribution network. Each no-load switch is connected through a positive and negative cabling connection brought in through the top of the connection compartment. Each cable connection must land on bus bar stabs that extend through the connection compartment into the drawer compartment to allow the no-load switch drawers to slide in and out of the connection

compartment bus bar connections. In traditional switchgear, this is achieved through stationary spring-loaded bus bar stabs that are the ”female” connection to the removable ”male” connection of the draw-out circuit breaker. That traditional connection is modeled here but naval designers will have the freedom to determine physical connection compartment connections during the design process.

The drawer compartment becomes an active component of the connection compartment and is placed in fig. 4.25. Solid allocations are placed next. The connection compartment requires solid conductor allocations representing connection bus bar stabs, connection cabling, and solid frame allocations be added as supplementary allocations. In this use-case, it is assumed that the connection compartment and drawer compartment are constrained to the same height. This may not be the case in all applications. If the two compartment heights are not constrained, the PDM Bay height will be taken as a maximum between the connection compartment and the drawer compartment height as informed by compartment compilation equations. Fig 4.26 reflects the conductor and frame solid allocation additions.

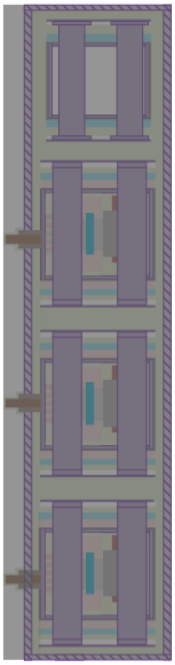

Figure 4.25: Active Component Placement of Connection Compartment

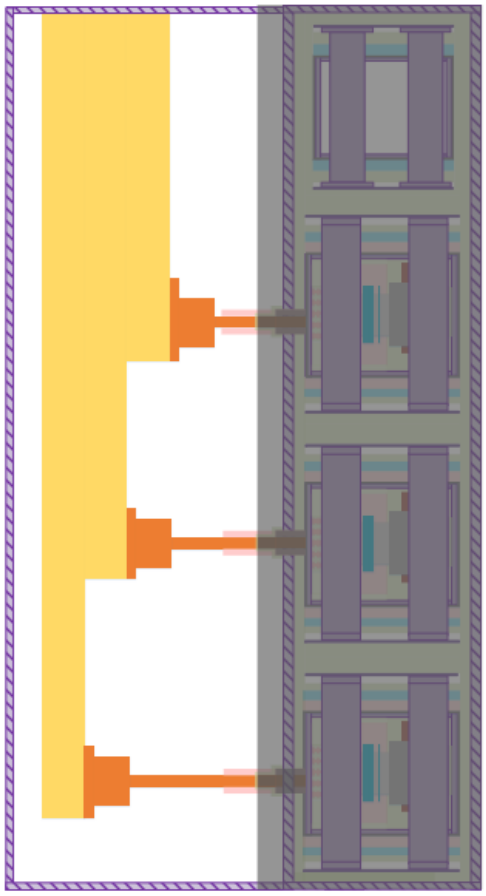

Figure 4.26: Solid Allocation Placement of Connection Compartment

Following the allocation and compilation process, supplementary allocations are subsequently added. Supplementary allocation determination of the active component drawer compartment and interconnection cabling assumes that insulation coordination has already taken place at the drawer level and through cable insulation, leaving thermal management as the only design decision to account for. As with the no-load switch and drawers, the choice is between liquid cooling or forced-air convection. Forced-air convection is implicitly chosen in this use-case, resulting in thermal air flow and accessibility allocations being prescribed as seen in fig. 4.27.

The bus bar connection stabs are assumed to be uninsulated bus bar and therefore insulation coordination must be considered. Fig. 4.28 reflects this with a decision node for insulation allocations. The bus bar connections are necessarily be left ungrounded

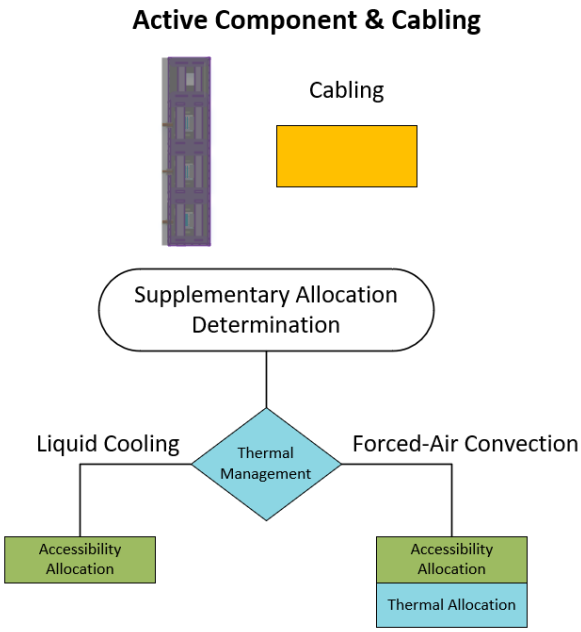

Figure 4.27: Active Component & Cabling Supplementary Allocation Determination

and forced-air convection is selected for thermal management to prescribe insulation, thermal, and accessibility supplementary allocations. The corresponding supplementary allocations are added to fig. 4.26 and are reflected in fig. 4.29.

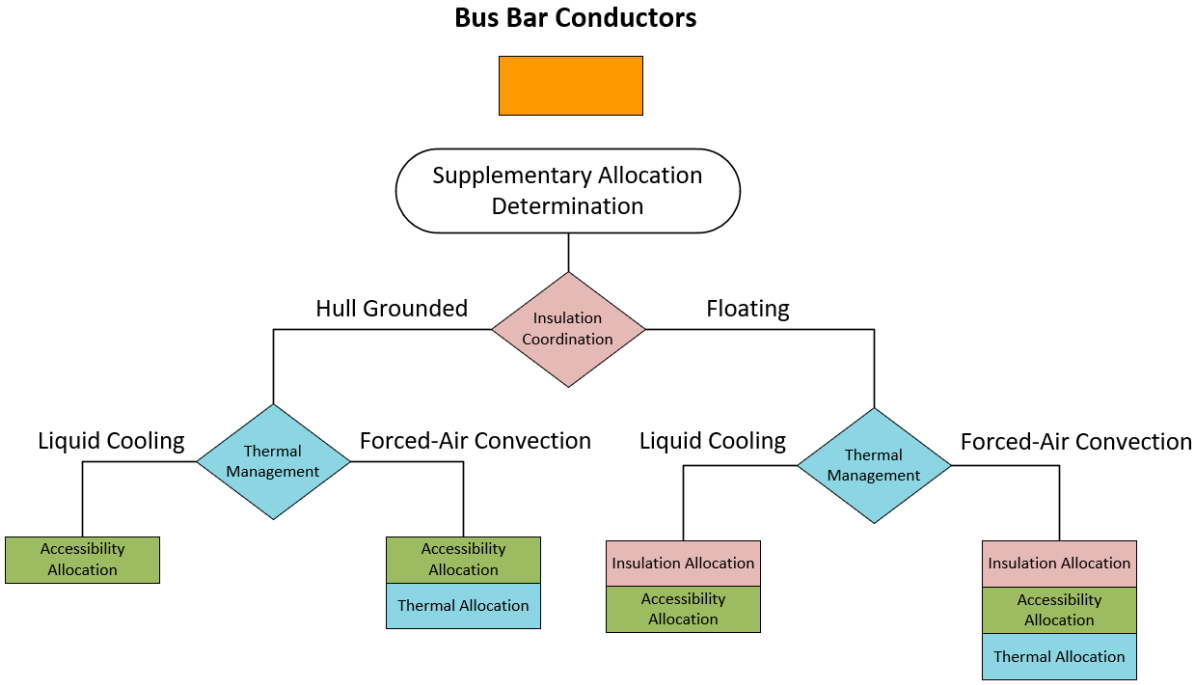

Figure 4.28: Bus Bar Conductor Supplementary Allocation Determination

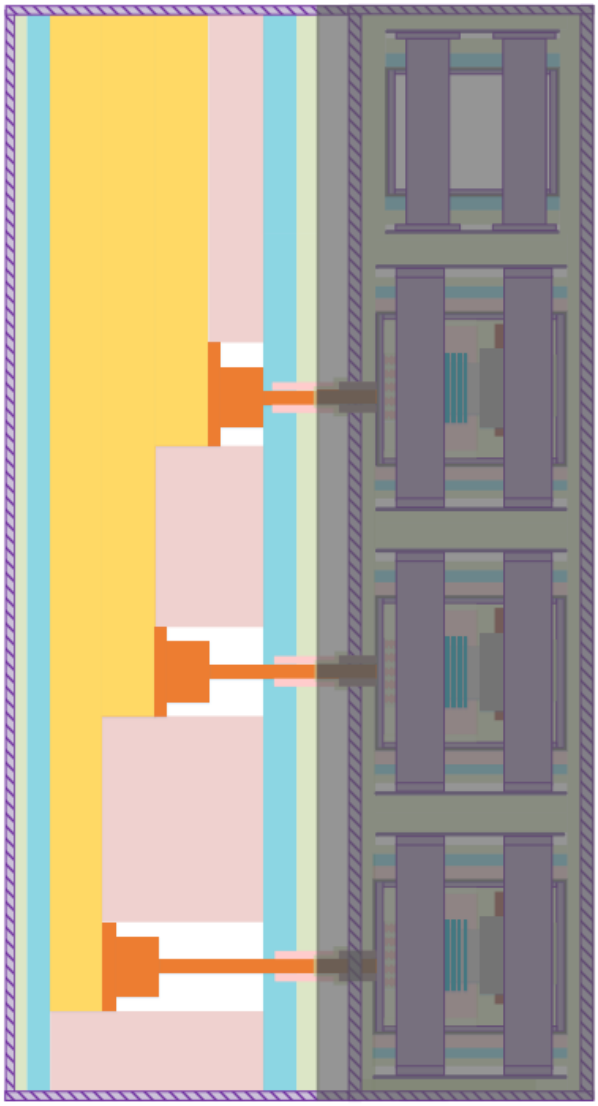

Figure 4.29: Supplementary Allocation Placement of Connection Compartment

First and second-pass dimensioning is performed on the fully allocated compilation in the x, y, and z, coordinate plane. Fig. 4.30 shows the first pass dimensioning in the y and z coordinate plane. Due to the absence of overlapping dimensions, 4.30 becomes the fully dimensioned drawing used in the compilation build-up. The connection compartment's dimensioning of the x-coordinate system will be presented in the following section as insulation stand-off distances are dictated by the number of adjacent compartments required by the bay. The maximum width between the adjacent connection compartments and drawer compartments will drive the bay's overall width.

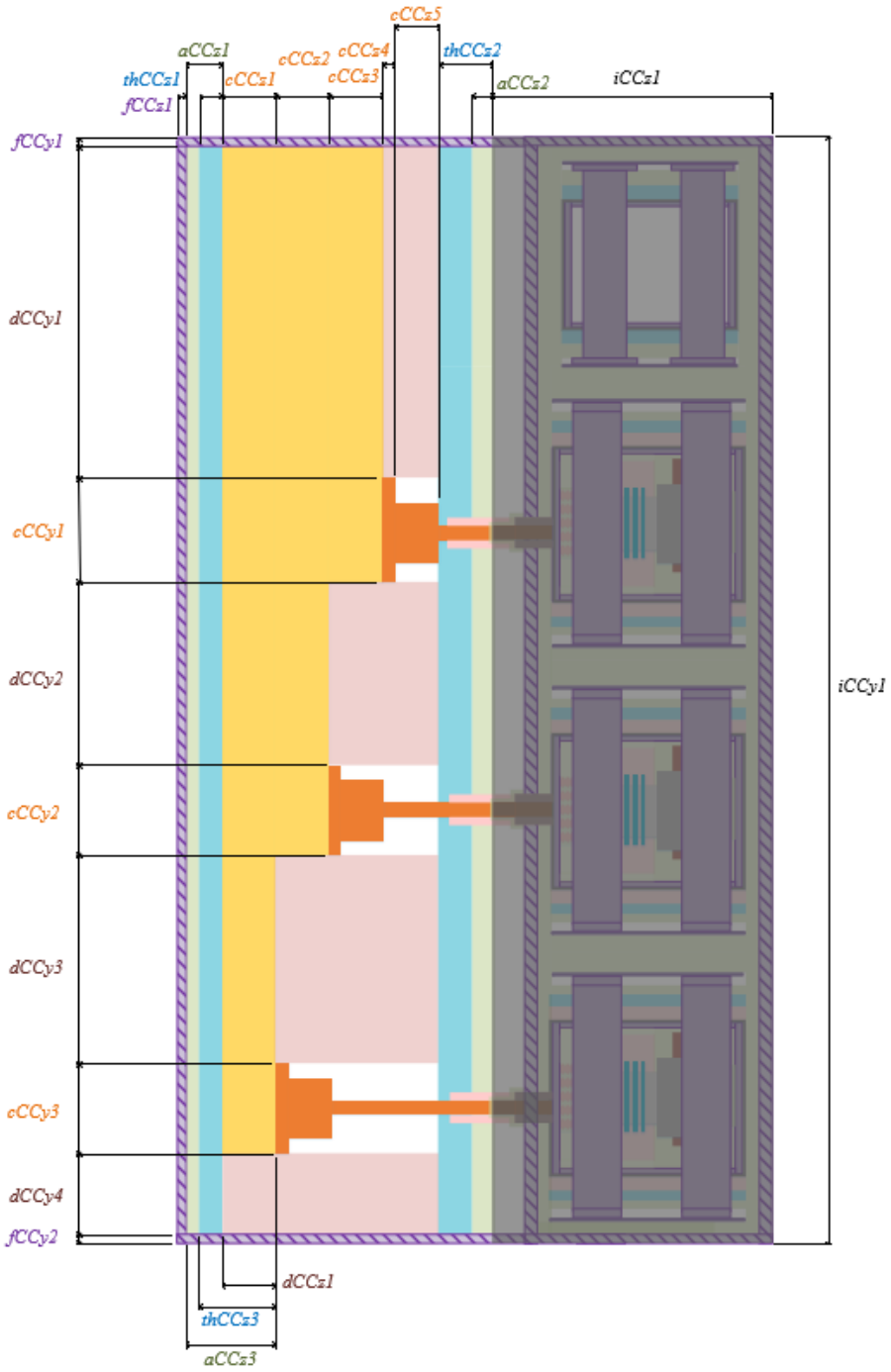

Figure 4.30: First & Second-Pass Dimensioning of Connection Compartment

Due to the dependence of the bay's overall width, height, and length on the number of no-load switches required, the drawer compartment, connection compartment, and bay build-up equations are presented in section 4.2.

4.1.6 PDM Bay

To demonstrate the allocation and compilation process at the bay ontological level, the figures introduced in this section assume that eighteen no-load switches, or nine modular no-load switch drawers, are required. Due to an assumed imposed height constraint, three adjacent compartments are required to house the required disconnects. Initiating the allocation and compilation process, the drawer and connection compartments are placed as active components of the bay as shown in figs. 4.31 and 4.32.

Supplementary allocations are subsequently added and determined by fig. 4.33. Insulation coordination is assumed accounted for in the drawer and connection compartment by added creepage and clearance stand-offs at the no-load switch drawers and connection compartment, leaving thermal management as the only decision node. As previously assumed the PDM bay will be forced-air cooled by heat exchangers located in each drawer compartment. Following 4.33 thermal air-flow and accessibility allocations are prescribed and added as reflected in figs. 4.34 and 4.35.

First, and the subsumed second-pass dimensioning, in the x-coordinate plane of the

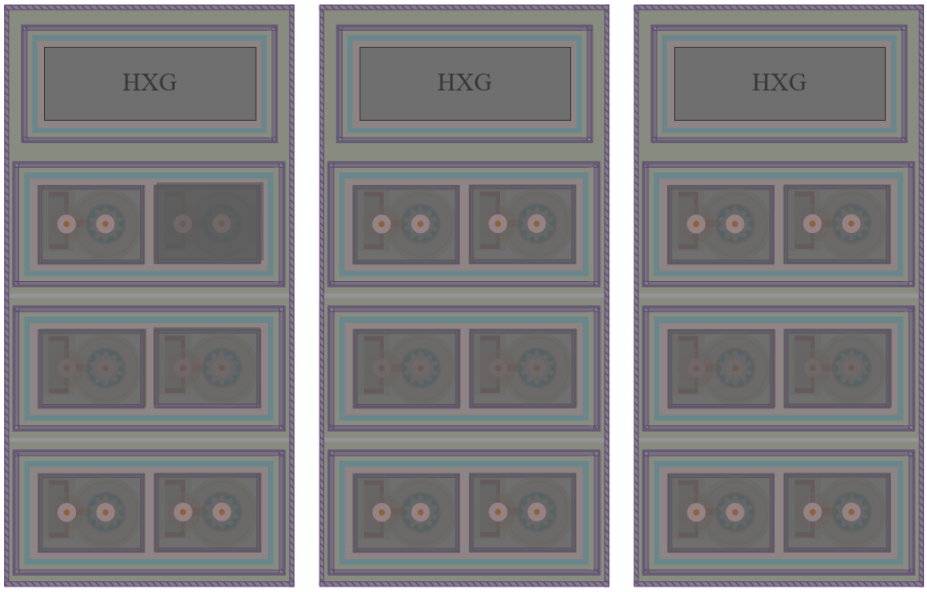

Figure 4.31: PDM Bay Active Component Placement

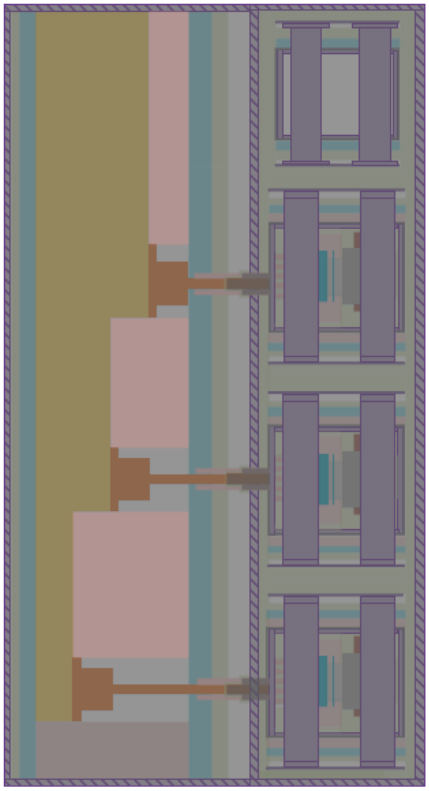

Figure 4.32: PDM Bay Active Component Placement

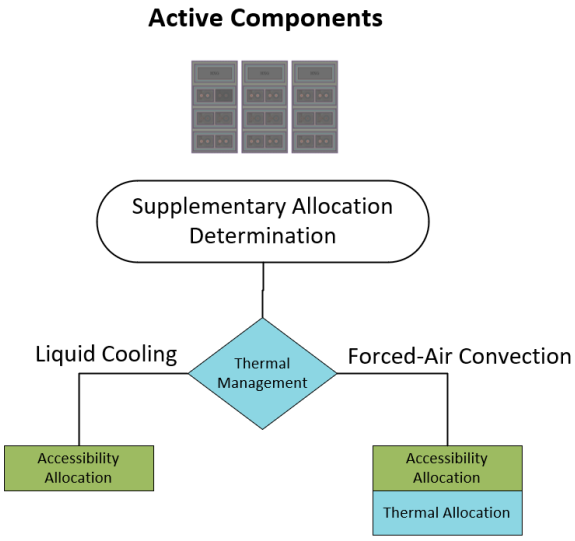

Figure 4.33: Supplementary Allocation Determination for PDM Bay

fully allocated bay is presented in figs. 4.36 to 4.38. Note that as with any allocation, allocations can be set to zero as design decisions are made. In practical application, thermal

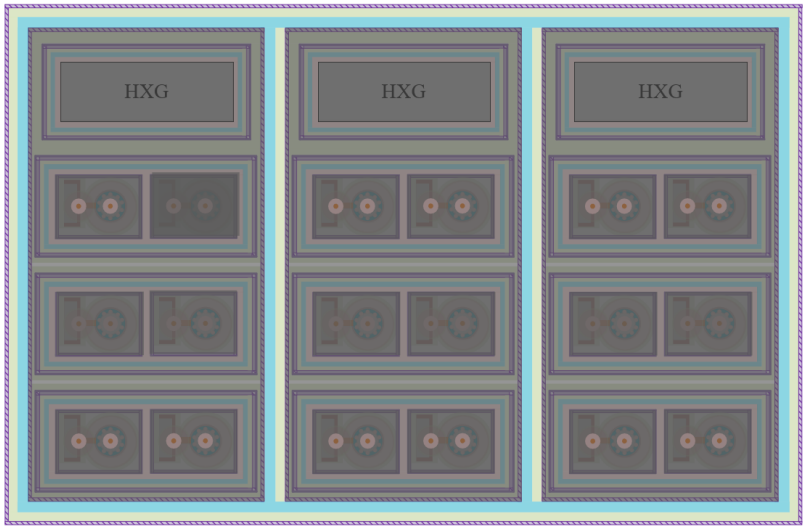

Figure 4.34: PDM Bay Supplementary Allocation Placement

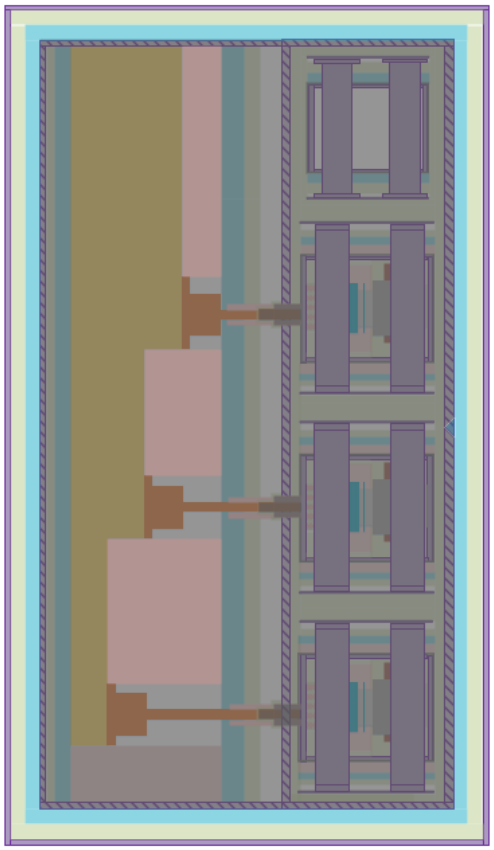

Figure 4.35: PDM Bay Supplementary Allocation Placement

air flow and accessibility, as represented by a_{By2} and th_{By2}, may not be feasibly added underneath compartments resulting in each allocation set to zero. The same is true for

the added frame structure represented by f_{By1} and f_{By2}. In this use case, it is added to provide protection from the shipboard environment but may be foregone and set to zero during practical implementation. Fig. 4.38 will be elaborated on in section 4.2.

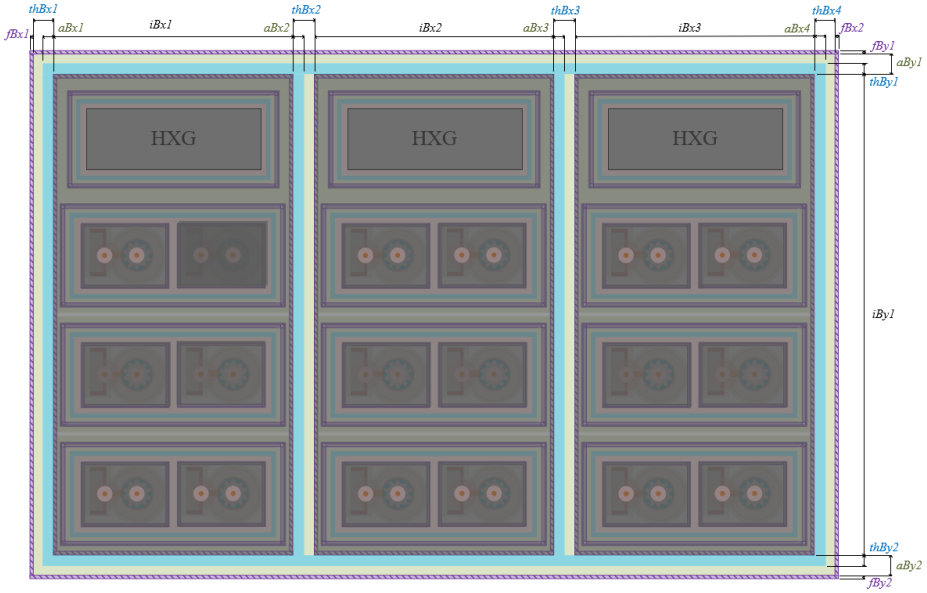

Figure 4.36: Dimensioned PDM Bay X-Direction

The resulting bay build-up equations will be presented in section 4.2 as the drawer compartment, connection compartment, and bay equations inform each other. With a fully dimensioned model complete the bay allocation and compilation process is complete.

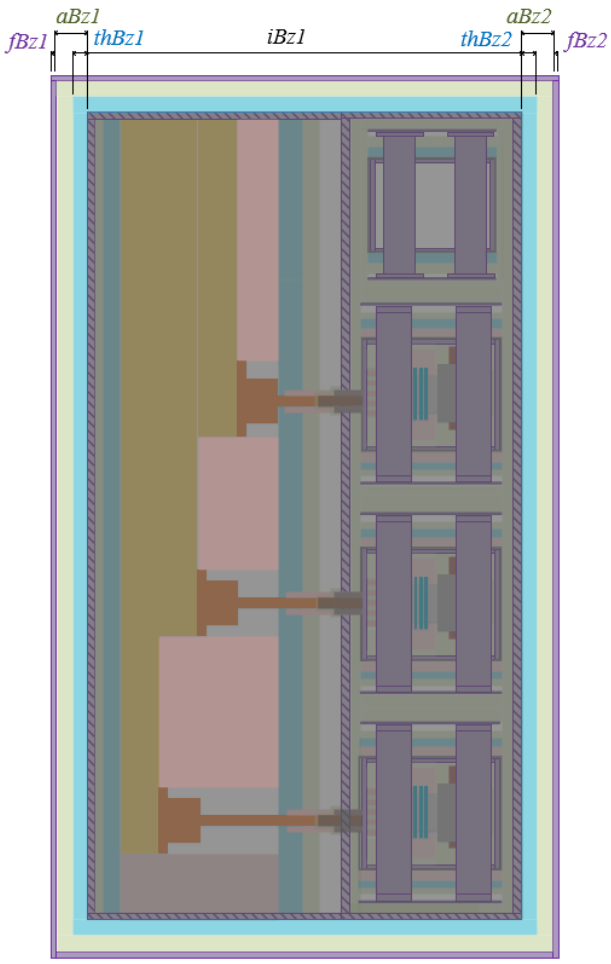

Figure 4.37: Dimensioned PDM Bay

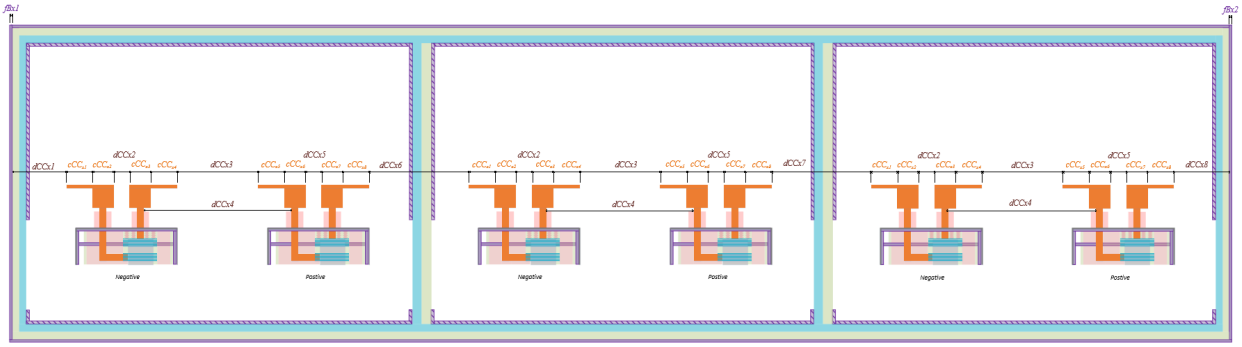

Figure 4.38: Dimensioned PDM Bay Connection Compartment X-Direction

4.2 PDM Metamodel MATLAB Code

Fig. 4.39 is a sequence diagram depicting how the PDM Metatest Matlab code is constructed and passes data between its multiple sub-functions. The metatest is comprised of multiple sub-functions that are called as shown in Fig. 4.39. The Metatest code builds upon the simulation code described in chapter 3 and nests the code scaling the individual no-load switch, called NLSw.m in section 4, into Switch_Drawers.m. The execution of the Metatest code is similar to NLSw.m. PDM_Metatest.m is the wrapper script that queries inputs directly from the designer and passes them to the sub-functions housed within. Four input arrays, categorized as design space variables (x), design requirements (r), design parameters (k), and operational vignettes (v), are passed to PDM_Metatest.m. Each array may, and often will, have multiple input arguments. The simulation code begins with the designer being asked the following questions to populate the four inputs:

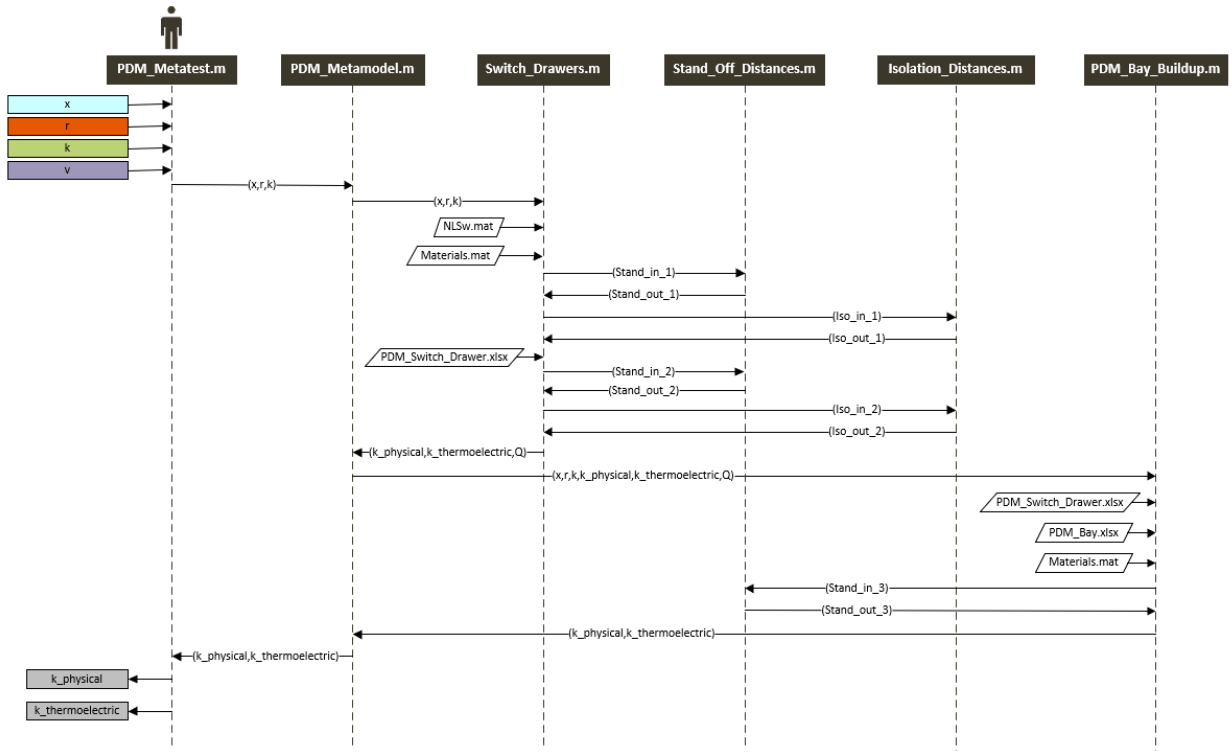

Figure 4.39: Bay Code Sequence Diagram

- Design Space Variables (x)
  - Rated connection voltage? (between 1,000 and 36,000 volts)
  - Rated connection current? (between 300 and 3500 amperes)
  - What is the inlet water temperature (deg C)?
  - What is the inlet mass flow rate (kg/s)?
- Design Requirements (r)
  - Maximum allowable bay height? (meters)
- Design Parameters (k)
  - How many in-zone connections are there? (between 0 and 10)
  - Is there a forward connection? (Enter 1 for YES and 0 for NO)
  - Is there an aft connection? (Enter 1 for YES and 0 for NO)
- Operational Vignettes (v)
  - How many in-zone connections are in the ON state?
  - What is the input connection current (A)?
  - Is the forward connection in the ON state? (Enter 1 for YES and 0 for NO)
  - What is the input forward connection current (A)?
  - Is the aft connection in the ON state? (Enter 1 for YES and 0 for NO)
  - What is the input aft connection current (A)?

Once queried, the inputs are stored in structures denoted x for design space variables, r for design requirements, k for design parameters, and v for operational vignettes. Structures x, r, and k are passed from PDM_Metatest.m to PDM_Metamodel.m. Operational vignettes (v) are not passed because the calculations requiring these inputs takes

place in PDM_Metatest.m. PDM_Metamodel.m is the sub-function that calls the compilation sub-functions Switch_Drawers.m and PDM_Bay_Buildup. It is in Switch_Drawers.m and PDM_Bay_Buildup that the various allocation types in the x, y, and z direction are built up into width, length, and height equations. Structures x, r, and k are passed from PDM_Metamodel.m to Switch_Drawers.m beginning the compilation process. Switch_Drawers.m first loads the initialized allocations of the test article no-load switch designed to 6000V and 2000A [38] from the input NLSw.mat file. The Materials.mat input is brought in to initialize the densities used for later weight calculations, modulus of elasticities for column buckling analysis, and insulation constants. The sub-function unpacks the design space variables and uses rated connection current to find a scaling ratio between the test article no-load switch and the current chosen by the designer. The scaling ratio *Iratio* is dived by the test article's initialized internal resistance to find a scaled resistance that is used to find the power loss for the designer selected no-load switch using eq. 4.7.

$$PowerLoss = RatedCurrent^2 * ScaledResistance \tag{4.7}$$

With scaled power losses found, Switch_Drawers.m uses the scaling ratio to scale the width of contactor cylinder, the width of the actuator cylinder, and the number of heat-sink fins, all of which are assumed to scale with current and subsequently power. Next, just as in NLSW.m, Switch_Drawers.m calls the sub-functions Stand_Off_distances.m and Isolation_Distances.m to calculate creepage and clearance distances that inform that insulation allocations. Fig. 4.39 shows single variables, Stand_in_1 and Iso_in_1, being passed to their respective sub-functions but in practice Stand_in_1 and Iso_in_1 are a list of the following variables:

- Stand_in_1
  - OVCat - Over-voltage Category
  - UAC - (UDC/sqrt(2)*.98)/2

  - UDC - Rated Voltage/2
  - ku - Voltage Tolerance
  - kr - Voltage Ripple
  - kp - Line-to-Ground Pulsing Factor
  - fr - AC Frequency
  - U_Nom - Line-to-Line Functional Insulation
  - U_INSUL_L - Line-to-Ground Functional Insulation
  - DC - DC System Marker

- Iso_in_1
  - OVCat - Over-voltage Category
  - U1 - Rated Voltage 1
  - U2 - Rated Voltage 2
  - ku1 - Voltage Tolerance 1
  - ku2 - Voltage Tolerance 2
  - kr1 - Voltage Ripple 1
  - kr2 - Voltage Ripple 2
  - kp1 - Line-to-Ground Pulsing Factor 1
  - kp2 - Line-to-Ground Pulsing Factor 2
  - fr - AC Frequency
  - U_Nom_1 - Line-to-Line Functional Insulation 1
  - U_Nom_2 - Line-to-Line Functional Insulation 2
  - DC1 - DC System Marker 1
  - DC2 - DC System Marker 2

An in-depth definition and description of the variables can be found in [23]. The variable lists *Stand_out_1* and *Iso_out_1* are returned to Switch_Drawers.m with both lists housing a prescribed air-gap clearance and creepage distance, denoted as *dClr* and *dCrp*, based upon the inputs of *Stand_in_1* and *Iso_in_1*. Each insulation allocation is assigned its appropriate *dClr* and *dCrp* value. With allocations initialized either through NLSw.mat, or Stand_Off_distances.m and Isolation_Distances.m, the compilation of the no-load switch can begin.

The width, length, and height of the no-load switch is compiled based on figs. 3.17 to 3.19 as in NLSW.m and the compilations remain the same as captured by eqs. (3.1), (3.2), (3.5) to (3.7), (3.9) and (3.10). As before, the max between directional compilations is taken as captured by eqs. (3.3), (3.8) and (3.11).

This ends the scaling of the individual no-load switch and marks the beginning of modularizing the scaled no-load switches into modular drawers. The compilation of the drawers begins by bringing in the drawers' initialed thermal, accessibility, and frame allocations to Switch_Drawers.m from PDM_Switch_Drawers.xlsx as show in fig. 4.39. These allocations correspond to figs. 4.4 and 4.5 in section 4.1.1. As when compiling the individual no-load switch, air-gap creepage and clearance distances are assigned to the insulation allocations by passing *Stand_in_2* and *Iso_in_2* to Stand_Off_distances.m and Isolation_Distances.m. The calculated creepage and clearance distances are returned through *Stand_out_2* and *Iso_out_2* and assigned to the appropriate insulation distances.

Before calculating the total drawer width, length, and height and ultimately passing k_physical and k_thermal to PDM_Metamodel.m, the code calculates the frame support length, f_{DSz3} and f_{DSz4}, based upon column buckling analysis. A safety factor of 2.0 is used along with an initialized frame width. The frame support height is a function of the no-load switch's height. The assembled drawers' total width, length, and height are calculated as informed by figs. 4.4 and 4.5. Unlike the individual no-load switch, each dimension in the drawer compilation only has one possible build-up so no maximum is

taken.

The weight of the assembled drawer is found by adding the calculated weight of two individual no-load switchs plus the weight of the drawer support frames and enclosure. As the mass was found for the no-load switch, the volume of the support frames and enclosure are found and then multiplied by the density of Aluminum 1100.

The packaged drawer's width, height, length, and mass are stored in *k_physical* along with the individual no-load switch's width, height, length, and mass and returned to PDM_Metamodel.m in addition to *k_thermal* and *alpha_SW*. *Alpha_SW* is no used by the designer but houses specific allocations either pulled in from PDM_Switch_Drawers.xlsx or scaled from the test article to be used in the PDM_Bay_Buildup.m compilation.

To begin building up the packaged no-load switch drawers into the drawer compartment, PDM_Metamodel.m passes the variable structures *x*, *r*, *k*, *k_physical*, *k_thermal*, and *alpha_SW* to PDM_Bay_Buildup.m as shown in fig. 4.39. PDM_Bay_Buildup.m begins by again pulling in the drawer's initialized thermal, accessibility, and frame allocations from PDM_Switch_Drawer.xlsx and assigning allocations to local variables. PDM_Bay_Buildup.m pulls in initialized thermal, accessibility, conductor, and frame allocations that pertain to the bay compilation from PDM_Bay.xlsx. The allocations are informed by figs. figs. 4.36 to 4.38. Materials.mat is pulled into PDM_Bay_Buildup.m to calculate component masses. Air-gap creepage and clearance distances are determined by passing the list of variables *Stand_in_3* to Stand_Off_Distances.m. *Stand_out_3* is returned and the appropriate creepage and clearance distances are assigned to the insulation allocations.

Next is the determination of how many drawers fit into a compartment and how many compartments are required based upon the number of switches determined in PDM_Metatest.m. The number of required switches is found by summing together the designer's answers to the questions asked in PDM_Metatest.m, categorized as design parameters (*k*), to determine the total number of switches required. Using *k* and the bay maximum height constraint, *r*, PDM_Bay_Buildup.m determines the number of switches

per bay and number of compartments per bay. Recall that a bay is comprised of adjacent compartments filled with drawers. When the number of drawers required, based upon the number of switches required, exceeds the available space for drawers in one compartment then a subsequent compartment is added. This continues until enough compartments are added to house the quantity of drawers required.

To find the height available for drawers in a compartment, the model subtracts the initialized bay z-direction frame allocations and heat exchanger drawer height from the determined height constraint (r). The difference is then divided by the drawer height calculated in Switch_Drawers.m to find the number of spaces available for drawers in one compartment. The model rounds down to the nearest integer as a fractional drawer is not practical. The model then determines if additional compartments are required by comparing the number of drawers required to the space available for drawers. If the number of spaces available for drawers is less than the number of drawers required, then additional compartments are added until all required drawers are placed. If the number of spaces available for drawers is greater than the number of drawers required then only one compartment is required and the bay height is driven by the drawer and connection compartment height. An important note is that in this use case additional compartments are assumed to be the same height as the first compartment for standardization even if the additional compartments are not fully filled with drawers. The length and height of each additional compartment is also assumed equal to the first compartment's dimensions.

To find the total width of the bay module, resulting from the required drawers as determined by the design parameters (k), the drawer compartment, connection compartment, and modular bay widths are evaluated. Equations (4.14) to (4.17) and (4.23) capture the build-up equations of the drawer compartment as informed by fig. 4.24 and **??**.

To find the total width of the Bay module the width of the connection compartment and drawer compartment, a function of required disconnects as queried from the designer, are evaluated with the maximum driving overall width. Equations (4.8) to (4.16)

capture the build-up equations informed by the bay fig. 4.36, connection compartment fig. 4.38, and drawer compartment fig. 4.24.

$$w_{Bay} = max(w_{ConnComp}, w_{DrComp}) \tag{4.8}$$

$$\begin{aligned} w_{ConnComp} = f_{Bx1} + d_{CCx1} + w_{stab} + d_{CCx3} + (2 \times (n_{comp} - 1) \times (w_{stab} + d_{CCx3})) \\ + w_{stab} + d_{CCx8} + f_{Bx1} \end{aligned} \tag{4.9}$$

Where, d_{CCx3} is equal to d_{CCx6}, d_{CCx7}, and d_{CCx8} in eq. 4.10 as each allocation for clearance requirements between conductors is energized to the same system voltage and will require the same clearance stand-off distance.

$$d_{CCx3} = d_{CCx6} = d_{CCx7} = d_{CCx8} \tag{4.10}$$

Where,

$$w_{stab} = c_{CCx1} + c_{CCx2} + d_{CCx2} + c_{CCx3} + c_{CCx4} \tag{4.11}$$

$$n_{comp} = \text{Required number of compartments} \tag{4.12}$$

$$w_{BayDr} = f_{Bx1} + max(a_{Bx1}, th_{Bx1}) + (n_{comp} \times (w_{DrComp} + max(a_{Bx2}, th_{Bx2}) \times (n_{comp} - 1))) + max(a_{Bx4}, th_{Bx4}) + f_{Bx2} \tag{4.13}$$

Where,

$$w_{DrComp} = max(w_{DrComp1}, w_{DrComp2}) \tag{4.14}$$

$$w_{DrComp1} = f_{Cx1} + a_{Cx1} + i_{Cx1} + a_{Cx2} + f_{Cx1} \tag{4.15}$$

$$w_{DrComp2} = f_{Cx1} + a_{Cx1} + i_{Cx2} + a_{Cx2} + f_{Cx1} \tag{4.16}$$

Where, thermal and accessibility allocations a_{Bx2} and th_{Bx2} from fig. 4.36 are assumed equal to a_{Bx3} and th_{Bx3} because of the standardized nature of modular equipment.

The length of the Bay module is a function of the connection and drawer compartment length as represented by eq. 4.17 and informed by figs. 4.30 and 4.37 and **??**. Equations (4.18) to (4.22) inform eq. 4.17. The connection compartment length will calculate dynamically as the number of drawers in each compartment changes with design decisions and disconnects required. Equations (4.19) and (4.20) capture the two dynamic build-ups of the connection compartment. Equation 4.19 captures the build-up when thermal and accessibility allocations, a_{CCz1} and th_{CCz1}, added to the connection cabling

drive the width and eq. 4.20 captures the case when insulation, thermal, and accessibility allocations added to the furthest extending connection stabs drive overall length. The length of the drawer compartment is captured in eq. 4.22 and is subsumed into the connection compartment build-up equations for ease of modeling.

$$l_{Bay} = f_{Bz1} + max(a_{Bz1} + th_{Bz1}) + i_{Bz1} + max(a_{Bz2} + th_{Bz2}) + f_{Bz2} \tag{4.17}$$

where,

$$i_{Bz1} = max(l_{Comp1}, l_{Comp2}) \tag{4.18}$$

where from fig. 4.30,

$$\begin{aligned} l_{Comp1} = {} & f_{CCz1} + max(a_{CCz1} + th_{CCz1}) + c_{CCz1} \times n_{Drawers} + c_{CCz4} + c_{CCz5} \\ & + max(a_{CCz2} + th_{CCz2}) + i_{CCz1} \end{aligned} \tag{4.19}$$

$$\begin{aligned} l_{Comp2} = {} & f_{CCz1} + max(a_{CCz3}, th_{CCz3}, d_{CCz1}) + ((c_{CCz4} + c_{CCz5}) \times n_{Drawers}) \\ & + max(a_{CCz2} + th_{CCz2}) + i_{CCz1} \end{aligned} \tag{4.20}$$

Where,

$$n_{Drawers} = \text{Number of Disconnects in Compartment} \tag{4.21}$$

where from fig. **??**,

$$i_{CCz1} = i_{Cz1} + f_{Cz1} \tag{4.22}$$

The height of the bay module is calculated as a maximum between the drawer and connection compartment height with the assumption that both compartment heights are set equal to their maximum. Bay length is calculated by eq. 4.23, as informed by fig. 4.36, which sets bay height to the maximum between eqs. (4.24) and (4.25), as informed by fig. 4.30 and **??**. Both compartments build-up dynamically as a function of the number of drawers per compartment, $n_{Drawers}$, to account for changes in design decisions and disconnects required by the designer.

$$h_{Bay} = max(h_{ConnComp}, h_{DrComp}) \tag{4.23}$$

where, from fig. 4.30

$$h_{ConnComp} = f_{CCy1} + d_{CCy1} + ((n_{drawers}) \times (c_{CCy1} + d_{CCy2})) + f_{CCy2} \tag{4.24}$$

Where, conductor and insulation allocations c_{CCy1} and d_{CCy2} from fig. 4.30 are assumed equal to c_{CCy2}, d_{CCy3}, c_{CCy3}, and d_{CCy4} as each conductor and its required clearance requirement is assumed equal for every no-load switch.

$$h_{DrComp} = i_{CCy1} = f_{Cy1} + (n_{drawers}) \times (i_{Cy1} + a_{Cy2}) + i_{Cy4} + a_{Cy2} + f_{Cy1} \tag{4.25}$$

Where, active component and accessibility allocations i_{Cy1} and a_{Cy2} from fig. 4.30 are assumed equal to i_{Cy2}, a_{Cy3}, i_{Cy3}, and a_{Cy4} as no-load switch drawer heights are equal and accessibility required between drawers is assumed equal.

Where,

$$i_{Cy4} = h_{HD} \tag{4.26}$$

$$i_{Cy1} = h_{DS} \tag{4.27}$$

The volume of the Bay is found by multiplying together the calculated bay width, length, and height as shown in Eq. 4.28 and is returned in k_physical.

$$v_{bay} = w_{Bay} \times l_{Bay} \times h_{Bay} \tag{4.28}$$

The weight of the Bay is found by adding the weight of all of the required drawers, the heat exchanger, the bay supports and enclosure, and the variable weight of the conductor stabs depending on the number of drawers required. Similiar to how the mass was found for the no-load switch and drawer, the volume of the bay support frames and enclosure are determined and then multiplied by the density of Aluminum 1100. The mass of the conductor stabs requires dynamic calculations to determine the number, and volume, of the required conductor stabs before being multiplied by the density of copper. Because the width, length, and height of each additional compartment is assumed equal to the first, even if the number of drawers inside of the last compartment are not equal to the first compartment, the last compartment's stab conductor volume could be different than the first compartment, meaning that the model can not simply multiply the stab volume

of the first compartment by the number of compartments required. To capture the last compartment's variable conductor volume, the model uses if statements to determine the number of stabs in the last compartment before computing their volume and adding it to the first and subsequent compartment conductor volumes. Their combined volume is multiplied by the density of copper to find the total weight of the conductor stabs. Once found, all weights are summed and the total weight of the bay is stored in *k_physical* to be returned.

With the bay width, height, length, volume, and mass calculated and stored in *k_physical*, *k_physical* and *k_thermal* are returned to PDM _Metamodel.m as shown in fig. 4.39. *K_physical* and *k_thermal* are then returned to PDM_Metatest.m and unbundled so that the no-load switch, drawer, and total bay width, height, length, volume, and weight are displayed in Matlab for the designer.

4.3 PDM Bay Metamodel Results

The outputs of the PDM bay metamodel are presented in figs. 4.40 to 4.44. Fig. 4.40 shows the bay's overall width, height, and length as system voltage increases from 5kV to 30kV with a fixed current of 2000A and height constraint of 3 meters. Notice that the bay's height, shown in green, is bounded by the three-meter constraint. Whenever the three-meter constraint is reached a subsequent increase in width is experienced as additional compartments are added to house the disconnect drawers that push the bay height above 3 meters. This is seen at 10kV and again at 16kV. The reader will also notice that bay width begins to linearly increase at 16kV as insulation requirements that drove the individual no-load switch's width and the no-load switch's drawer width begin to drive overall bay width. This again highlights that performance metrics of the lowest modular assembly will inform performance metrics at the system level.

Total PDM bay mass is presented in fig. 4.41 and reflects the insights gained from fig. 4.40. Note that when an additional compartment is added due to the imposed height

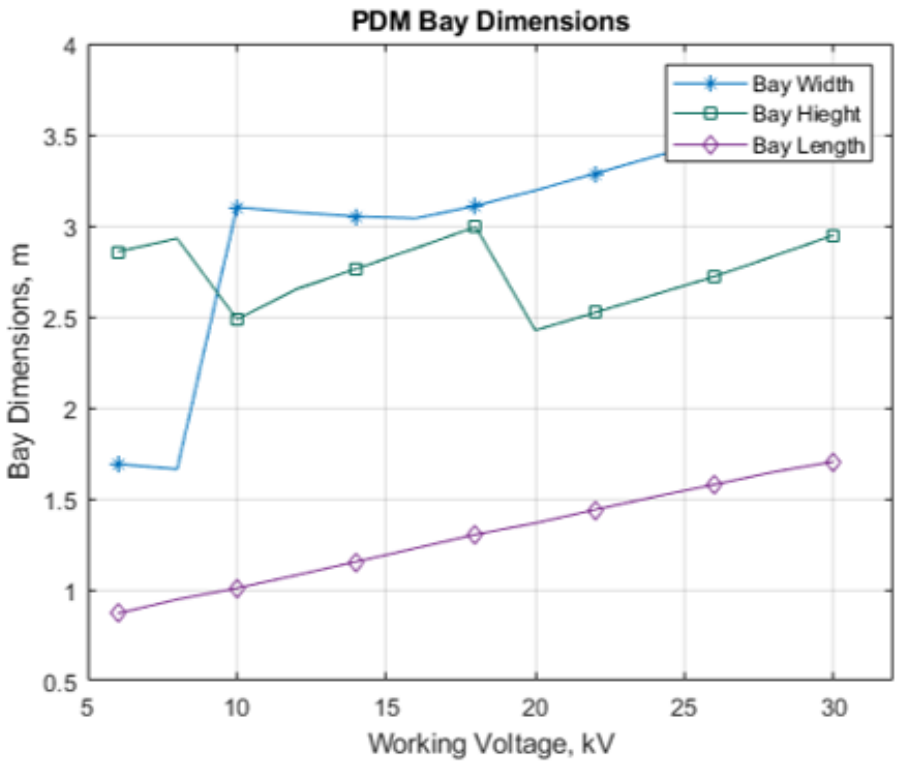

Figure 4.40: PDM Bay Dimensions

constraint at 10kV, bay mass has a corresponding increase. This is again experienced at 16kV when insulation requirements begin to increase frame size and subsequently PDM bay mass.

In fig. 4.42 the power density between the complete bay assembly is compared against the power density of the active component no-load switch and heat exchanger drawers that comprise the compartments and bay. The comparison again demonstrates the loss in power density, performance metrics in a general sense, as active components are modularized and built into a modular distribution network. The bay's power density is labeled Bay PD and shown in orange while the no-load switch and heat-exchanger drawers' combined power density is labeled Active Component PD and shown in blue. As seen in fig. 4.42, once insulation, thermal, and accessibility allocations are added to the compartment and bay assembly power density peaks at 3.65 MW/m^2 at 16kV compared to the active components' 7.45 $MW/^2$. Note that at 10kV the bay's power density experiences a de-

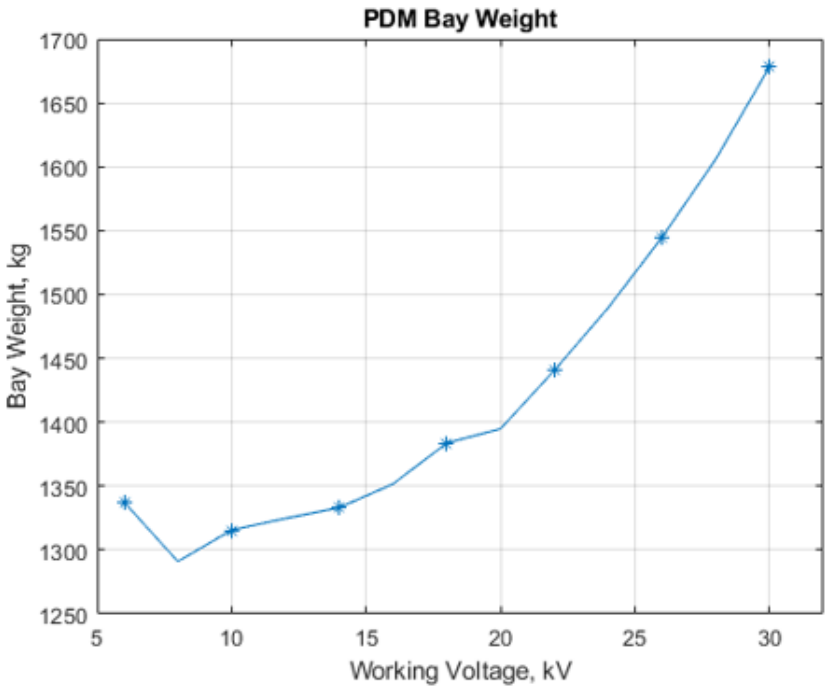

Figure 4.41: PDM Bay Mass

crease in slope as the bay width in fig. 4.40 is approximately doubled to reflect an additional compartment. This is seen again at 17kV as the bay's 3-meter height constraint is reached, before linearly decreasing as bay width, height, and length continue increasing linearly above 17kV.

Fig. 4.43 compares specific power between the bay assembly and its active component building blocks. The loss in specific power between the bay and its active component drawers is less pronounced than power density as increasing creepage and clearance requirements continue to drive overall volume but do not contribute to overall mass. Specific power increases for both the bay and active components begin to flatten at 17kV as the bay's increasing frame weight, as dictated by increasing width, length, and height, begins to dominate overall assembly weight. A key insight from the presented MOPs suggests that power density and specific power gains will likely be negated by increased insulation requirements above a certain distribution voltage threshold. This insight can be counter-intuitive as increases in distribution voltage will necessarily increase power

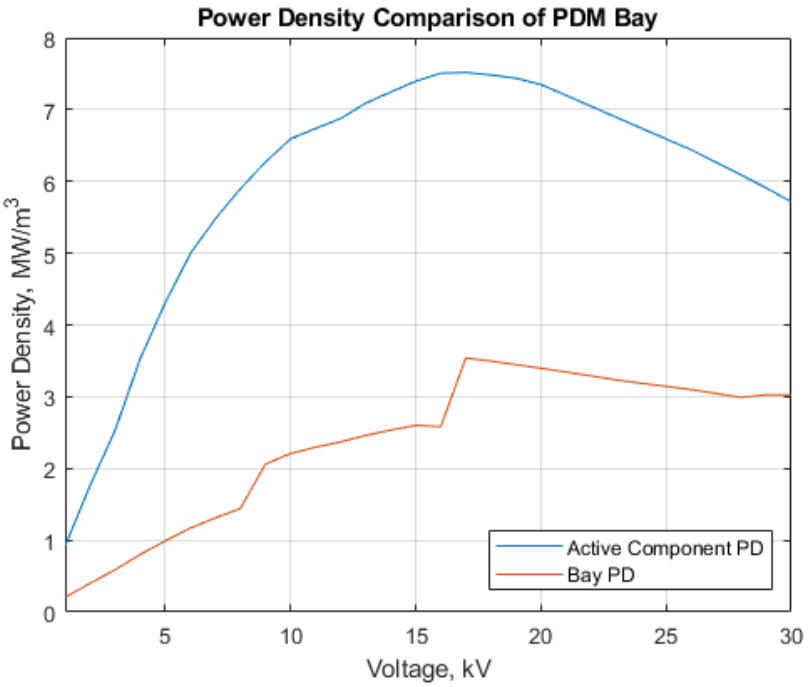

Figure 4.42: PDM Power Density Comparison

throughput, but as insulation, thermal, and accessibility requirements are considered and incorporated into the meta-model these power throughput gains are often negated.

The final result as shown in fig. 4.44, compares the bay's power density as bus voltage increases from 5kV to 30kV to the bay's calculated specific power. This is representative of the MOP Pareto fronts produced by the VPP that designers will use to select for design solutions as a trade-off between stakeholder needs, here MOPs. Both trends suggest diminishing returns on power density and specific power gains above 17kV. While no definite findings can be made from fig. 4.44 as stakeholder needs are left undefined, the MOP comparisons will provide transparency into design decisions' impact on MOPs, which designs will ultimately use to evaluate equipment and system performance.

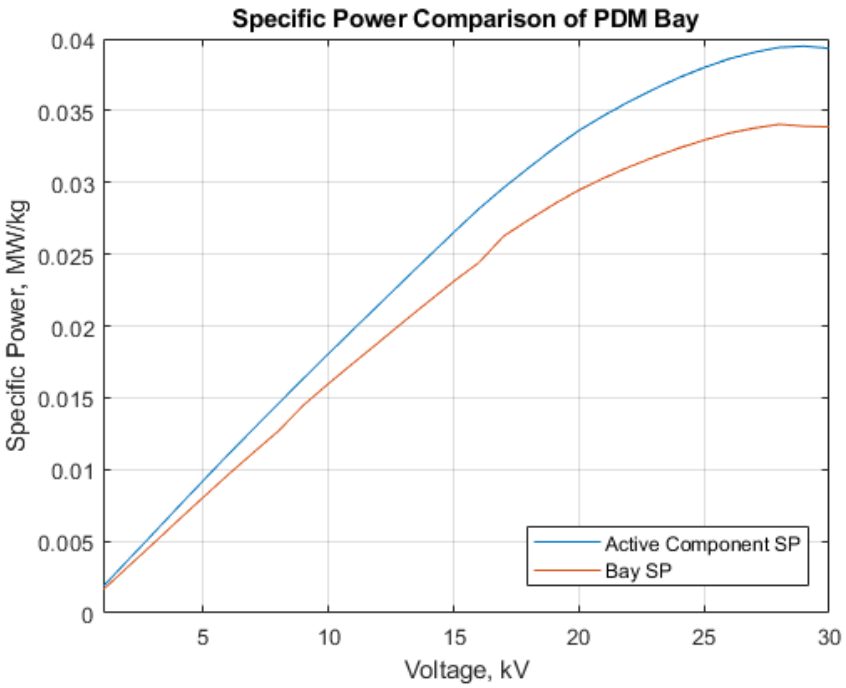

Figure 4.43: PDM Specific Power Comparison

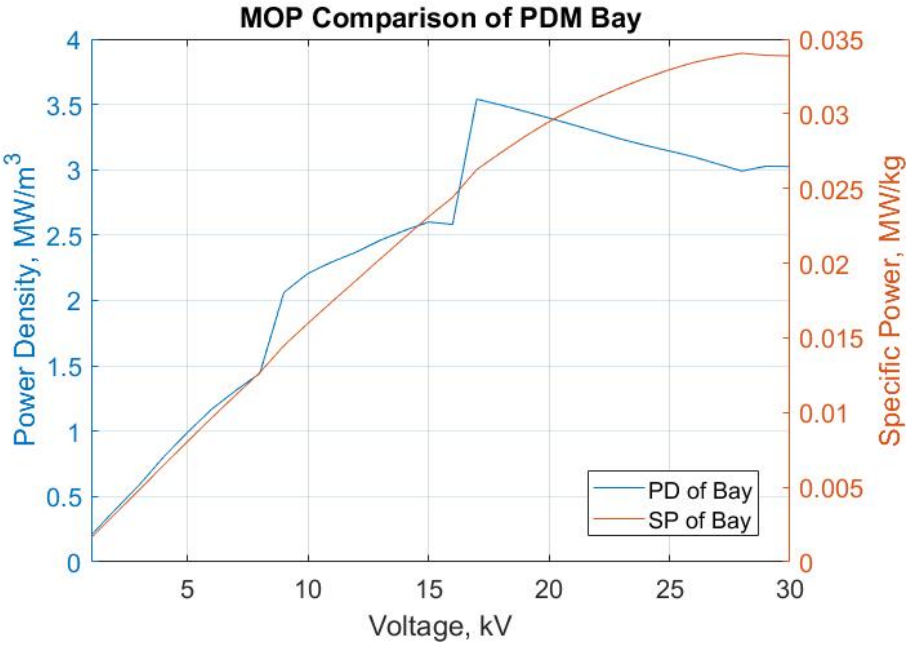

Figure 4.44: PDM MOP Comparison

CHAPTER 5
CONCLUSION AND FUTURE WORK

In this thesis, an allocation and compilation methodology is proposed to enable the modularization of power electronic technology for use in modular naval distribution networks. A use-case is employed on a power distribution module comprised of multiple no-load DC disconnect switches to demonstrate the methodology's applicability to all ontological levels of a modular distribution network. First, the methodology is applied to the power distribution module's least replaceable units as a demonstration of the generic process. Then the LRU building blocks are modularized into drawers with performance metrics calculated as a function of distribution bus voltage from 5kV to 30kV. The calculated MOPs, power density and specific power specifically, suggest diminishing returns on performance gains once a distribution bus voltage of 16kV is reached as insulation coordination requirements begin to dominate space claim. This insight holds true as no-load switch drawers are modularized into drawer compartments and the functionally defined PDM. A connection compartment, accounting for interconnection requirements imposed on the assembly when integrated into a distribution network, is added allowing for transparency into the effect modularization has on performance metrics. A scalable metamodel is produced from the methodology for use in the S3D's LEAPS database. MOPs calculated by the metamodel are compared for distribution bus voltages from 5kV to 30kV with the insight that insulation coordination requirements imposed by bus voltages above 16kV holds true at all ontological levels of the modularized technology.

Future work will involve integrating physics-based scaling laws for thermal, insulation, and structural spatial allocations present in this methodology as fundamental research matures. The incorporation of physics-based scaling laws will remove the inherent conservativeness of standards-based allocations as employed in this use-case. Future

work will also include applying this methodology to complete distribution powertrains utilized in the IPS and NiPEC architectures. Further insights will be gained into equipment modularization effects on system-level performance metrics as this methodology, in conjunction with the VPP, produces optimal, scalable, metamodels for S3D. Additional design variables, representing design choices, such as liquid cooling water temperature, grounding scheme, and current selection will also be incorporated into future applications of this methodology.

REFERENCES

[1] N. Doerry, J. Amy, and C. Krolick, "History and the status of electric ship propulsion, integrated power systems, and future trends in the us navy," *Proceedings of the IEEE*, vol. 103, no. 12, pp. 2243–2251, 2015.

[2] N. Doerry and K. McCoy, "Next generation integrated power system: NGIPS technology development roadmap," Naval Sea Systems Command Washington DC, Tech. Rep., 2007.

[3] Z. Tu, W. Zhang, and W. Liu, "Deep Reinforcement Learning-Based Optimal Control of DC Shipboard Power Systems for Pulsed Power Load Accommodation," *IEEE Transactions on Smart Grid*, vol. 14, no. 1, pp. 29–40, 2023.

[4] N Doerry and J Amy, "{MVDC} Shipboard Power System Considerations for Electromagnetic Railguns," (pp. 15–16).

[5] J Kuseian, "Naval power systems technology development roadmap-distribution a-14 may 2013," *Electric Ship Office-PM320*,

[6] C. M. Cooke, C Chryssostomidis, and J Chalfant, "Modular integrated power corridor," in *2017 IEEE Electric Ship Technologies Symposium (ESTS)*, IEEE, 2017, pp. 91–95.

[7] R Soman, M Steurer, T Toshon, and M. O. Faruque, "Investigation of Scaling Laws of Modular Multilevel Converters for Sizing Breaker-less MVDC Architectures," no. May, 2016.

[8] J. Chalfant, "Early-stage design for electric ship," *Proceedings of the IEEE*, vol. 103, no. 12, pp. 2252–2266, 2015.

[9] R. Soman, M. M. Steurer, T. A. Toshon, M. O. Faruque, and R. M. Cuzner, "Size and weight computation of mvdc power equipment in architectures developed using the smart ship systems design environment," *IEEE Journal of Emerging and Selected Topics in Power Electronics*, vol. 5, no. 1, pp. 40–50, 2017.

[10] J. Chalfant, B. Langland, D. Rigterink, C. Sarles, P. Mccauley, D. Woodward, A. Brown, and R. Ames, "Smart Ship System Design (S3D) Integration with the Leading Edge Architecture for Prototyping Systems (LEAPS)," *2017 IEEE Electric Ship Technologies Symposium, ESTS 2017*, pp. 104–110, 2017.

[11] S. Stipetic, D. Zarko, and M. Popescu, "Scaling laws for synchronous permanent magnet machines," *2015 10th International Conference on Ecological Vehicles and Renewable Energies, EVER 2015*, 2015.

[12] R. C. Zowarka, "Physical scale modeling to verify energy storage inductor parameters," *IEEE Transactions on Magnetics*, vol. 20, no. 2, pp. 219–222, 1984.

[13] S. D. Sudhoff, G. M. Shane, and H. Suryanarayana, "Magnetic-equivalent-circuit-based scaling laws for low-frequency magnetic devices," *IEEE Transactions on Energy Conversion*, vol. 28, no. 3, pp. 746–755, 2013.

[14] S. Yang and J. C. Ordonez, "Optimal cooling channel layout in a hot enclosure subject to natural convection," *Journal of Heat Transfer*, vol. 141, no. 11, pp. 1–12, 2019.

[15] R. Cuzner, S. Cruz, F. Ferrese, and R. Hosseini, "Power converter metamodeling approach for the smart ship design environment," in *Electric Ship Technologies Symposium (ESTS), 2017 IEEE*, IEEE, 2017, pp. 118–125.

[16] R. M. Cuzner, D. C. Gross, and M. Steurer, "Determining Parameter Objectives via Model-Based Engineering," *2023 IEEE Electric Ship Technologies Symposium, ESTS 2023*, no. 1650470, 2023.

[17] R. M. Cuzner, R. Soman, M. M. Steurer, T. A. Toshon, and M. O. Faruque, "Approach to scalable model development for navy shipboard compatible modular multilevel converters," *IEEE J. Emerg. Sel. Topics Power Electron*, vol. 5, no. 1, pp. 28–39, 2017.

[18] R. Cuzner, R. Siddaiah, and T. Nguyen, "Applying a Virtual Prototyping Process to Generate Pareto Optimal Solutions for a Modular Multi-Level MVAC to MVDC Converter," *IEEE International Symposium on Industrial Electronics*, vol. 2019-June, pp. 2039–2046, 2019.

[19] R. Cuzner, M. Vygoder, and R. Siddaiah, "Power Conversion and Distribution Equipment Metamodels for Dependable Design of Shipboard Integrated Power and Energy Systems," in *2018 IEEE International Conference on Electrical Systems for Aircraft, Railway, Ship Propulsion and Road Vehicles and International Transportation Electrification Conference, ESARS-ITEC 2018*, Institute of Electrical and Electronics Engineers Inc., Jan. 2019, ISBN: 9781538641927.

[20] A. Challita, "High Speed , Medium Voltage Direct Current Isolation Device," no. May, pp. 1–10, 2014.

[21] S. Hundertmark, "Investigations on the energy chain for a naval railgun," *IEEE Transactions on Plasma Science*, vol. 48, no. 11, pp. 3991–3996, 2020.

[22] I. R. McNab, F. Stefani, M. T. Crawford, M. Erengil, C. Persad, S. Satapathy, H. Vanicek, T. Watt, and C. Dampier, "Development of a naval railgun," *2004 12th Symposium on Electromagnetic Launch Technology*, vol. 41, no. 1, pp. 76–80, 2004.

[23] R. Cuzner and W. Koebel, "Application of IEC-61800-5 Insulation Coordination to Shipboard Equipment Scaling Studies," 2021, pp. 1–11.

[24] "Adjustable speed electrical power drive systems - Part 5-1: Safety requirements - Electrical, thermal and energy," *IEC 61800-5-1*, 2018.

[25] T. Damle, C. Park, J. Ding, P. Cheetham, M. Bosworth, M. Steurer, R. Cuzner, and L. Graber, "Experimental setup to evaluate creepage distance requirements for shipboard power systems," in *2019 IEEE Electric Ship Technologies Symposium (ESTS)*, IEEE, 2019, pp. 317–323.

[26] J. Choi, N. Guo, T. Damle, J. Ding, R. Nguyen, C. Park, and L. Graber, "Testbed to Study the Surface Charge Distribution along DC Standoff Insulators for All-Electric Ships," in *2020 Electrical Insulation Conference*, Jun. 2020.

[27] A. Cavallini, D. Fabiani, and G. C. Montanari, "Power electronics and electrical insulation systems Part 1: Phenomenology overview," *IEEE Electrical Insulation Magazine*, vol. 26, no. 3, pp. 7–15, 2010.

[28] ——, "Power electronics and electrical insulation systems-part 2: life modeling for insulation design," *IEEE Electrical Insulation Magazine*, vol. 26, no. 4, pp. 33–39, 2010.

[29] ——, "Power electronics and electrical insulation systems-Part 3: Diagnostic properties," *IEEE Electrical Insulation Magazine*, vol. 26, no. 5, pp. 30–40, 2010.

[30] R. Cuzner, M. Vygoder, and R. Siddaiah, "Power conversion and distribution equipment metamodels for dependable design of shipboard integrated power and energy systems," in *2018 IEEE International Conference on Electrical Systems for Aircraft, Railway, Ship Propulsion and Road Vehicles & International Transportation Electrification Conference (ESARS-ITEC)*, IEEE, 2018, pp. 1–8.

[31] "Military specification: Electric power equipment, basic requirements," *Mil-DTL-917E*, 1993.

[32] R. Siddaiah, R. M. Cuzner, J. Ordonez, C. Dimarino, and J. Chalfant, "Virtual Prototyping Process : Enabling Shipboard Sizing and Arrangement of a Power Electronics Power Distribution System," *2023 IEEE Electric Ship Technologies Symposium, ESTS 2023*, pp. 1–10, 2023.

[33] R. Cuzner and R. Siddaiah, "Derivation of power system module metamodels for early shipboard design explorations," in *Electric Ship Technologies Symposium (ESTS), 2019 IEEE*, IEEE, 2019.

[34] R. Siddaiah, R. Cuzner, and T. Nguyen, "Applying a virtual prototyping process to generate pareto optimal solutions for a modular multi-level mvac to mvdc converter," in *2019 IEEE 28th International Symposium on Industrial Electronics (ISIE)*, IEEE, 2019, pp. 1–8.

[35] U. Navy, "Switchgear, Power, Hard-Mounted, Medium Voltage, Naval Shipboard," *MIL-DTL-32483*, no. August, 2013.

[36] ——, "Mechanical Vibrations of Shipboard Environment," *MIL-STD-167-1*, 1974.

[37] U.S. Navy, *Military Specification: Shock Tests, H.I. (High-impact) Shipboard Machinery, Equipment, and Systems, Requirements*, March. 1989, ISBN: 6451973904.

[38] S. Castellan, R. Menis, A. Tessarolo, and G. Sulligoi, "Power electronics for all-electric ships with MVDC power distribution system: An overview," in *2014 Ninth International Conference on Ecological Vehicles and Renewable Energies (EVER)*, IEEE, 2014, pp. 1–7.

Appendices

APPENDIX A

CLEARANCE AND CREEPAGE DISTANCE DETERMINATION FOR FREQUENCIES GREATER THAN 30K KHZ

Frequency Creepage Distances .png

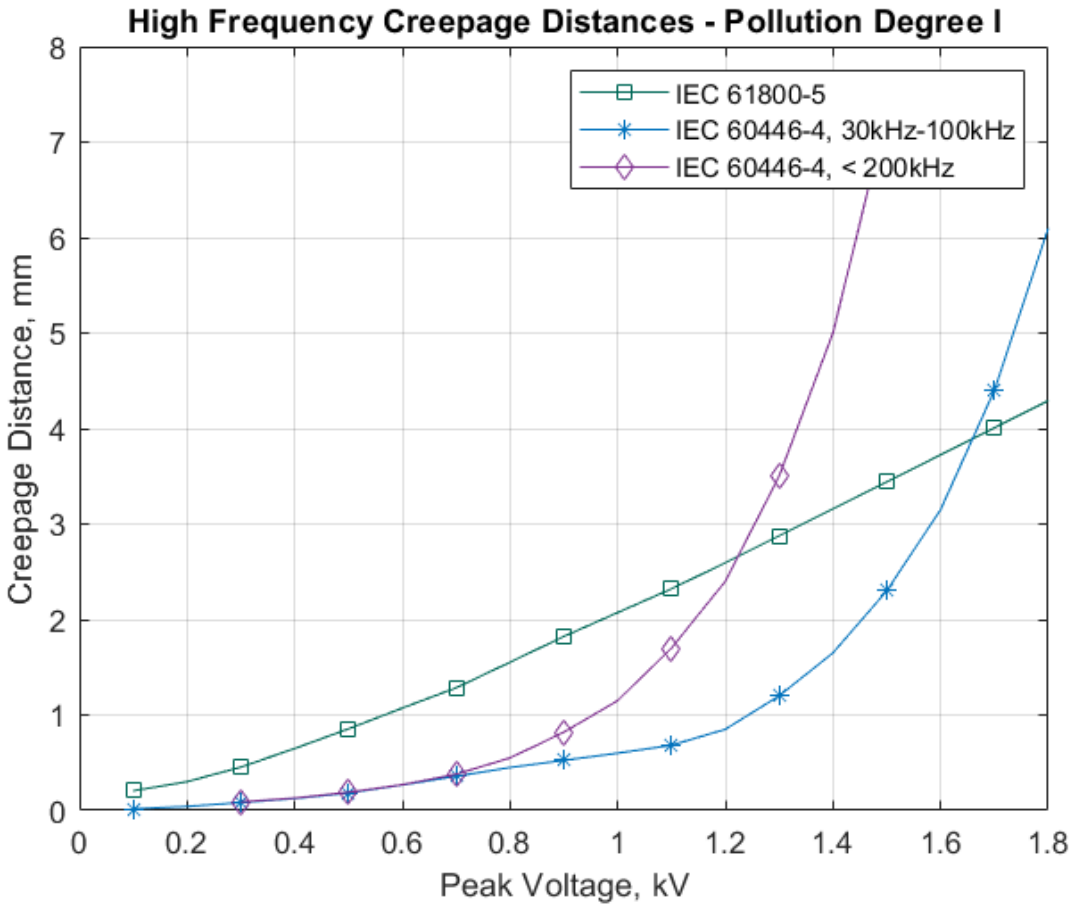

Figure A.1: High Frequency Creepage Distances

Frequency Clareance Distances.png

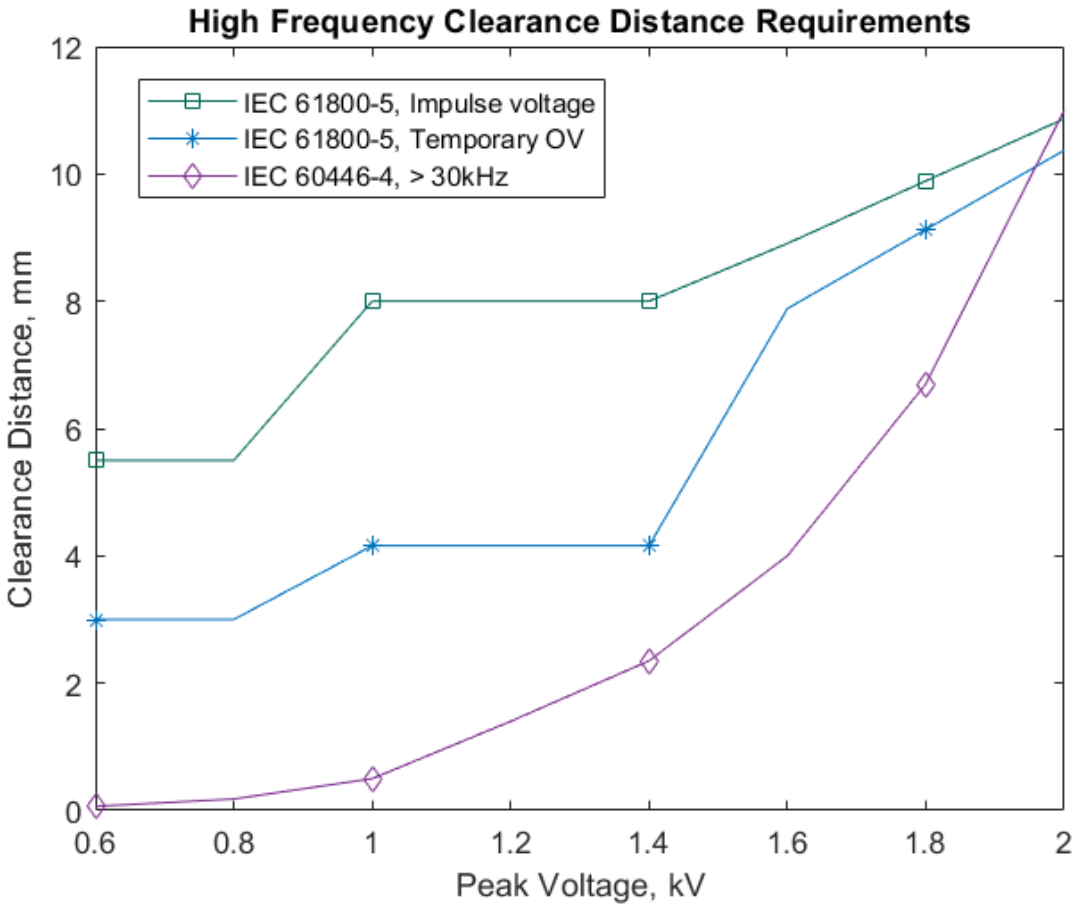

Figure A.2: High Frequency Clearance Distances